DOE/BC/10327-20
(DE84012729)

DEVELOPMENT AND VERIFICATION OF SIMPLIFIED PREDICTION MODELS FOR ENHANCED OIL RECOVERY APPLICATIONS

CO_2 (MISCIBLE FLOOD) PREDICTIVE MODEL—FINAL REPORT

Work Performed for the Department of Energy
Under Contract No. DE-AC19-80BC10327

Date Published-October 1984

Scientific Software-Intercomp
Denver, Colorado

U. S. DEPARTMENT OF ENERGY

FOSSIL ENERGY

DISCLAIMER

This report was prepared as an account of work sponsored by an agency of the United States Government. Neither the United States Government nor any agency thereof, nor any of their employees, makes any warranty, express or implied, or assumes any legal liability or responsibility for the accuracy, completeness, or usefulness of any information, apparatus, product, or process disclosed, or represents that its use would not infringe privately owned rights. Reference herein to any specific commercial product, process, or service by trade name, trademark, manufacturer, or otherwise, does not necessarily constitute or imply its endorsement, recommendation, or favoring by the United States Government or any agency thereof. The views and opinions of authors expressed herein do not necessarily state or reflect those of the United States Government or any agency thereof.

Printed in the United States of America. Available from:
National Technical Information Service
U.S. Department of Commerce
5285 Port Royal Road
Springfield, VA 22161

NTIS price codes
Paper copy: $14.50
Microfiche copy: $4.50

DOE/BC/10327-20
Distribution Category UC-92a

DEVELOPMENT AND VERIFICATION OF SIMPLIFIED PREDICTION MODELS FOR ENHANCED OIL RECOVERY APPLICATIONS

CO_2 (MISCIBLE FLOOD) PREDICTIVE MODEL—FINAL REPORT

George W. Paul, *Principal Investigator*
Scientific Software-Intercomp
1801 California Street
Denver, Colorado 80202

R. M. Ray, *Technical Project Officer*
Bartlesville Project Office
P.O. Box 1398
Bartlesville, Oklahoma 74005

TECHNOLOGY TRANSFER BRANCH
BARTLESVILLE PROJECT OFFICE
U.S. DEPARTMENT OF ENERGY
BARTLESVILLE, OKLAHOMA

Work Performed for the Department of Energy
Under Contract No. DE-AC19-80BC10327

Date Published—October 1984

FOREWORD

This contract, DE-AC19-80BC10327, is a natural extension of contracts DE-AC19-78BC00048 and DE-AC19-78BC00051 which developed a simplified predictive model for the surfactant-polymer process. This contract report details the results of development of a simplified predictive model for the steam drive process which is useful for estimating the enhanced recovery potential of specific properties. This model, as with the surfactant-polymer model, contains algorithms to predict the oil recovery of a 5-spot pattern, and, given the necessary information, the economics of the project from the single pattern to full field development. Data for all fluids from injectants to produced fluids are calculated and reported in a model run. After development, this model was evaluated by task group members of the National Petroleum Council for use in their 1984 EOR Potential Study. The Council task group members made many recommendations to update, correct deficiencies, and add to the capabilities of the model. Unfortunately, this report was initiated prior to the final changes being performed, and, as such, this report does not contain all improvements suggested by the NPC representatives. This model as reported does satisfy all contractual obligations for the development of the model.

This contract report is one of two submitted under the referenced contract. The second report, yet to be published, is on the development of a simplified predictive model for the CO_2 miscible drive process. That miscible report will be published in the immediate future.

The development of these simplified predictive models was the direct result of a desire to perform national EOR potential studies that were based on individual reservoir properties. This EOR potential would then be the accurate attainable and would reflect current technology as it was currently understood. The very nature of the design of these models allows the user to update the technology as technological advances are made or to estimate the result of technology sensitivities which are useful in prioritizing R&D programs. As there is usually a vast difference between technically recoverable oil and economically recoverable oil, each model has its own economic routines which can also be used to determine the effects of sensitivites not only to prices/costs but also to changes due to technological advances/changes.

While this steam drive model is extremely useful as a measuring tool, the user needs to be aware that it is not appropriate for in-depth, reservoir-specific engineering studies and should be used only to predict the potential for applying the steam drive process to a reservoir or group of reservoirs. In-depth evaluation should then follow using methods based upon standard industry practices before project implementation.

TABLE OF CONTENTS

		Page
ABSTRACT		
LIST OF TABLES		
LIST OF FIGURES		
ACKNOWLEDGEMENTS		
I.	INTRODUCTION	
	A. Purpose and Scope	1
	B. Assumptions, Limitations, and Applicability of CO_2 Predictive Model (CO2PM)	2
	C. Previous CO_2 Models	3
II.	FRACTIONAL FLOW MODEL	
	A. Scaled Equations	6
	B. Results Without Viscous Fingering	12
	C. Results With Viscous Fingering	15
	D. Comparison of Fractional Flow Model With Numerical Simulator	17
	E. Comparison of Fractional Flow Model to Laboratory Experiment	19
	F. Calculating Average Concentrations Behind the Fronts	21
	G. Correction For Finite Slug Size	22
	H. Modification For Layering	24
III.	INCLUDING GRAVITY IN ONE-DIMENSIONAL THEORY	
	A. Scaling Parameter	26
	B. Simulation Results	26
	C. Effective Koval Factor	27
IV.	AREAL SWEEP CORRECTIONS	
	A. Areal Sweep Correlation	29
	B. Combining Areal Sweep With One-Dimensional Theory	31

TABLE OF CONTENTS (Cont.)

		Page
V.	COMPARISON OF CO2PM WITH FIELD DATA AND NUMERICAL SIMULATION	
	A. Selection of CO_2 Field Cases	35
	B. Comparison of CO2PM With Slaughter Pilot	35
	C. Comparison of CO2PM With Simulation For Denver Unit	36
VI.	CO2PM ECONOMIC MODEL	
	A. General Description	37
	B. Annual Balance Sheet	39
	C. Taxes	42
	D. Debt Financing	44
	E. Escalation and Discounting	44
	F. Uncertainty	46
	G. Results and Profitability Indices	47
NOMENCLATURE		50
REFERENCES		55
TABLES		58
FIGURES		64
APPENDICES		
	A. Method of Characteristics Fundamentals	A-1
	B. Effect of Gravity Segregation on Miscible Flood Oil Recovery	B-1
	C. Calculation of Rate and Slug Size Multipliers for Layers	C-1
	D. Description of CO2PM Routines	D-1

ABSTRACT

A screening model for CO_2 miscible flooding has been developed consisting of a reservoir model for oil rate and recovery and an economic model. The reservoir model includes the effects of viscous fingering, reservoir heterogeneity, gravity segregation and areal sweep. The economic model includes methods to calculate various profitability indices, the windfall profits tax, and provides for CO_2 recycle. The model is applicable to secondary or tertiary floods, and to solvent slug or WAG processess. The model does not require detailed oil-CO_2 PVT data for execution, and is limited to five-spot patterns. A pattern schedule may be specified to allow economic calculations for an entire project to be made. Models of similar architecture have been developed for steam drive, in-situ combustion, surfactant-polymer flooding, polymer flooding and waterflooding.

LIST OF TABLES

		Page
Table 1	Reservoir and Fluid Propeties for 1-D Simulations	58
Table 2	Reservoir Properties for 2-D Cross-section Simulations	59
Table 3	CO2PM Input Data For Slaughter Case	60
Table 4	CO2PM Input Data For Denver Unit Case	62

LIST OF FIGURES

		Page
Figure 1	Phase Boundaries in Ternary Equilibria	64
Figure 2a	Schematic Composition Path Diagram	65
Figure 2b	Schematic Flux-Concentration Plot	65
Figure 2c	Time-Distance Diagram	66
Figure 2d	Effluent Histories	67
Figure 3	Relative Permeabilities and Fractional Flow for SACROC Example	68
Figure 4	Composition Path Diagram for No-Fingering Cases	69
Figure 5	Effluent Histories for Four No-Fingering Cases	70
Figure 6	Fractional Flow Construction for $J_1 \rightarrow I_2$	71
Figure 7	Fractional Flow Construction for $J_2 \rightarrow I_1$	72
Figure 8	Fractional Flow Construction for $J_2 \rightarrow I_2$	73
Figure 9	Composition Path Diagram for Fingering Cases	74
Figure 10	Effluent Histories for Four Fingering Cases	75
Figure 11	Comparison of CO2PM with Simulator for Secondary Case	76
Figure 12	Comparison of CO2PM With Simulator for Tertiary Case (WAG = 0, KOVAL = 10)	77
Figure 13	Comparison of CO2PM with Simulator for Tertiary Case (WAG = 2, KOVAL = 10)	78
Figure 14	Comparison of CO2PM with Simulator for Tertiary Case (WAG = 0, KOVAL = 5)	79
Figure 15	Production Curves for Coreflood	80
Figure 16	Fractional Fluxes	81
Figure 17	Comparison of CO2PM with Coreflood Results	82
Figure 18a	Schematic of Fractional Flux-Concentration Curve	83
Figure 18b	Schematic of Flux Profile	83
Figure 19	Average Concentration Behind Front	84
Figure 20	Schematic of Correction Procedure for Finite Slugs	85
Figure 21	Relative Permeability Curves	86
Figure 22	Effect of Relative Permeability on Single Layer Recovery	87
Figure 23	Effect of Pattern Size on Recovery	88
Figure 24	Normalized Rate vs. t_h/t_v	89
Figure 25	Normalized Rate vs. Koval Factor	90

LIST OF FIGURES (Cont.)

		Page
Figure 26	Gravity Correction Factor vs. t_h/t_v	91
Figure 27	Schematic of Contacted and Invaded Area in 1/4 5-Spots	92
Figure 28	Areal Sweep Correlations	93
Figure 29	Schematic of Behavior of Average Concentrations	94
Figure 30	Cumulative Oil Produced for Experiment C-1-6	95
Figure 31	Comparison of CO2PM with Slaughter Pilot (3 layers, VDPL = 0.48)	96
Figure 32	Comparison of CO2PM with Slaughter Pilot (1 layer, VDP = 0.48)	97
Figure 33	Comparison of CO2PM with Slaughter Pilot (1 layer, VDP = 0.25)	98
Figure 34	San Andres Relative Permeability	99
Figure 35	Comparison of Flow Capacity-Storage Capacity Relations	100
Figure 36	Comparison of CO2PM with Simulator for Denver Unit	101
Figure A-1a	Characteristic Construction for General One Dependent Variable Problem	102
Figure A-1b	Characteristic Construction for Special Case	102
Figure A-2a	Characteristics for Two-Variable Problem	103
Figure A-2b	Characteristics for Centered Simple Wave	104
Figure D-1	CO2PM Flow Diagram	105

ACKNOWLEDGEMENTS

The following persons are acknowledged for their contributions to the work: L. W. Lake of U. Texas, Austin; from Scientific Software-Intercomp, A. Arya, S. R. Aydelotte, T. L. Gould, J. E. McElhiney, A. R. Merchant, and M. B. Moranville; and from the National Petroleum Council Miscible Task Group, A. Emanuel (Chevron), E. Cook (Mobil), P. Leonard (Exxon), and W. Miller (Shell).

I. INTRODUCTION

A. Purpose and Scope

One goal of the Bartlesville Energy Technology Center (BETC) of the U. S. Department of Energy is to possess the capability to identify reservoirs for enhanced oil recovery (EOR). Towards the fulfillment of this goal, the development of a reservoir data base and a series of simplified performance prediction models for the various EOR processes is essential.

Such a program was begun in 1978 under BETC's contract to Gary Energy Co./Intercomp to screen the mid-continent and California regions for micellar-polymer candidate reservoirs. Under that contract, Intercomp constructed both a reservoir data base[1] and a simplified performance prediction model for micellar-polymer flooding.[2] Recognizing the strength of such an approach, Intercomp, in 1980, initiated for BETC the development of predictive models for the carbon dioxide (CO_2) miscible flooding[3] and steam drive[4] processes. Subsequently, Intercomp/Scientific Software-Intercomp developed waterflood, polymer flood, and in-situ combustion models for the National Petroleum Council (NPC). The suite of models was used by NPC in their 1983 study of the EOR potential of U.S. reservoirs.

The basic idea of the predictive models is to allow rapid and inexpensive screening for EOR based on economic profitability, rather than on a series of arbitrary technical constraints. Thus, the performance prediction models were developed to satisfy the following criteria:

1. They should be direct and easy to use, requiring a relatively small amount of computer software.

2. They should use technical information readily available from primary or secondary producing operations in the reservoir data base, or, at the least, they should point toward information that should be included in the reservoir data base.

3. They should be accurate enough to evaluate the EOR process/candidate reservoir, at least in a relative sense for a particular EOR process among a group of candidates, or for a particular reservoir among a group of processes.

The architecture of the models developed to date is basically the same: an oil recovery versus time algorithm is computed, the results of which are input to the economic calculations. EOR process variables are integrated into the oil recovery algorithm. An example is the effect of lowering the viscosity of oil by heating; in the steam drive process, this effect influences the oil mobility and thus its recovery. The economic calculations require estimates of process costs, reservoir development costs, and operating costs. These economic elements, when properly considered on a time scale with oil production, allow computation of discounted cash flow economics. The economic evaluation provides the ultimate measure of EOR potential.

B. Assumptions, Limitations and Applicability of CO_2 Predictive Model

This report summarizes the development of the CO_2 miscible flood predictive model (CO2PM). The CO2PM combines the ability to handle complex mechanistic calculations usually available only through full numerical simulation with the low operating cost of the less technically sophisticated hand-held calculator models.

The oil rate and recovery algorithm includes treatments for a number of effects and conditions: fractional flow, areal sweep, reservoir heterogeneity, viscous fingering, and gravity segregation. A one-dimensional fractional flow theory was developed for first-contact miscible displacements in the presence of a second immiscible phase. The theory is based on a specialized version of the method of characteristics known as coherence or simple wave theory. The theory incorporates the Koval[5] factor method to account for unstable miscible displacements (fingering). An extension of the Koval approach is used to model the influence of gravity segregation. Reservoir heterogeneity is accounted for by allowing up to five layers in the model. The fractional flow theory with gravity and heterogeneity dependence is corrected for areal sweep with a generalization of Claridge's[6] procedure to first-contact miscible floods of arbitrary WAG ratios and arbitrary initial conditions.

The CO2PM assumes that the displacement is fully miscible and that the Koval factor method adequately describes fingering and gravity effects. Due to boundary condition restrictions in the method of characteristics, the CO2PM should not be used with a Koval factor below about 2.0 (very stable miscible displacement). The model does not calculate fluid injectivity and assumes that the reservoir can take any specified injection rate. The model also assumes steady-state displacement with constant injection rate and WAG ratio.

The CO2PM can be used for a wide range of initial reservoir conditions. It can be used for both secondary (mobile oil present) and tertiary recovery. It can predict performance for continuous CO_2 injection or for any WAG process. Ultimate chase fluid is limited to water. The model is limited to five-spot patterns.

In the CO2PM, CO_2 and water are simultaneously injected in a proportion determined by the WAG ratio. This is not a true WAG process but the overall recoveries should not be influenced by this factor. The reservoir fluid properties and formation volume factors are kept constant during the oil recovery calculations, but this assumption should not affect the results in the majority of cases. The fractional flow calculations are performed under the assumption of no free gas saturation in the reservoir. Finally, the model may not accurately predict the bypassing of heavy oils by more mobile CO_2. However, in such cases the displacement will most likely be immiscible.

The model requires minimum data and defaults are available for most of the input data. Defaulting is useful for quickly screening a large number of reservoirs. However, caution should always be exercised with default values, particularly for economic data. When examining a particular reservoir for CO_2 flooding potential, specific data for the reservoir in question should be used; otherwise, misleading results may be obtained. Extensive data defaulting defeats the purpose of screening models such as the CO2PM.

Implied by the above assumptions is that the reservoir performance calculations are limited to single patterns. To estimate multi-pattern project behavior, a pattern development schedule may be specified. Single pattern results are superposed with the schedule for more realistic project behavior. This pattern superposition

is used in the economic calculations to time cash flow so that estimates of timing, costs, and revenues for an entire project may be made.

To estimate the economic potential of a project, after-tax cash flow is calculated from the estimated revenues and expenditures. These include drilling and well workover costs, CO_2 compression and recycle costs, depreciation, fixed and variable overhead, water treating and disposal costs, royalties, severance, state and federal taxes, windfall profits taxes, cost and price escalations, and debt financing. A lumped parameter uncertainty model is incorporated into the economic calculations to estimate risk, allowing for the variation of overall project performance within an 80 percent confidence interval.

C. Previous CO_2 Models

Prior to undertaking the development of the CO2PM, several existing oil recovery algorithms for CO_2 flooding were investigated. These include the Lewin method[7] and a modified Koval method.

The Lewin method was developed by an empirical fit of recovery curves from field projects. The method is restricted to projects with a 0.7 HCPV CO_2 slug injection followed by water. This method was coded and the produced oil volumes reported in Lewin's example calculations for the Crossett, North Cowden and Keystone projects were duplicated. The produced CO_2 volumes reported were determined to be in error and this was verified by Lewin.

The modified Koval method was based on the original work of Koval[5] as modified by Claridge[6] for areal sweep, and further modified for trapped oil saturation and Hawthorne's[8] gravity stabilization effect. All of these modifications apply only to those cases where water is immobile, which corresponds to a secondary flood. The modified Koval method was validated against laboratory data and numerical simulation.

All of the methods investigated were found lacking in two critical areas for practical application of a CO_2 predictive model: 1) how to handle WAG floods, and 2) how to compute the delay time prior to oil breakthrough in tertiary floods. In the Lewin model, the delay time was set at 0.2 HCPV, which may be reasonable for some field projects,

but not for others. Delay time is indicative of oil bank formation due to fractional flow of the miscible CO_2 - oil mixture and water. Thus, a "grassroots" oil bank fractional flow formulation was undertaken for the CO2PM.

The integration of the theoretical elements of fractional flow, gravity, and areal sweep are discussed in Sections II-IV of this report. Although not required for running the model, these sections will enable the reader to obtain an understanding of what is in the model and why. Section V discusses the comparison of the CO2PM with field results and with numerical simulation. An explanation of the subroutines and a flow diagram of the CO2PM is given in Appendix D. Economics are presented in Section VI. Because there are so many options in the economic calculations, this section should be carefully read before executing the model. One option of note in the economics is that the user may bypass the oil recovery calculations altogether and enter an oil rate versus time curve directly into the economics program.

II. FRACTIONAL FLOW MODEL

The basis for the CO_2 predictive model is a one-dimensional solution to the fractional flow equation by the method of characteristics (MOC). A brief exposition on the MOC is given in Appendix A. Here we use those results as a starting point to solve for oil recovery as a function of dimensionless time.

A. Scaled Equations

Consider the displacement of oil (i=2) by a first-contact miscible solvent (i=3) in the presence of a third immiscible component, water (i=1). If these three components are distributed between an aqueous (j=1) and oleic (j=2) phase, the mass conservation in one dimension is

$$\frac{\partial C_i}{\partial t_D} + \frac{\partial F_i}{\partial x_D} = 0, \quad i = 1, 2, 3, \tag{1}$$

where

x_D = Dimensionless distance = x/L

t_D = Dimensionless time in pore volumes = $\int_0^t q dt / V_p$

and

C_i = Overall concentration of species i (volume i/total volume)

$$C_i = C_{i1} S_1 + C_{i2} S_2, \quad i = 1, 2, 3 \tag{2a}$$

F_i = Overall fractional flux of species i (volume i flowing/ total volume flowing)

$$F_i = C_{i1} f_1 + C_{i2} f_2, \quad i = 1, 2, 3. \tag{2b}$$

In Equations (2) $f_j(S_j)$ and S_j are the fractional flow and saturation of phase j; C_{ij} is the phase concentration of species i in phase j (volume i in j/volume j). The C_i and C_{ij} are, therefore, volume fractions. Equation (1) is based upon ideal mixing, incompressible

fluids and rock, and no dispersion.[9] In what follows we will also neglect capillary pressure and gravity, although the latter may be included in the f_j without added complexity. Note the t_D is based on total pore volume, not hydrocarbon pore volume. Since the C_i's and F_i's sum to unity, there are only two independent Equations (1) which we arbitrarily select to be the equations for oil and solvent.

The equilibria relations for the phase concentrations C_{ij} are equilibrium vaporization ratios

$$K_i = C_{i2}/C_{i1} \ . \tag{3}$$

Note that these are not the traditional equilibrium K-values, used in hydrocarbon vapor-liquid equilibria calculations, which are defined as ratios of mole fractions. The traditional K-values may be corrected to volume ratios, since temperature and pressure are fixed, so that the form (3), while untraditional, will allow the same flash calculation procedures. Therefore, with the K_i specified, and the C_i known, the saturation or volume fraction of phase 2 follows from the solution to

$$\sum_{i=1}^{3} C_{i2} - \sum_{i=1}^{3} C_{i1} = \sum_{i=1}^{3} \frac{C_i(1-K_i)}{1 + S_2(K_i-1)} = 0 \ . \tag{4}$$

With S_2 determined from (4) by a trial and error solution, the phase concentrations follow from

$$C_{i2} = \frac{C_i}{1 + S_2(K_i-1)} \ , \quad i = 1, 2, 3 \tag{5}$$

and Equation (3). There being three concentration variables (two independent), the overall and phase concentrations may be easily represented on a triangular diagram. The phase boundaries (C_i - curves where one phase is present in an infinitestimal amount) follow directly from Equation (4). The binodal curve separating a two phase environment with a single aqueous phase is

$$\sum_{i=1}^{3} C_i K_i = 1 \tag{6a}$$

and that defining the binodal curve between a two phase and single oleic phase is

$$\sum_{i=1}^{3} C_i/K'_i = 1 \ . \tag{6b}$$

Equations (6a) and (6b) follow from (4) by setting $S_2 = 0$ and 1, respectively. Figure 1 shows the phase boundaries calculated by Equations (6). Once these are determined, the two-phase region may be covered with equilibrium tie lines which connect phase concentrations in equilibrium.

The fractional flow terms in Equation (2b) are

$$f_1 = 1 + \left[\frac{k_{r2}\ \mu_1}{k_{r1}\ \mu_2}\right]^{-1} \tag{7}$$

and $f_2 = 1-f_1$. In Equation (7) the relative permeabilities k_{r1} and k_{r2} are functions of the phase saturations, and the phase concentrations C_{ij}. The viscosities μ_1 and μ_2 are functions of the C_{ij}. These functionalities must be prespecified.

The foregoing remarks and Equations (2) - (7) imply that we may regard F_2 and F_3 as functions of C_2 and C_3; therefore, Equation (1) becomes

$$\frac{\partial C_2}{\partial t_D} + F_{22}\ \frac{\partial C_2}{\partial x_D} + F_{23}\ \frac{\partial C_3}{\partial x_D} = 0 \tag{8a}$$

$$\frac{\partial C_3}{\partial t_D} + F_{32}\ \frac{\partial C_2}{\partial x_D} + F_{33}\ \frac{\partial C_3}{\partial x_D} = 0 \tag{8b}$$

where $F_{23} = (\partial F_2/\partial C_3)_{C_2}$, etc. Equations (8) are of the reducible form given in Appendix A with (C_2,C_3) corresponding to (u,v). The partial derivatives F_{22}, F_{23}, F_{32}, and F_{33} are known functions of C_2 and C_3, though they cannot be expressed in closed form. Instead, they may be approximated to high accuracy as, for example,

$$F_{32} = \frac{F_3(C_2 + \epsilon\ ,\ C_3) - F_3(C_2,\ C_3)}{\epsilon} \tag{9}$$

where ϵ is small compared to C_2.

To use the coherence theory, express Equation (1) as

$$\frac{\partial C_i}{\partial t_D} + \left(\frac{\partial F_i}{\partial C_i}\right)_{x_D} \frac{\partial C_i}{\partial x_D} = 0, \quad i = 2, 3. \tag{10}$$

Equation (10) is rigorously correct, although of little use since the two derivatives $(\partial F_i / \partial C_i)_{x_D}$ are not known functions of (C_2, C_3) unless $C_2(x_D, t_D)$ and $C_3(x_D, t_D)$ are known--which is the solution. (To follow these procedures it is highly important to distinguish between F_{22} and $(\partial F_2 / \partial C_2)_{x_D}$). Equation (10) does, however allow the definition of a concentration velocity (the velocity of a fixed concentration) as

$$v_{C_i} = \left(\frac{\partial F_i}{\partial C_i}\right)_{x_D}, \quad i = 1, 2, 3. \tag{11}$$

Because of the dimensionless coordinates, x_D and t_D, all velocities from this point on are normalized by the bulk fluid velocity (specific velocities). In a coherent wave region, as discussed in Appendix A, the concentration velocities of all components are equal.

$$v_{C_2} = v_{C_3} = \frac{dF_2}{dC_2} = \frac{dF_3}{dC_3} = \sigma . \tag{12}$$

The total derivatives in Equation (12) follow because of the relation $C_2 = C_2(C_3)$ in coherent waves. To find this relation express Equation (12) as an eigenvalue problem by expanding the total differentials dF_2 and dF_3:

$$\begin{pmatrix} F_{22} & F_{23} \\ F_{32} & F_{33} \end{pmatrix} \begin{pmatrix} dC_2 \\ dC_3 \end{pmatrix} = \begin{pmatrix} dC_2 \\ dC_3 \end{pmatrix} \sigma \tag{13}$$

Then the characteristic equation has two eigenvalue roots given by

$$\sigma^{\pm} = 1/2 \left(-(F_{22} + F_{33}) \pm ((F_{22} - F_{33})^2 + 4 F_{32} F_{23})^{1/2}\right) . \tag{14}$$

Note that, as required above, σ^+ (the "fast" path) is always greater than σ^- (the "slow" path). The components of the eigenvector can be expressed in two equivalent forms

$$\left(\frac{dC_2}{dC_3}\right)_{\sigma^\pm} = \frac{F_{23}}{F_{22} - \sigma^\pm} \tag{15a}$$

$$\left(\frac{dC_3}{dC_2}\right)_{\sigma^\pm} = \frac{F_{32}}{F_{33} - \sigma^\pm} \tag{15b}$$

Either of Equations (15) may be used to determine $C_2 = C_2(C_3)$, although in practice, one form may be more convenient than the other. In composition space the integration of Equations (15) gives two families of curves corresponding to the fast and slow paths. The sequence of paths that satisfy the initial and boundary conditions for a particular problem is the composition route. The fast path portion of the composition route must pass through the initial conditions, the slow path position through the injected conditions. In between these extremes there are an infinite number of mathematical solutions corresponding to arbitrary switching from fast to slow paths. There exists, however, only one possible physical solution as the concentration velocities must decrease monotonically (but not continuously) from initial to injected conditions. The unique composition route, therefore, is that with only one switching point corresponding to the fast path through the initial conditions, and the slow path through the injected conditions. The velocity of any point on the composition route is given by Equation (14). Points of intersection on the composition route between the fast and slow paths have two concentration velocities. These points correspond to the constant state regions in x_D-t_D space. The fast path corresponds to the fast wave, and the slow to the slow wave.

We note the correspondence between the MOC and coherence theories by comparing Equations (A-10) and (14), and Equations (A-13) and (15). Finally, we note that the mapping from x_D - t_D space (characteristic space C) to composition space (image space Γ) is not one-to-one (points map to regions, etc.) because of the vanishing Jacobian.

More often than not it happens that the concentration velocity, calculated in Equation (14), does not monotonically decrease in the upstream (toward the injected conditions) direction along the fast and/or slow path segments. When this happens, a physical solution is realized by introducing shocks. A shock is simply a discontinuity in any physical variable -- here the concentration and fractional flows.

Shocks are idealizations of physical phenomena in that if dissipative effects, such as capillary pressure and dispersion, were to be included in Equation (1), they would not occur. In the limit of large macroscopic length scales, dissipative effects are small, and shock calculations portray actual front behavior reasonably well.

When shocks form, the entire preceding mathematical development is valid except that all differential changes are replaced by finite differences expressing the change in a quantity between the upstream and downstream of the shock. In particular, Equation (12) becomes the integral coherence condition

$$v_{\Delta C_2} = v_{\Delta C_3} = \frac{\Delta F_2}{\Delta C_2} = \frac{\Delta F_3}{\Delta C_3} . \tag{16}$$

In principle, Equation (16) defines an entirely new set of paths beginning at the initial and injected conditions. In practice, the paths calculated by Equations (15) are not much different from those of Equation (16), though the velocity must be corrected in the shock regions. A given fast or slow path segment, moreover, may contain one or more portions which are sharpening and are spreading. If we accept that the path calculated by the differential condition is close to that calculated by the integral condition, the estimate of the shock regions follows an exact analogue to the Buckley-Leverett construction. These comments are illustrated by Figure 2, which shows a hypothetical example of the composition paths, routes, shock calculation, x_D - t_D diagram, and effluent history. Figure 2a gives the composition path diagram with fast path through initial composition (I), slow path through injected composition (J), and intersection point (A). Along the I-A-J composition route a curve of F_3 versus C_3 may be plotted as in Figure 2b. A curve of F_2 versus C_2 would be equivalent, from Equation (12), except for identical scale factors on both axes. Clearly on neither path does the concentration velocity monotonically decrease (note that at A the concentration velocity discontinuously falls, however). The points A' and A" simultaneously satisfy the differential and integral conditions, Equations (12) and (16); hence,

$$v_{\Delta C_3} = \frac{\Delta F_3}{\Delta C_3} = \frac{F_3(C_{3A}') - F_3(C_{3I})}{C_{3A}' - C_{3I}} = \left(\frac{dF_3}{dC_3}\right)_{C_{3A}'} = \sigma^+(C_{3A}') \quad (17a)$$

$$v_{\Delta C_3} = \frac{\Delta F_3}{\Delta C_3} = \frac{F_3(C_{3A}) - F_3(C_{3A}'')}{C_{3A} - C_{3A}''} = \left(\frac{dF_3}{dC_3}\right)_{C_{3A}''} = \sigma^-(C_{3A}''). \quad (17b)$$

The graphical solution to Equations (17) is shown in Figure 2b. The analogy to the Buckley-Leverett construction is obvious. Note that in Equations (17) we have written F_3 and $\sigma \pm$ as functions of C_3 only because of the relation $C_3 = C_3(C_2)$ in Figure 2a. In order to avoid nonphysical velocities, the concentration velocities v_{C_3} are replaced by $v_{\Delta C_3}$ for $C_{3I} < C_3 < C_{3A}'$ and $C_{3A} < C_3 < C_{3A}''$. Outside these segments the velocities calculated by Equation (14) apply. Note that there is the possibility that the shock velocity from A to A" is greater than $\sigma^+(C_{3A}')$. If this happens it indicates that there is substantial disagreement between the differential and integral composition paths. The x_D - t_D space corresponding to the composition space of Figure 2a is in Figure 2c. In MOC terminology Figure 2a is the image space Γ of the characteristic space C in Figure 2c for a centered simple wave. Note the similarities with Figure 2b of Appendix A. The most useful result from Figures 2a and 2c is the effluent history plot, Figure 2d. This is a plot of F_3 or C_3 (or F_2-C_2) along a line $x_D = 1$ in x_D - t_D space. The time axis should, therefore, reflect the arrival and passage of the various shocks and spreading waves at the outflow end. In the results given below we show only composition path diagrams and effluent histories based on the overall fractional flow F_i.

B. Results Without Viscous Fingering

The results shown in this section are based on the displacement of both oil and water by simultaneous injection of solvent and water. The oil and water have essentially no mutual solubility ($K_1 = 0.01$, $K_2 = 100$), and the solvent a limited solubility ($K_3 = 20$) in the aqueous phase. Solvent and oil are miscible in all proportions. The relative permeability data are analytic functions fitted to published data[10] for the SACROC CO_2 flood, and are shown in Figure 5. We assume the aqueous and oleic phase relative permeabilities to be unaffected by

the solvent. This assumption eliminates interfacial tension[11] and mobile water[12] effects, though these could be easily included if we knew their effect on relative permeability. The pure-component water, oil, and solvent viscosities are 0.5, 0.38, and 0.037 cp, respectively. The solubility of solvent in the aqueous phase, the phase viscosities, and whether or not the displacement is first-contact miscible depend on the reservoir temperature and pressure. The equilibrium constant K_3, in particular, may be related to published solubility data[13] for CO_2 solvents as

$$K_3 = 1 + (2.38 \times 10^3)/R_{sw} \tag{18}$$

where $R_{sw}(T, P)$ is the CO_2 solubility in water in SCF/STB. Without the aqueous phase, the analogous problem for immiscible and developed miscibility floods has been worked by Dumore et al.[14]

Figure 4 shows the composition path diagram for these conditions. Because of the limited solubilities, the single phase regions are quite small near the water apex, and along the solvent-oil binary axis. The K-values appreciably affect the displacement by determining the tie lines, which are also shown on Figure 4. Lines of constant residual phase saturations delineate the zones where two phases flow. The topology of the fast and slow paths is similar to that described by Helfferich,[15] though less complex. Fast paths begin (lower left) at the residual oleic phase line, follow the tie lines for some distance, then deviate upward to the solvent-water binary axis. Slow paths begin (upper right) at the residual aqueous phase boundary, follow tie lines, and then also deviate to the solvent-water axis. Note the deviation from the tie lines occurs at the same point for both paths; thus, the tie lines everywhere coincide with composition paths. The concentration velocities change continuously along each tie line path; on each non-tie line path the velocities are constant, and are shown on the figure. The points on the tie lines where both paths deviate correspond to singular compositions where $\sigma^+ \rightarrow \sigma^-$. The locus of these points is a curve which could have been constructed by setting the discriminant of Equation (14) to zero. This singular curve is not a composition path because the locus of points with zero discriminant does not, in general, coincide with the solution to Equation (15).

We consider in Figure 4 four special cases or specific composition routes: i) pure solvent (J_1) displacing secondary oil (I_1), ii) pure solvent (J_1) displacing tertiary oil (I_2), iii) water-alternating-gas (solvent), WAG (J_2), displacing secondary oil (I_1), and iv) WAG (J_2) displacing tertiary oil (I_2). The solution to any other set of initial and injected conditions would readily follow from Figure 4. The injected conditions are represented on the composition path diagram though, in all probability, the injected flux is what would usually be specified. Thus, if W_R is the WAG ratio in reservoir volumes, we have

$$W_R = \left(\frac{F_1}{F_3}\right)_{x_D=0} = \left(\frac{C_{11}f_1 + C_{12}f_2}{C_{31}f_1 + C_{32}f_2}\right)_{x_D=0} \simeq \left(\frac{1 - f_2}{f_2}\right)_{x_D=0} \qquad (19a)$$

from which we have

$$(f_2)_{x_D=0} = \frac{1}{1 + W_R} \quad . \qquad (19b)$$

The f_2 in Equation (19b) is the oleic phase fractional flow for solvent-water. The saturation, and hence, the overall concentration associated with a specified W_R may be calculated from the solvent-water fractional flow curves, and Equation (4). We have assumed that alternating water and solvent is equivalent to simultaneous injection. For the pure solvent injection cases (W_R = 0) there is a very slow indifferent wave[16] from composition J_1 to J_1' which we will ignore by taking the injected composition for these cases to be J_1'. The effluent histories for these cases are shown in Figure 5.

The composition route for the $J_1' \longrightarrow I_1$ case does not switch since the initial and injected points are on the same fast path. The path has a constant concentration velocity resulting in the expected piston-like displacement shown in the upper panel of Figure 5. The solvent front is not retarded by the solubility in the aqueous phase because of concomitant swelling of this phase due to the ideal mixing assumption. The $J_1 \longrightarrow I_2$ case follows the slow path to J_1' where it switches to a fast path that is tangent to the oil-water axis at the singular curve. This path gives a spreading wave up to a point near

J_2' on the oil-water axis and proceeds directly to I_1. The switch from a fast back to a slow path at the singular curve is permissible since the composition velocities are equal there. For this route both waves are shocks (Figure 5). The $J_2 \longrightarrow I_2$ case switches again at J_2' then proceeds to I_2, both again being shocks. Comparing all the effluent histories in Figure 5 reveals that, for these cases that ignore viscous fingering, there is no obvious advantage to using the WAG process except, perhaps, for a greater solvent efficiency.

All four cases in Figure 5 may be obtained by simpler methods because in none of the cases is there simultaneous three component flow. In fact, for any case where the injected overall composition is leaner in C_3 than J_2'', or richer than S_1, the problem can be solved by considering two component flow only. Figures 6 - 8 give the graphical construction for three of the Figure 5 cases (see reference 17 for details). Where the injected composition is between J_2'' and S_1, a remarkably narrow class, the slow path intersects the J_1''-S_2 fast path at a three flowing phase composition point. Reference 18 gives an analogous result for polymer floods.

There are two additional insights from the simplified constructions, however. One is that we can estimate the velocity of the residual water fronts, constructed in Figures 6 - 8, and shown in Figure 5. The second is that we can estimate is the velocity of a chase water front behind the solvent, illustrated in Figures 6 - 8. The latter condition could be used to calculate an optimal solvent volume.

C. Results with Viscous Fingering

None of the foregoing includes what is generally conceded to be the most serious problem in miscible flooding, viscous fingering. Unfortunately, no satisfactory way exists for including this phenomenon into the equations. In what follows we use a modification of the theory originally presented by Koval,[5] bearing in mind the limitations of this theory. Koval accounted for viscous fingering by using immiscible concepts--fractional flow--to model miscible displacements. This can be justified because of near-segregated flow in a fingering displacement. To modify our equations in this way we alter the definition of F_i, Equation (2b), to

$$F_i = C_{i1} f_1 + f_{i2} f_2 \ , \ i = 1, 2, 3 \tag{20}$$

where f_{i2} is a "fractional flow" of component i in the oleic phase. Based on segregated flow in the oleic phase this would be

$$f_{i2} = \frac{C_{i2}/\ \mu_i^{\,o}}{C_{12}/\ \mu_1^{\,o} + C_{22}/\ \mu_2^{\,o} + C_{32}/\ \mu_3^{\,o}} \ , \ i = 1, 2, 3 \tag{21}$$

where the $\mu_i^{\,o}$ are pure component viscosities. By analogy to Koval we modify (21) as

$$f_{32} = \frac{C_{32}}{C_{12}\left(\dfrac{\mu_3^{\,o}}{\mu_1^{\,o}}\right) + \dfrac{C_{22}}{K_{val}} + C_{32}} \tag{22a}$$

$$f_{22} = \frac{C_{22}/K_{val}}{C_{12}\left(\dfrac{\mu_3^{\,o}}{\mu_1^{\,o}}\right) + \dfrac{C_{22}}{K_{val}} + C_{32}} \tag{22b}$$

$$f_{12} = 1 - f_{22} - f_{32} \tag{22c}$$

where K_{val} is the Koval factor

$$K_{val} = H\ [0.78 + 0.22(\mu_2^{\,o}/\ \mu_3^{\,o})^{1/4}]^4 \tag{23a}$$

and H is the heterogeneity factor. In an earlier report[2], H was referred to as M_{eff}, and was expressed as a function of the Dykstra-Parsons coefficient (VDP)

$$\log_{10} H = VDP/(1-VDP)^{.2} \tag{23b}$$

Using equations (20) - (23) with K_{val} = 8.1 (note that this is fixed for a given case), the composition path diagram is shown in Figure 9 and the effluent history in Figure 10. Compared to the no-fingering

case, Figures 4 and 5, there are substantial changes. First, there is much less tracking of the tie lines by the composition paths. Second, there is no singular curve. Third, as expected, there is less tendency for shocks to form, Figure 10. Fourth, the time scale is elongated; it requires two or more times the throughput for equivalent recovery for the fingering cases (compare Figures 5 and 10). Finally, for any of the cases with a mobile water saturation, there is a simultaneous breakthrough of oil and solvent, with the bulk fo the oil production occurring after breakthrough. Since this latter observation is characteristic of solvent floods in which no precautions have been taken to prevent fingering, the fingering case seems more realistic.

The qualitative features of the composition path are like those discussed above. The most interesting deviation is the existence of a second path route from J_2 to I_1. This route contains a shock portion from J_2 to J_2', a spreading portion, and then a second shock to I_1. By comparing cases with common initial conditions, we may judge the effectiveness of the WAG process. In all cases, the WAG attains complete oil sweep-out earlier than the pure solvent cases. The WAG also delays solvent breakthrough in all cases, though for tertiary cases, it also delays oil breakthrough. Since the analysis presented here is limited to one-dimensional cases with no mobile water trapping, it is not surprising that we cannot make a general statement about the effectiveness of the WAG. Finally, we note that there are large regions of three component flow; hence, there are no simplified methods for the fingering cases.

D. Comparison of Fractional Flow Model Model with Numerical Simulator

In order to validate the fractional flow calculations, the CO2PM was compared in 1-D with Scientific Software-Intercomp's equation of state compositional reservoir simulator (COMP II).

The reservoir and fluid properties used in the runs are listed in Table 1. This system was initialized at various conditions and simulated with various WAG ratios and Koval factors. The same runs were repeated with the predictive model and the results compared.

Four cases are described in detail here:

1. Initial oil saturation = 0.70 (secondary recovery condition), WAG = 0, Koval = 10.
2. Initial oil saturation = 0.26 (tertiary recovery condition), WAG = 0, Koval = 10.
3. Initial oil saturation = 0.26 (tertiary recovery condition), WAG = 2, Koval = 10.
4. Initial oil saturation = 0.26 (tertiary recovery condition), WAG = 0, Koval = 5.

Case 1:

In this case, the reservoir was initialized at connate water saturation (mobile oil present). The oil rate, CO_2 rate, and oil recovery are shown in Figure 11. The solid lines are the results from the simulator and the symbols represent the results from the CO_2 predictive model. This convention is used for all subsequent results. As the system is initialized at connate water saturation, oil is produced immediately at a very high rate. The oil rate remains constant until breakthrough and then decreases continuously. CO_2 production starts at breakthrough and increases continuously. The results obtained from the predictive model are nearly identical to the COMP II results. This verifies the mathematical basis for the fractional flow approach.

Case 2:

In this and subsequent cases, the system was initialized at residual oil saturation. Since initially no mobile oil is present, the oil rate should be zero until breakthrough. However, in the predictive model a very small amount of oil is produced at a constant rate until breakthrough (Figure 12). This is due to the boundary condition constraints in the fractional flow model which do not allow initialization exactly at residual oil saturation. However, this should not influence the overall recovery. The breakthrough time in COMP II is somewhat earlier than that given by the predictive model, and the peak oil rate in COMP II is lower than that in the predictive model. Total recoveries compare favorably.

Case 3:

In the simulator, CO_2 and water were injected in an alternating WAG process. In the predictive model, CO_2 and water must be injected simultaneously. Because simultaneous injection only approximates a WAG process, we should expect higher recoveries from the fractional flow model. As in Case 2, breakthrough occurs earlier and the peak oil rate is smaller in COMP II than in the predictive model (Figure 13). The overall recovery is indeed less in COMP II.

Case 4:

In this case the conditions were similar to Case 2 except that a lower Koval factor was used. The results follow the trends of the previous cases (Figure 14).

The fractional flow model in the CO2PM matches the simulation results in 1-D reasonably well. Either increasing the number of grid blocks or injecting CO_2 and water simultaneously in the numerical simulation runs would improve the comparison with the fractional flow model.

E. Comparison with Laboratory Experiment

The previous section showed the comparison of the results of the one-dimensional fractional flow model to the results of numerical simulation. Here we compare the fractional flow solution to experimental results from run C-1-6, a tertiary non-WAG displacement of Brookhaven crude oil in a Berea core at 1800 psig and 109° F, presented by Whitehead et al.[19] The experimental results as presented by these authors are shown in Figure 15. These results were converted to reservoir volumes and fractional fluxes as shown in Figure 16. This correction involved tabulating the oil, gas, and water produced at each data increment and correcting the gas to reservoir volumes by multiplying by the gas formation volume factor of $B_g = 2.75 \times 10^{-3}$ ft^3/SCF. In doing this we are assuming all of the produced gas less that originally associated with the oil (R_s = 276 SCF/STB) is CO_2. The Figure 16 results show clean water production initially followed by simultaneous breakthrough of the oil and CO_2. Obviously the CO_2 is

fingering through the oil and we should use a $K_{val} > 1$ to match the results.

Data used in the fractional flow model came from several sources. We used the following oil-water relative permeabilities from Delshad[20]

$$k_{ro} = 0.717 \left(\frac{0.637 - S_w}{0.247} \right)^{1.41} \tag{24}$$

$$k_{rw} = 0.058 \left(\frac{S_w - 0.61}{0.247} \right)^{1.48}$$

In addition, we took the oil viscosity estimated to be 6.76 cp at these conditions,[21] the water viscosity to be 1 cp, and the CO_2 viscosity to be .06 cp.[22] Finally, we selected the heterogeneity factor H = 7 from the original Koval paper for a Berea core. Note that there are now no free parameters left in the fractional flow formation. The match we will show, therefore, is not a history match, but represents what one might estimate a priori with the CO2PM, and from literature data sources.

Figure 17 shows the comparison between the experimental results of experiment C-1-6 (Figure 16) and the results of the CO2PM. The top plot shows oil fractional flux (cut), and the bottom plot shows both water and solvent fractional flux. Note that the CO2PM accurately predicts the breakthrough time of oil and solvent, accurately predicts the peak oil fractional flow, but deviates somewhat from the experimental data at times after breakthrough. This deviation could almost certainly be removed by history matching. In fact, note that the water cut is the most accurate of the three fluxes at long times. This suggests that the water-oil relative permeability used for the comparison is reasonably accurate, and that the match could be improved simply by raising the Koval heterogeneity factor. Given the empirical nature of the heterogeneity factor, uncertainties in converting the cumulative data in Figure 15 to fluxes, and other data uncertainities, the comparison in Figure 17 is remarkably good, particularly considering that the displacement was not first-contact miscible.[19]

We do not show other comparisons to experimental data, though several exist in the literature, because the qualitative aspects of such

displacements and the results of the fractional flow model are in substantial agreement for tertiary floods: the CO_2 and oil break through together, peak oil rate follows closely after oil breakthrough, and oil production tails out over a substantial number of injected pore volumes. A comparison of the results of the entire CO2PM to a field case will be considered in Section V. The results of the comparison to experiment C-1-6 will be used as an illustration in the following sections.

F. Calculating Average Concentrations Behind the Fronts

In order to include areal sweep in the CO2PM we must estimate the average concentration of the three components behind the tip of the displacement front. We assume that the displacement qualitatively follows the form of experiment C-1-6 and that the fractional flux-concentration curve is like the one shown in Figure 18a. Experience to date with sensitivity studies run on the CO2PM failed to reveal a single case that deviates from this behavior. The development here parallels that first derived by Welge for oil-water fractional flow.[23]

Consider a concentration profile of a solvent-water mixture displacing an oil-water mixture (Figure 18b). The average concentration of component i for any region behind the leading edge of the front is

$$\overline{C_i} = \int_0^{x_{D1}} C_i dx_D , \qquad i = 1, 2, 3 \tag{25}$$

where x_{D1} is a position behind the leading edge. After breakthrough we will take x_{D1} to be at the outflow end of the one-dimensional system. Since x_{D1} is in either the constant or the spreading portion of the profile, we can integrate Equation (25) by parts and replace the integrand by

$$x_D = \left(\frac{dF_i}{dC_i}\right) t_D = F_i' t_D . \tag{26}$$

This yields

$$\overline{C_i} = (x_D C_i)_{x_D = x_{D1}} - \int_0^{x_{D1}} t_D \frac{dF_i}{dC_i} dC_i , \quad i = 1, 2, 3 . \tag{27}$$

Since t_D is an independent variable it passes through the integration sign and the integration may be performed analytically to give

$$\overline{C_i} = (x_D\, C_i)_{x_D=x_{D1}} - t_D \left[(F_i)_{x_D=x_{D1}} - (F_1)_{x_D=0} \right] , \; 1 = 1,2,3 \; . \quad (28)$$

At the effluent end and after breakthrough, $x_{D1} = 1$ giving

$$\overline{C_i} = (C_i)_{x_D=1} - t_D \left[(F_i)_{x_D=1} - F_{iJ} \right] , \; i = 1, 2, 3 \; . \quad (29)$$

Every term on the right side of Equation 29 is known: the inflow end flux F_{iJ} is specified, the outflow flux $(F_i)_{x_D=1}$ as a function of t_D comes from the composition routes, and the concentration $(C_i)_{x_D=1}$ corresponding to $(F_i)_{x_D=1}$ is from the fractional flux-concentration relation, Figure 18a. The average concentration in the medium after breakthrough may be calculated from Equation 28. The results of this calculation applied to the data of experiment C-1-6 are shown on Figure 19. This figure also shows the average concentrations of the three components based on an overall material balance of the experimental data. Since experimental average concentrations may be converted to concentrations at the end of the medium from Equation 29, the fractional flow theory suggests a procedure whereby simultaneous three-phase fractional fluxes may be derived from experimental data in exactly the same manner as that used by Welge for oil-water fractional flow.

G. Correction for Finite Slug Size

The expense of miscible solvents is such that they cannot be injected indefinitely even if the oil recovery is extremely good. Thus, the solvent/water mixture is injected in a finite amount or slug of size t_{DS} as shown in Figure 20. The total amounts of solvent and water

injected are, therefore, $F_{3J}t_{DS}$ and $F_{1J}t_{DS}$, both expressed as a fraction of total pore volume. In the CO2PM we assume the chase fluid is water. In practice, a wide variety of chase fluids are used (including water), but we cannot model chase fluids that are miscible with the CO_2 and, perhaps, not miscible with the reservoir oil. This is because if the chase fluids were to penetrate regions where oil and CO_2 are flowing simultaneously (an extremely likely circumstance unless very large slugs are used) miscibility would be lost, and one of the primary assumptions underlying the fractional flow theory would be seriously violated. The correction for a finite slug followed by water is somewhat ad hoc, but our experieince with the compositional simulator indicates that the treatment is fairly accurate.

Let us assume that after some dimensionless time t_{DS} of solvent/water injection we switch to a water chase fluid. Since the chase water is more viscous than the solvent, and since it is miscible with the slug water we assume the chase water displaces the material ahead of it in a piston-like fashion. However, it is also reasonable to assume that the chase water displaces only the amount of oil in the system in the hydrocarbon phase in excess of the residual oil saturation, as $C_{22}(S_2-S_{2r})$. Similarly, chase water displaces the solvent in the system only up to the amount of solvent in the hydrocarbon phase over and above the residual oil saturation, or $C_{32}(S_2-S_{2r})$. We correct the average concentrations in the system of the previous section in the following manner:

1. On the continuous solvent curve (that calculated in the previous section) locate the average oil and solvent concentrations corresponding to t_{DS}.

2. Flash the average concentrations at this point to determine the average hydrocarbon phase saturation (S_2) and composition (C_{22}, C_{32}) in the system.

3. Calculate the incremental solvent and oil production associated with the chase fluid injection. These are $C_{32}(S_2-S_{2r})$ and $C_{22}(S_2-S_{2r})$.

4. Subtract the incremental oil production from the average oil concentration in the system at t_{DS}. In a similar manner, add the incremental solvent production to the average solvent concentration at t_{DS}.

5. Return to the continuous solvent curve and find the value of dimensionless time that corresponds to the ultimate oil production calculated in step 4.

6. For all dimensionless times greater than that calculated in step 5 set the average concentrations to the ultimate values, and the fractional flows of solvent and water equal to zero.

This procedure is illustrated in Figure 20. In addition to the above assumptions, we are further assuming that the oil production functions between the onset of chase fluid injection and ultimate recovery are the same as in the continuous solvent/water case. With the one-dimensional fractional flow theory corrected in this manner, the correction for areal sweep efficiency (Section IV) remains valid since this deals with average concentrations.

H. Modification for Layers

Koval's theory applies to secondary (no mobile water) miscible floods. In the CO2PM, the Koval factor only affects the fractional flow of oil and CO_2 in the oleic phase. As K_{val} becomes large, oil fractional flow approaches zero (Equations 22a and 22b). The displacement of water is independent of K_{val} and is only affected by the oil-water permeability. For secondary cases, the CO2PM gives solvent breakthroughs approximately equal to $1/K_{val}$ in accordance with Koval's theory and with experimental observation. However, breakthrough in a tertiary flood is only a function of the viscosity assigned to the oleic phase. As K_{val} becomes large, CO_2 displaces water, and that breakthrough is the earliest that can be expected when using the CO2PM.

Experience with the model showed that CO_2 and oil breakthroughs in tertiary floods are somewhat later than observed. This was compensated for by allowing up to five equal thickness layers to be specified in the CO2PM. All layers are assigned the same, user-specified VDP. Thus, K_{val} will be the same in each layer. A measure of heterogeneity among the gross layers, VDPL, must also be specified. VDPL may be obtained from the results of waterflood

performance. Generally, VDP will be somewhat less than VDPL. In the CO2PM, VDPL is used to calculate the permeabilities of the individual layers (Appendix C). The layer permeabilities, which are normalized to represent the average reservoir permeability specified to the model, are then used to scale rate and slug size for the various layers.

III. INCLUDING GRAVITY IN ONE-DIMENSIONAL THEORY

A. Scaling Parameter

Numerical simulation was used to develop a correlation of vertical sweep as a function of the extent to which gravity segregation occurs. The viscous-to-gravity forces were characterized by the ratio of the time required for a fluid particle to travel the distance between the wells (t_h) to the time required for fluid to move from the bottom of the reservoir to the top (t_v) due to gravity forces. As shown in Appendix B, for a five-spot pattern, this ratio is given by

$$\frac{t_h}{t_v} = 2.5271 \left(\frac{k_v}{k_h}\right)\left(\frac{A}{h}\right)\left(k_h h\right) \frac{\Delta\rho}{Q\,\mu} \qquad (30)$$

where

k_v = vertical permeability, md
k_h = horizontal permeability, md
A = five-spot pattern size, acres
h = reservoir thickness, feet
$\Delta\rho$ = water-CO_2 density difference, g/cc
Q = injection rate, RB/D
μ = CO_2 viscosity, cp

B. Simulation Results

All simulation runs were made with the COMP II model utilizing the miscible option. A 2-D variable cross-section model of 1/8 of a five-spot was used. The same fluid system was used in all runs, and the equation of state parameters input were based on the following fluid data at 230° F:

Pressure	Density (lb/ft^3)		Viscosity (cp)	
	CO_2	Oil	CO_2	Oil
2900 psi	27.374	39.786	.036	.287
5000 psi	41.987	41.166	.057	.358

In addition, the oil and solution gas had the following properties:

Stock tank oil gravity	40.89° API
Stock tank gas gravity	0.996
Solution gas-oil ratio	1059 SCF/STB

The Koval factor in all runs was set at 2.75 for both the horizontal and vertical directions. A wide range of reservoir characteristics were used to vary the dimensionless scaling parameter t_h/t_v. Table 2 summarizes the additional data for individual runs. Figure 21 shows the two sets of relative permeability curves used in the simulation runs. Figure 22 shows the effect of these relative permeability curves on oil recovery. The effect of pattern size on recovery is shown in Figure 23.

In developing the vertical sweep correlations, the effects of displacement efficiency due to variations in relative permeability curves and total volume of CO_2 injected were accounted for by normalizing peak oil rates to the peak rate for no gravity (t_h/t_v = 0). A plot with the scaling parameter as independent variable versus normalized rate is shown in Figure 24.

C. Effective Koval Factor

Next, the 1-D fractional flow model in CO2PM was used to determine the influence of Koval factor on oil recovery. A series of 1-D runs were made with the predictive model in which the Koval factor was changed. The peak oil rates were then normalized with respect to the base case (Koval factor = 2.75) and a plot of Koval factor versus normalized peak oil rate made (Figure 25).

From the COMP II runs, it was concluded that as t_h/t_v increases, peak oil rate decreases, oil recovery decreases, and oil breakthrough occurs earlier. Moreover, the fractional flow model showed that the same results can be obtained by increasing the Koval factor. Figures 24 and 25 were then used to develop a crossplot for a multiplying factor (F) as a function of t_h/t_v. This correlation is a straight line on semi-log paper and is shown in Figure 26. The equation of the line is:

$$F = 0.565 \log t_h/t_v + 0.870 \qquad (31)$$

with the condition that $F \geq 1$. The modified Koval factor is then F times the K_{val} of Equation (23).

In order to calculate the effect of gravity on oil recovery and rates, the following procedure is used in the CO_2 predictive model:

1. Read in the user-specified Koval factor or calculate it on the basis of fluid viscosities and reservoir heterogeneity (Equation 23).

2. Calculate dimensionless scaling parameter, t_h/t_v, from Equation 30.

3. Calculate the multiplying factor F, from Equation 31.

4. Calculate the modified Koval factor by multiplying the Koval factor calculated in step 1 by the factor F.

5. Use the new Koval factor in the oil recovery calculations.

IV. AREAL SWEEP CORRECTIONS

Considerable work was published in the early petroleum literature on correlating areal sweep efficiency with pattern type, mobility ratio, and throughput. In this section we include the effects of areal sweep in the calculations of the previous sections using a generalization of the technique originally presented by Claridge.[6]

A. Areal Sweep Correlation

Since we are including viscous fingering in the fractional flow theory explicitly, it is important not to include it in the areal sweep correlation. Claridge anticipated this event and addressed it by defining an "invaded area" sweep efficiency as shown in Figure 27. He determined that the areal sweep correlation of Caudle and Witte[24] most nearly approximated the invaded area sweep and derived equations to describe it for flow in a confined 5-spot. Figure 28 shows the comparison between the experimental and calculated sweep efficiencies using Claridge's Equations (1) through (6). He also gave a procedure for combining areal and displacement sweep for secondary, non-WAG displacements. The CO2PM uses a generalization of Claridge's procedure to first-contact floods of arbitrary WAG ratios, and arbitrary initial conditions. This generalization is described and illustrated in this section.

The invaded area is the area defined by a curve connecting the extreme tips of the viscous fingers, Figure 27, and given by the product of E_A, the invaded area sweep efficiency, and the pattern area. E_A as a function of dimensionless time and mobility ratio is given in Claridge's paper and not repeated here. In Figure 27 the contacted area is the area actually occupied by the solvent fingers.

Central to this procedure is the idea of average concentrations behind the front. The average concentrations in the contacted area are $(C_1, C_2, C_3)_j$, the injected concentrations. We define the average concentrations in the invaded zone to be $(\overline{C_1}, \overline{C_2}, \overline{C_3})$ where

$$\overline{C_i} = \frac{\text{Volume of component i in invaded zone}}{\text{Volume of invaded zone}} \qquad (32)$$

The $\overline{C_i}$ are functions of time through the fractional flow theory in Section II. If E_A and the $\overline{C_i}$ are both known as functions of time, the cumulative production of component i is

$$N_i = qtF_{ij} - V_p E_A (\overline{C_i} - \overline{C_{ij}}), \quad 1 = 1, 2, 3 \tag{33}$$

from an overall material balance. In Equation (33), q is the injection/production rate, V_p the total pore volume and t is time. All volumes in this equation are in reservoir volumes. For oil, in particular, we can write

$$N_{2D} = E_A \left(1 - \frac{\overline{C_2}}{C_{2I}}\right) \tag{34}$$

where N_{2D} is the cumulative oil produced expressed as a fraction of oil in place at the start of solvent injection. To express oil recovery as a fraction of original (at discovery) oil in place, Equation (34) should be multiplied by the ratio of C_{2I} and the original oil saturation $(1 - S_{wc})$.

The $\overline{C_i}$ terms in Equations (33) and (34) may be expressed as functions of dimensionless time through the Welge integration procedure applied to the flux-concentration curve of Figure 18.

$$\overline{C_i} = \begin{cases} \overline{C_i}^o & \text{for } t_D < t_D^o \\ (C_i)_{x_D = 1} - t_D \left[(F_i)_{x_D = 1} - F_{ij} \right] & \text{for } t_D > t_D^o \end{cases} \tag{35}$$

where $\overline{C_i}^o$ is the average concentration of component i behind the invaded zone front prior to breakthrough, and t_D^o is the dimensionless time at breakthrough, both quantities coming from the fractional flow theory. Note that the second expression of Equation (35) is the same as Equation (29).

Figure 29 shows the average solvent and oil concentrations versus a dimensionless time t_{D1}. We begin here to use t_{D1} as the time variable for the C_i, and t_{D2} for E_A since, in general, neither function depends explicitly on the actual dimensionless time, t_D, in Equation (34). We relate t_{D1}, t_{D2}, and t_D to each other below. From Figure 18 we see that the average concentrations all begin at $\overline{C_1}^o$, remain constant until breakthrough, and then gradually approach the concentrations corresponding to the injected fluxes at large t_{D1}. Breakthrough occurs at $t_{D1} = (1 + W_R)\overline{C_3}^o$. Also plotted on Figure 29 are curves showing the average concentration in the one-dimensional system versus t_{D1} (dotted lines). These curves begin at the initial value C_{iI} of each concentration, and decrease linearly to $\overline{C_i}^o$ at breakthrough; after breakthrough they coincide with the average concentration behind the leading edge of the front. System average concentrations are not used in the following development, and are shown on Figure 29 only for completeness.

B. Combining Areal Sweep with One-Dimensional Theory

Imagine a one-dimensional permeable medium with $\overline{C_2} = \overline{C_2}(t_{D1})$ and $\overline{C_3} = \overline{C_3}(t_{D1})$ known from fractional flow theory. The medium is homogeneous except for certain time-varying regions from which flow is excluded. If we focus only on the regions that are not excluded, the concentrations and fractional fluxes are those given by the one-dimensional theory. These variables depend on a dimensionless time that is normalized by a volume that does not include the regions from which flow is excluded,

$$t_{D1} = \frac{\text{Volume solvent + water injected}}{\text{Volume invaded}} \quad . \tag{36}$$

If we identify the flow-excluded regions with the uninvaded regions in Figure 27, the dimensionless time t_{D1} becomes

$$t_{D1} = t_D/E_A \quad . \tag{37}$$

On the other hand, consider a homogeneous 5-spot pattern with $E_A = E_A(t_{D2})$ known, into which is being injected solvent and water

simultaneously. If we regard the oil and water in the invaded region as being part of the rock matrix, the appropriate dimensionless time t_{D2} becomes

$$t_{D2} = \frac{\text{Volume solvent injected}}{\text{Volume solvent in pattern}} \tag{38}$$

which may be decomposed into

$$t_{D2} = \frac{\text{Volume solvent injected}}{\text{Volume solvent + water injected}} \times$$

$$\frac{\text{Volume solvent + water injected}}{\text{Volume of pattern}} \times \frac{\text{Volume of system}}{\text{Volume solvent in pattern}} . \tag{39}$$

After breakthrough, t_{D2} may be written in our terminology as

$$t_{D2} = t_D/(1 + W_R)\overline{C_3} \quad .$$

Equations (37) and (40) are the relations among the various dimensionless times. Claridge calls t_{D1} and t_{D2} the "apparent" pore volumes injected for the appropriate variable. t_D may be eliminated between Equations (37) and (40) to give

$$t_{D1} = \frac{t_{D2}}{E_A} \overline{C_3}(1 + W_R) \quad . \tag{41}$$

The definitions in Equations (37) and (40) may be verified by observing that when breakthrough happens in an areal sense, it also happens in the one-dimensional system. Thus, at breakthrough we have $t_{D2} = E_A$, and $\overline{C_3} = \overline{C_3}^o$ from which follows $t_{D1} = (1 + W_R)\overline{C_3}^o$ from Equation (41). Figure 29 shows that this is indeed the correct dimensionless time for the one-dimensional system.

The procedure to calculate the correct t_{D1}, t_{D2}, and t_D is iterative. We assume that we know $\overline{C_i} = \overline{C_i}(t_{D1})$ from fractional flow theory, and $E_A = E_A(t_{D2})$ from the Claridge correlations. The procedure for combining areal and displacement sweep efficiency is

1. Estimate the mobility ratio M to be used in the areal sweep correlation. Following Craig,[25] we take M to be the mobility ratio based on the average concentrations behind the front at breakthrough

$$M = (\lambda_{rt})_{\overline{C_i}^o} / (\lambda_{rt})_{C_{iI}} \tag{42}$$

The numerical value of M does not change during a run.

2. For this value of M find the breakthrough areal sweep efficiency $t_{D2}^o = E_A^o$. This is done by linear interpolation of the breakthrough sweep efficiency in Figure 28. The dimensionless breakthrough time for the combined areal and displacement sweep is $t_D^o = E_A^o(1 + W_R)\overline{C_3}^o$ from Equation 40. The calculations begin at t_D^o.

3. Fix $t_D > t_D^o$.
4. Pick $t_{D1} > \overline{C_3}^o(1 + W_R)$.
5. Calculate $\overline{C_3}(t_{D1})$ from fractional flow.
6. Calcualte t_{D2} from Equation (40).
7. Estimate $E_A(t_{D2})$ from areal sweep correlation.
8. Calculate t_{D1} from Equation (37).
9. Test for convergence. If the t_{D1} estimates in steps 4 and 8 differ by less than some small pre-set tolerance, the procedure has converged. If not we must re-estimate t_{D1} and return to step 4.
10. Calculate cumulative oil produced from Equation (34), and the combined fractional flow of each component from

$$F_i^T = \left(1 - \frac{dE_A}{dt_{D2}}\right) F_i(t_{D1}) + \frac{dE_A}{dt_{D2}} F_{iI} \quad . \tag{43}$$

11. Increment t_D and return to step 3 for a new time-step. The entire procedure continues until t_D is larger than some pre-set maximum. Our experience has been that the above iterative procedure converges in 2-4 iterations per time step by simple direct substitution. The combined fractional flow in Equation (43) represents contribution

from the invaded zone (first term), and the univaded zone (second term) with all expressions being evaluated at consistent values of t_{D1}, t_{D2}, and t_D.

The derivatives in Equation (43) must be numerically evaluated. Once $F_i^T(t_D)$ is known we calculate component rates in standard volumes as

$$q_i = qF_i^T/B_i, \qquad i = 1, 2, 3 \tag{44}$$

corresponding to a real time t

$$t = V_p t_D/q \quad . \tag{45}$$

Figure 30 shows the results of the correction for areal sweep applied to the CO2PM calculation on the experiment C-1-6, Figure 17. The y-axis plots cumulative oil produced as a fraction of initial oil in place at the start of solvent injection, and the x-axis plots each of the three dimensionless times. Note how the combined areal and displacement sweep run breaks through earlier than the other two, and, except for early time, is everywhere smaller. The combined fractional oil recovery at a particular dimensionless time is not simply the product of displacement and areal sweep at that time. The correct dimensionless time for consistently evaluating the latter two is given by Equations (37) and (40). Figure 30 shows that the combined oil recovery is roughly equally dependent on areal and displacement sweep effects.

V. COMPARISON OF CO2PM WITH FIELD DATA AND NUMERICAL SIMULATION

A. Selection of CO_2 Field Cases

The primary criteria used to select CO_2 field floods for comparison with the CO2PM was that the projects must have extensive and complete production data that are clearly the result of a CO_2 flood. Examination of the literature showed that only six projects satisfied this criteria: Crosset (for which the distinction between primary production and CO_2 response is tenuous), Kelly-Snyder (Phase I and pilot), Little Creek, Lick Creek, and the Slaughter Estate Unit (SEU) pilot.

Lick Creek was eliminated on the basis of not being first contact miscible. Of the remaining projects, enough data (reservoir characterization, production data, etc.) could be found from the literature for only the SEU pilot.

B. Comparison of CO2PM with Slaughter Pilot

The actual and predicted responses for the SEU pilot are compared for three CO2PM runs in Figures 31-33. Table 3 shows a listing of the CO2PM input based on literature data.[6,7] The oil-water relative permeabilities used in the CO2PM were

$$k_{rw} = 0.34\left(\frac{S_w - .08}{0.58}\right)^{1.78}$$
$$k_{ro} = \left(\frac{0.66 - S_w}{0.58}\right)^{2.55} \qquad (46)$$

Figure 34 shows the comparison of these equations to published data.[27] The initial oil fractional flow of 0.13 was set from the observed initial water-oil ratio of about 8. For the base case three-layer CO2PM run (Figure 31), VDPL = 0.48 was based on the geologic

zonation.[26] VDP was set to zero, which gives a K_{val} = 2.70 (H = 1) for each layer. The matching parameter used in the CO2PM was the reservoir injection rate. A value of 390 RB/D was selected for the comparison since this gave the best compromise between peak oil rate and the time of peak rate. The SEU pilot averaged 360 RB/D of solvent and water (the WAG ratio was one) allocated to the pilot during solvent injection, and 986 RB/D during chase gas injection. The history match value falls within this range.

Comparison of Figures 31 and 32 shows the merits of using a multi-layered approach in the CO2PM. With one layer (Figure 32), even an appropriate value of VDP = 0.48 (for this case H = 3.52, K_{val} = 9.5), Figure 35 and Reference 2, gives a poor representation of the field performance. In order to obtain a reasonable match of the observed behavior using one layer (Figure 33), VDP must be arbitrarily lowered to 0.25 (H = 1.84, K_{val} = 4.96). These results indicate that the Koval approach must be augmented by layering if reasonable results for tertiary and near tertiary floods are to be obtained with the CO2PM.

C. Comparison of CO2PM with Simulation for Denver Unit

The CO2PM is compared with Shell Oil Co.'s WASSIM simulator for he Denver Unit, Wasson Field (Figure 36). Shell also supplied the CO2PM input data shown in Table 4. Figure 36 shows the CO2PM run as a three layer case, compares reasonably well with the Shell results. As in the Slaughter example, the CO2PM could not match the simulator unless layering was used.

VI. CO2PM ECONOMIC MODEL

A. General Description

Analytical techniques have been available for about the past 20 years for evaluating the potential profitability of investments, usually in terms of return on investment. This evaluation is derived from the net cash flow expected during the forecasted economic life of a project. The future annual cash flow schedule, in turn, is based on forecasts of key revenue and cost parameters (oil/gas sales, oil/gas prices, capital requirements, development schedules, fixed and variable operating costs, and various tax/depreciation scenarios). Because funds that are earned sooner are more valuable, future earnings are discounted, by compound-interest methods, to a present value for use in calculating various quantitative measures of profitability.

The CO2PM economic model is used to convert predicted performance data from the reservoir algorithm into a cash flow analysis extending over the life of the project. This analysis combines forecasts of revenue, costs, expenses, and taxes into an annual balance sheet. The cash flow analysis provides a more realistic measure of CO_2 flood performance than net CO_2/cumulative oil ratios or other technical yardsticks.

The economic model will permit management to judge whether a proposed project development strategy meets the company standards for return on investment. Alternatively, the model can be used to develop an economic ranking of various pattern flood projects available to the company at a given time. This second type of usage can yield an economic "screening" of CO_2 projects, depending on the profitability criteria chosen.

The model also permits an evaluation of the uncertainty of future earnings as a result of changes in key forecast variables and thus an evaluation of project risk (upside potential and downside risk). The parameter method of evaluating uncertainty is used, due to its simplicity and reasonable accuracy.

The model requires four types of data in order to perform a meaningful economic screen:

1. Reservoir Production Function for a Pattern (oil, gas, water, CO_2 rates versus time). A feature has been incorporated in the model to allow externally generated performance data to be input directly into the economic model, thereby bypassing the reservoir algorithm calculations. Using this option, results from, for example, physical modeling or detailed reservoir simulation may be analyzed in a consistent manner.

2. Project Definition (pattern development schedule, CO_2 recycle, compression, and/or separation, pipeline length, number of wells drilled, water handling, etc.). Once the performance of a single pattern has been determined, a schedule of the number of patterns per year to be initiated is used to superpose the pattern rates into an overall project performance. This procedure implicity assumes that all patterns in the project perform identically (i.e., second year oil and water rates for every pattern are the same regardless of when the pattern comes on stream). Also superposed are the capital cost of drilling and equipping wells associated with developing each pattern.

3. Economic Parameters. These include prices, costs, tax rates, discount rate, escalation (inflation) rates, and capital schedule.

4. Range of Uncertainty for Key Parameters. The model treats uncertainty by predicting the probability of project present value. Low, most likely, and high values of cost and price parameters are required. This allows for an evaluation of the uncertainty of further earnings due to variations in critical values and thereby provides a measure of project risk. Details of the uncertainty method are discussed in Section VI-F.

The model computes several types of after tax profitability criteria which can be used separately or in some combined weighted fashion for project screening:

1. Discounted Cash Flow (DCF)
   - Present Value (PV) Profit

2. Payout (Present Value)
   - Time required for PV profit to equal PV investment

3. Investment Efficiency
   - Present Value Profit to Investment (P/I) Ratio

4. Internal Rate of Return (DCFROR)
   - Discount rate that reduces DCF to zero

B. Annual Balance Sheet

For each year of the project, a balance sheet is constructed as follows:

Project Revenue	
Net Oil Sold (Less Royalty)	
Net Gas Sold (Less Royalty)	
	Total Revenue (R)
Project Costs	
Severance Tax	
Fixed Operating Cost	
Variable Operating Cost	
CO_2 Purchase Cost*	
CO_2 Treating Cost**	
Produced Water Treating Cost	
Well Workover Cost	Total Operating Cost (O)
	Net Operating Income (NOI)
Capital	
Working Capital (WC)	
Tangible Capital (CT)	
Intangible Capital (CI)	
Debt Interest Cost	
Net Borrowing	
Principal Repayment	Total Capital (C)
	Cash Flow Before Taxes

*Net including any benefit from recycle.

**If CO_2 is recycled, it must be separated from the produced stream and recompressed to injection conditions.

Taxes

Excise (Windfall) Tax (WPT)
State Income Tax (SIT)
Federal Income Tax (FIT)
Intangibles and Depreciation
Investment Tax Credit

Total Taxes (T)

Cash Flow After Taxes (P)

That is, for each year of the project after tax profit is given by:

$$P = R - O - C - T \tag{47}$$

where O is the total operating costs, the total capital is

$$C = WC + CT + CI \tag{48}$$

and the taxes are

$$T = WPT + SIT + FIT \quad . \tag{49}$$

Net revenue is given by

$$R = (P_O V_O + P_G V_G)(1 - Y_r) \tag{50}$$

where

P_O = Price of oil, \$/BBL
P_G = Price of gas, \$/MCF
V_O = Annual volume of oil, BBL
V_G = Annual volume of gas, MCF
Y_r = Royalty rate

The annual operating cost is given by

$$O = S + F + O_V V_O + O_{WT} V_W + O_P V_P + P_I V_I + W_{WO} \tag{51}$$

where

S = Severance tax = RX_{SEV}

X_{SEV} = Severance tax rate

F = Fixed annual operating cost, \$/yr

O_V = Variable operating cost, \$/BBL oil

O_{WT} = Produced water lifting, treating, separating, disposal, and reinjection cost, \$/BBL water

V_W = Annual volume of produced water, BBL

O_P = CO_2 separation and recompression cost, \$/MSCF

V_P = Annual volume of produced CO_2, MSCF

P_I = Price of CO_2, \$/MSCF

V_I = Net volume of CO_2 purchased, MSCF

W_{WO} = Well workover and maintenance, \$/yr.

Once the annual operating cost is determined, the working capital required to finance the short term float in each year is given by

$$WC = (O_i - O_{i-1}) \frac{NWC}{12} \tag{52}$$

where $(O_i - O_{i-1})$ represents the change in operating costs in a year, and NWC is the months of working capital required.

The annual net operating income is given by

$$NOI = R - O \quad , \tag{53}$$

and the before tax income is

$$BTI = NOI - WC - CT - CI \ . \tag{54}$$

This value is an intermediate variable used for before tax screening. However, the NOI from equation (53) is used to develop the tax requirements.

C. Taxes

The excise (windfall) tax is computed in the model based upon the assumption of tertiary oil. No attempt has been made to include computations based on incremental economics over continued secondary or primary operations. The windfall price difference is based on

$$P_W = P_O - P_{BO} \tag{55}$$

where

P_{BO} = Base price of oil escalated at inflation rate

P_W = Windfall price difference

The windfall price difference is subject to a net income limitation (NIL) computed as

$$P_{NIL} = (NOI - C_{DW})/V_{ON} \tag{56}$$

where

C_{DW} = Capital depreciation by units of production

V_{ON} = Net oil sold = $V_O(1 - Yr)$.

If P_{NIL} is less than P_W, then P_{NIL} is used as the basis for the windfall excise tax (WPT) as follows:

$$WPT = V_{ON}(1 - X_{SEV})\ P_W\ X_{WPT} \tag{57}$$

where

X_{WPT} = Windfall tax rate.

Since the WPT is subject to phase out at some future date, the model decrements the tax rate over a finite period beginning at a specified date.

State income tax (SIT) can be complex in some situations, but for the purposes of screening, we have simply based it on net operating income:

$$SIT = NOI \; X_S \tag{58}$$

where

X_S = state income tax rate.

A similar approach is taken for federal income taxes (FIT):

$$FIT = (NOI - WPT - SIT - C_{DF} - C_I) \; X_F - T_{CR} \tag{59}$$

where

C_{DF} = Depreciation of tangible capital

C_I = Intangible capital

X_F = Federal tax rate

T_{CR} = Investment tax credit.

Two methods of depreciating capital are allowed. The first is a straight line technique in which equal amounts of tangible capital per year are depreciated over a set period of time. The second method is the scheduled five year depreciation of the Accelerated Capital Recovery System (ACRS) according to the 1981 Tax Act.

Any investment tax credit not used in a given year may be carried forward to future years, but the tax credit may not be used to generate negative federal income taxes. During early years of the operation of a project, negative NOI may result in negative FIT which can be used to shelter income from other projects if desired. Alternatively, setting negative FIT values to zero assumes that negative cash flows cannot be used to offset other income. This provides a more severe test of project profitability.

The total undiscounted cash flow for the project is based upon the sum of the annual cash flows calculated over the economic life of the project. Economic life may be calculated as the point of maximum

after tax cash flow, or as the point of maximum cumulative net operating income. The second method may extend the economic life beyond the time when negative after tax annual cash flows are occurring.

D. Debt Financing

The economic model also allows for a percentage of tangible and intangible capital to be borrowed. The model calculates a debt schedule consisting of:

1. Debt added per year;
2. Principal repaid per year;
3. Interest paid per year; and
4. Principal balance at end of year.

A fixed interest rate is used for these calculations, and loan repayments are in equal annual installments similar to home mortgage payments. Loan payment may be delayed and the loan need not be completely repaid at the end of the project, implying that the loan will be paid off elsewhere. If loan payment is delayed, accrued interest will increase loan principal. Annual interest payments are deducted from taxable income, and interest and principal payments are made from the after tax cash flow.

E. Escalation and Discounting

In order to properly evaluate each of the annual calculations, the prices and costs must be escalated to account for inflation. Each parameter in the model may be escalated at a different rate by the relation:

$$E_i = A_i \, (1 + e_A)^{i-1} \tag{60}$$

where

A_i = Annual cost or price in year i

E_i = Escalated value

e_A = Escalation rate.

The model includes two discounting options: annual (year end) and semi-annual (mid-year). For annual discounting the method is

$$PVP_i = \frac{P_i}{(1 + X_{DR})^i} \tag{61A}$$

$$DCF = \sum_{1}^{NPL} PVP_i \tag{61B}$$

where

PVP_i = Present value of parameter P in year i

X_{DR} = Discount rate

NPL = Years of economic life

DCF = Discounted cash flow.

The present value of each variable is computed by the model, so that a present value comparison of revenues and operating costs can be made. For mid-year discounting the method is:

$$PVP_i = \frac{P_i}{(1 + X_{DR})^{i-1/2}} \tag{62}$$

The model also has a "constant dollar" discounting option which allows undiscounted cash flows to be adjusted by an average inflation rate prior to normal compound interest discounting. The procedure then becomes:

$$P_{CD_i} = \frac{P_i}{(1 + X_{INF})^{i-1/2}} \tag{63A}$$

$$PVP_i = \frac{P_{CD_i}}{(1 + X_{DR})^{i-1/2}} \tag{63B}$$

where

X_{INF} = Average inflation rate during project

P_{CD} = Constant dollar profit.

This method is more technically correct than the procedure outlined in Equations (61-62), however, current industry practice is to set the "threshold" discount rate at a higher value to compensate for inflation.

F. Uncertainty

The parameter method present by Davidson and Cooper[28] is used to compute uncertainty in present value. This method deals with the parameters of the probability distributions rather than the distributions and, with reasonable assumptions about distribution form, can estimate the probability of achieving various levels of present value.

The parameter method requires that the uncertain parameters must be statistically independent. For this reason, the uncertainty in performance of the reservoir is considered as a single parameter. Other variables, such as costs, revenues and expenses, should be mutually independent. If dependence between parameters is established, the parameters should be re-arranged to minimize dependence if possible. In the economic model, unit prices, costs, and capital are defined as the uncertain variables, in addition to the uncertainty in oil production. Escalation, inflation and tax rates are treated as certain and constant values over the life of the project. These definitions constitute the first step of the uncertainty analysis.

The second step is to estimate the mean and variance of each of the uncertain variables. The mean is the weighted average value of all possibilities found in the probability distribution of a parameter, and the variance is the weighted average of all squares of differences from the mean. To simplify this task, three values of a parameter are used to define the mean and variance:

1. Low value - a value of the parameter small enough so that only a 10 percent chance exists of a smaller value;

2. The most-likely value; and

3. High value - a value large enough that there is only a 10 percent chance of a higher value.

The mean and variance of the parameter are calculated from these three values. [28, 29]

Finally, the means and variances are combined into other quantities of interest, such as revenues, expenses, and costs. Once combined, the assumption of a resulting log-normal distribution is made. At this point, the mean and variance of the present value are known and estimations of present value at 10, 50, and 90 percent probability computed.

G. Results and Profitability Indices

The calculated mean present value (50 percent) is presented in various formats to allow the direct comparison of costs and benefits. Additionally, various "technical" measures of project performance are made, including economic life, cumulative oil produced, gross oil sold, net oil sold, discounted net oil sold, and cumulative CO_2 - oil ratio. These measures may be helpful to operators intending to maximize oil recovery instead of cash flow.

The present value of project revenues, costs and expenses are also reported to allow for an analysis of the components of project present value. The final economic results are presented in terms of four parameters:

1. Discounted Cash Flow (DCF), which represents the present value profit of the project;

2. Payout, which is the time required for present value profit to equal present value investment;

3. Internal Rate of Return (DCFROR), which is a measure of the discount rate that reduces the DCF to zero; and

4. Investment Efficiency (P/I), which is the present value per dollar invested.

The strengths and weaknesses of these criteria are discussed in detail by Capen, et al.[30] DCF is the most widely accepted measure of project performance but it fails to recognize capital limitations and requires the specification of a discount rate. The problem of not recognizing capital limitations may result in the situation of a company identifying the project with the greatest wealth being returned while lacking the resources to perform the project, therefore this measure is not recommended for project screening. If DCF is used, a uniform discount rate should be applied to all cases considered, generally a discount rate based upon a company's average cost of capital.

Payout as an economic measure does provide an important measure of project performance. Since payout does not consider cash flow after the payout period ends, it is a poor ranking criteria. The advantage of including payout in the analysis allows for the recognition of minimum operating time required for a project, which can be important to operators seeking short-term returns when unstable environments make long operating periods unlikely.

The Internal Rate of Return, also known as the Discounted Cash Flow Rate of Return, is a very popular economic criteria, and this measure obviates the need to specify a discount rate as in DCF. Problems with this criteria may result when comparing projects at different discount rates, since a project at a lesser DCFROR may have a greater present value at a company's costs of capital.

The Investment Efficiency, or Profit-to-Investment Ratio (P/I) is the ratio of the projects total profit to the total investment required. The P/I is preferred because it gives a method of ranking projects in

such a way as to maximize the profit per dollar invested. However it does have a weakness for expense intensive projects, such as CO_2 flooding. In these types of projects, unusually high P/I ratios can result due to the relatively low capital requirements, since the purchase of CO_2 is expensed. To compensate for this we have added working capital to the model which partially compensates for high expense/capital ratios. A similar measure to P/I ratio, the Profit-to-Expense Ratio (P/E), is also computed by the model.

The task of ranking various projects by the above technical and economic criteria is not a simple one. The key to the accuracy of the ranking is consistency, so that the relative ordering of projects does not involve comparing "apples with oranges". A combination of common criteria must be used, for example, ranking by P/I only projects with payouts of less than five years and a DCFROR greater than fifteen percent.

NOMENCLATURE

A	=	pattern area, acres, or coefficient in Equation (A-1)
A_1, A_2	=	coefficients in Equations (A-6a) and (A-6b)
B	=	coefficient in Equation (A-1)
B_1, B_2	=	coefficients in Equations (A-6a) and (A-6b)
C	=	concentration, vol. fr., or locus of characteristic curve in x-t space
C_1, C_2	=	coefficients in Equations (A-6a) and (A-6b)
d	=	differential operator
D_1, D_2	=	coefficients in Equations (A-6a) and (A-6b)
E	=	coefficient in Equation (A-1)
E_A	=	areal sweep efficiency
E_1, E_2	=	coefficients in Equations (A-6a) and (A-6b)
f	=	fractional flow, phase flux/total flux
F	=	multiplying factor for correcting Koval factor for gravity
F_i	=	Overall fractional flux of species i, volume i flowing/total volume flowing
h	=	thickness, ft
H	=	heterogeneity factor, dimensionless, or total thickness, ft

NOMENCLATURE (Cont.)

k	=	permeability, md
k_r	=	relative permeability
K_i	=	equilibrium vaporization ratio, vol. fr. i in oleic phase/vol. fr. i in aqueous phase
K_{val}	=	Koval factor, dimensionless
L	=	injector-producer distance, ft, or linear operator (directional derivative)
M	=	mobility ratio, dimensionless
N	=	number of layers
N_i	=	cumulative production of component i, bbl
N_{2D}	=	cumulative oil produced, fr. OIP at start of CO_2 injection
p	=	probability
q	=	steady-state injection/production rate, bbl/day
Q	=	injection rate, bbl/day
R_s	=	solution gas-oil ratio, MCF/STB
R_{sw}	=	CO_2 solubility in water, SCF/STB
S	=	saturation, fraction
s	=	parameter along curve C
t	=	time, days
t_{DS}	=	hydrocarbon pore volumes of water and CO_2 injected as WAG

NOMENCLATURE (Cont.)

u	=	dependent variable in Equation (A-1)
v	=	dependent variable in Equation (A-1)
VDP	=	Dykstra-parsons coefficient within a layer
VDPL	=	Dykstra-Parsons coefficient among multiple layers
$\bar{v}_h$	=	frontal velocity for five-spot, ft/day
v_{Ci}	=	concentration velocity of species i, dimensionless
V_p	=	total pore volumes, bbl
W_R	=	injected WAG ratio, vol. water/vol. CO_2
X	=	distance, ft
α	=	parameter along curve C
β	=	parameter along curve C
Γ	=	image space
Δ	=	finite difference operator
ϵ	=	constant in Equation (9)
λ_1 λ_2	=	multipliers in Equation (A-7)
λ_{rt}	=	total relative mobility, cp^{-1}
μ	=	viscosity, cp
ρ	=	density, g/cc
σ	=	concentration velocity of all components in coherent wave region
∂	=	partial differential operator

NOMENCLATURE (Cont.)

Subscripts

D	=	dimensionless
h	=	horizontal
i	=	component, or layer
j	=	phase
I	=	initial condition
J	=	injected condition
N	=	number of dependent variables
o	=	oil
r	=	residual
s	=	total derivative wrt s
t	=	partial derivative wrt t
v	=	vertical
w	=	water
wc	=	connate water
x	=	total derivative wrt x
1	=	water (component), aqueous (phase)
2	=	oil (component), oleic (phase)
3	=	CO_2 (component)
'	=	derivative
o	=	at breakthrough
+	=	fast composition path
-	=	slow composition path
$\bar{\ }$	=	average behind front

NOMENCLATURE (Cont.)

Acronyms

CO2PM	=	CO_2 predictive model
WAG	=	water alternating gas

Economics Nomenclature

Contained in Section VI

REFERENCES

1. Selection of Reservoirs Amenable to Micellar Flooding, First Annual Report, U. S. Department of Energy Report DOE/BC/00048-20 (December, 1980).

2. Paul, G. W., Lake, L. W., Pope, G. A. and Young, G. B.: "A Simplified Predictive Model for Micellar-Polymer Flooding," Paper SPE 10733 presented at the California Regional Meeting of SPE, San Francisco, March 24-26, 1982.

3. Paul, G. W., Lake, L. W. and Gould, T. L.: "A Simplified Predictive Model for CO_2 Miscible Flooding," Paper SPE 13238 presented at SPE Fall Meeting, Houston, September 16-19, 1984.

4. Aydelotte, S. R. and Pope, G. A.: "A Simplified Predictive Model for Steamdrive Performance," J. Pet. Tech. (May, 1983) 991-1002.

5. Koval, E. J. : "A Method for Predicting the Performance of Unstable Miscible Displacements," Soc. Pet. Eng. J. (June, 1963) 145-154.

6. Claridge, E. L.: "Prediction of Recovery in Unstable Miscible Flooding," Soc. Pet. Eng. J. (April, 1972) 143-155.

7. Economics of Enhanced Oil Recovery, Final Report, U. S. Department of Energy Report DOE/ET/12072-2 (May, 1981).

8. Hawthorne, R. G.: "Two-Phase Flow in Two-Dimensional Systems-Effects of Rate, Viscosity and Density on Fluid Displacement in Porous Media," Trans. AIME (1960) 219, 81-87.

9. Lake, L. W., Pope, G. A., Sepehrnoori, K., Carey, G.: Isothermal Multiphase, Multicomponent Equations for Fluid Flow in Permeable Media, Center of Enhanced Oil and Gas Recovery Research, University of Texas (1981).

10. Dicharry, Roy M., Perrymann, T. L., and Ronquille, J. D.: "Evaluation and Design of a CO_2 Miscible Flood Project - SACROC Unit, Kelly-Snyder Field," J. Pet. Tech. (November, 1973) 1309-1318.

11. Rosman, A., and Zana, E.: "Experimental Studies of Low IFT Displacements by CO_2 Injection," Paper SPE 6723 presented at SPE 52nd Annual Meeting, Denver, Colo., October 9-12, 1977.

12. Stalkup, F. I.: "Displacement of Oil by Solvent at High Water Saturation," Soc. Pet. Eng. J. (December, 1970) 337-348.

REFERENCES (Cont.)

13. Crawford, H. R., Neill, G. H., Lucy, B. J., and Crawford, P. B. "Carbon Dioxide -A Multipurpose Additive for Effective Well Stimulation," J. Pet. Tech. (March, 1963) 237-242.

14. Dumore, J. M., Hagoort, J., and Risseeuw, A. S.: "An Analytical Model for One-Dimensional Three-Component Condensing and Vaporizing Gas Drives," Paper SPE 10069 presented at SPE 56th Annual Meeting, San Antonio, Texas, October 5-7, 1981.

15. Helfferich, F.: "Theory of Multicomponent, Multiphase Displacement in Porous Media," Soc. Pet. Eng. J. (February, 1981) 51-62.

16. Hirasaki, G. J.: "Application of the Theory of Multicomponent Multiphase Displacement to Three-Component, Two-Phase Surfactant Flooding," Soc. Pet. Eng. J., (April, 1981) 191-204.

17. Pope, G. A.: "The Application of Fractional Flow Theory to Enhanced Oil Recovery," Soc. Pet. Eng. J. (June, 1980) 191-205.

18. Essacson, E. L. Global Solution of a Riemann Problem for a Non-Strictly Hyperbolic System of Conservation Laws Arising in Enhanced Oil Recovery, NSF PAV-78-08066, Rockefeller University (1981).

19. Whitehead, W. R., Kimbler, O. K., Holden, W. R., and Bourgoyne, A. T.: Investigations of Enhanced Oil Recovery Through Use of Carbon Dioxide, U. S. Department of Energy Report DOE/MC/03106-9 (July, 1981).

20. Delshad, M.: Measurement of Relative Permeability and Dispersion for Micellar Fluids in Berea Rock, M.S. Thesis, The University of Texas, (1981).

21. Coleman, H. J., Shelton, E. M., Nichols, D. T., and Thompson, C. J.: Analyses of 800 Crude Oils from United States Oil Fields, U. S. Department of Energy Report BETC/RI-78/14, (November, 1978).

22. Goodrich, J. H., Target Reservoirs for CO_2 Miscible Flooding--Final Report, U. S. Department of Energy Report DOE/MC 08241-17, (October, 1980).

23. Welge, H. J.: "A Simplified Method for Computing Oil Recovery by Gas or Water Drive," Trans. AIME (1952) 195, 91-98.

REFERENCES (Cont.)

24. Caudle, B. H., and Witte, M. D.: "Production Potential Changes During Sweepout in a Five-Spot Pattern": Trans. AIME (1959) 216, 446-448.

25. Craig, F. F. Jr.: The Reservoir Engineering Aspects of Waterflooding, SPE Monograph Vol. 3, Society of Petroleum Engineers of AIME, Dallas, Texas (1971).

26. Rowe, H. G., York, S. Derryl, and Ader, J. C.: "Slaughter Estate Unit Tertiary Pilot Performance, " J. Pet. Tech. (March, 1982) 613-620.

27. Ader, J. C., and Stein, M. H.: "Slaughter Estate Unit CO_2 Pilot Reservoir Description via a Black Oil Model Waterflood History Match," Paper SPE 10727 presented at Third Joint SPE/DOE Symposium on Enhanced Oil Recovery, Tulsa, April 4-7, 1982.

28. Davidson, L. B. and Cooper, D. O.: "A Simple Way of Developing a Probability Distribution of Present Value," J. Pet. Tech. (September, 1976) 1069-1078.

29. Parratt, L. G.: Probability and Experimental Errors in Science, John Wiley and Sons, New York, 1961.

30. Capen, E. C., Clapp, R. V., and Phelps, W. W.: "Growth Rate - A Rate of Return Measure of Investment Efficiency," J. Pet. Tech. (May, 1976) 531-543.

31. Helfferich, F., and Klein, G.: Multicomponent Chromatography, Marcel Dekker, New York, 1970.

32. Ames, William F.: Numerical Methods for Partial Differential Equations, Academic Press, San Francisco, 1977.

33. Jeffrey, A. and Taniuti, M.: "Nonlinear Wave Propagation with Applications to Physics and Magnetohydrodynamics," Academic Press, New York, 1964.

34. Courant, R. and Friedrichs, K.O.: Supersonic Flow and Shock Waves, Springer-Verlag, New York, 1948.

35. Courant, R. and Hilbert, D., Methods of Mathematical Physics, Interscience Publishers, Vol. I, 1962.

36. Parsons, R. W.: "Velocities in Developed Five-Spot Patterns," J. Pet. Tech. (May, 1974) 550.

TABLE 1

RESERVOIR AND FLUID PROPERTIES FOR 1-D SIMULATIONS

Number of Grid Blocks in X-Direction	50
Number of Grid Blocks in Y-Dirction	1
Number of Grid Blocks in Z-Direction	1
Grid Block Dimension in X-Direction	20 ft
Grid Block Dimension in Y-Direction	25 ft
Grid Block Dimension in Z-Direction	25 ft
Formation Porosity	.20
Formation Permeability	2000 md
Initial Water Saturation	.74
Connate Water Saturation	.30
Residual Oil Saturation	.26
Formation Pressure	3750 psia
Formation Temperature	200°F
Water Formation Volume Factor	1.0 RB/STB
Oil Formation Volume Factor	1.63 RB/STB
Solution Gas-Oil Ratio	0.01 SCF/STB
Oil Specific Gravity	0.7
Gas Specific Gravity	1.0683
Oil Viscosity	0.35 cp
Water Viscosity	0.51 cp
CO_2 Viscosity	0.037 cp

TABLE 2

RESERVOIR PROPERTIES FOR 2-D CROSS-SECTION SIMULATIONS

Permeability	102 md
k_v/k_h	0.1
Porosity	0.176
Thickness	16.7 ft
Residual Oil Saturation	0.2
Connate Water Saturation	0.2
Water Injection Rate	3500 BW/D
CO_2 Injection Rate	5000 MCF/D

TABLE 3

CO2PM INPUT DATA FOR SLAUGHTER CASE

Slaughter Estate Run - WAG = 1.0, T_{DS} = 1.5, 3 Layers

Formation Properties

Porosity	0.1130	
Net Thickness	77.5	ft
Pattern Area	12.29	acres
Permeability	6.0	md
Depth	5000.0	ft
Vert/Horiz Permeability Ratio	0.01	
Formation Pressure	2000.0	psia
Formation Temperature	105.0	°F
Reservoir Water Salinity	50000.	ppm

Initial Conditions

Initial Oil Fractional Flow	0.1300	
Reservoir Injection Rate	390.0	BBL/D
Injected WAG Ratio	1.00	
Water Viscosity	0.8023	cp
Oil Viscosity	2.0000	cp
CO_2 Viscosity	0.0740	cp
Water Volume Factor	1.0000	RB/STB
Oil Volume Factor	1.2200	RB/STB
CO_2 Compressibility Factor	0.3091	1/psi
CO_2 Volume Factor	0.4000	RB/MCF
Water Density	1.0265	g/cc
CO_2 Density	0.7709	g/cc
CO_2 Density	48.1	lb/cu ft
CO_2 Solubility in Water	137.2	SCF/BBL
Oil Solution Gas Content	600.0	SCF/BBL

Relative Perm Curves

Oil Relative Perm Curvature	2.55
Water Relative Perm Curvature	1.78
Oil Relative Perm End-Point	1.000
Water Relative Perm End-Point	0.340
Irreducible Water Saturation	0.080
Residual Oil Saturation	0.310

TABLE 3 (Cont.)

RELATIVE PERMEABILITY TABLE

Water Saturation	Oil Kro	Water Krw	Fraction Water	Deriv DFW/DSW
0.0800	1.0000	0.0000	0.0000	0.000
0.1105	0.8774	0.0016	0.0046	0.290
0.1410	0.7644	0.0056	0.0181	0.600
0.1715	0.6607	0.0116	0.0420	0.980
0.2020	0.5661	0.0194	0.0786	1.435
0.2325	0.4802	0.0286	0.1302	1.953
0.1630	0.4027	0.0399	0.1980	2.493
0.2935	0.3334	0.0525	0.2818	2.989
0.3240	0.2718	0.0665	0.3790	3.357
0.3545	0.2177	0.0821	0.4844	3.518
0.3850	0.1708	0.0990	0.5910	3.431
0.4155	0.1305	0.1173	0.6914	3.114
0.4460	0.0967	0.1370	0.7793	2.634
0.4765	0.0688	0.1579	0.8513	2.080
0.5070	0.0464	0.1802	0.9063	1.537
0.5375	0.0292	0.2037	0.9457	1.058
0.5680	0.0165	0.2285	0.9718	0.672
0.5985	0.0079	0.2546	0.9877	0.381
0.6290	0.0028	0.2819	0.9960	0.179
0.6595	0.0005	0.3103	0.9994	0.054
0.6900	0.0000	0.3400	1.0000	0.000

Layer Multipliers based on Dykstra-Parsons = 0.480

Layer	Perm,md	Rate Mult	Dim Pore Vol Mult
1	9.96	0.55318	1.65953
2	5.28	0.29332	0.87995
3	2.76	0.15351	0.46052

TABLE 4

CO2PM INPUT DATA FOR DENVER UNIT CASE

Formation Properties		
Porosity	0.1220	
Net Thickness (Pay	178.0	ft
Pattern Area	71.10	acres
Permeability	8.2	md
Depth	5200.0	ft
Vert/Horiz Permeability Ratio	0.00	
Formation Pressure	2200.0	psia
Formation Temperature	105.0	°P
Reservoir Water Salinity	1000.	ppm
Initial Conditions		
Initial Oil Fractional Flow	0.0010	
Reservoir Injection Rate	1068.0	BBL/D
Injected WAG Ratio	0.50	
Water Viscosity	0.8284	cp
Oil Viscosity	1.3000	cp
CO_2 Viscosity	0.0700	cp
Water Volume Factor	1.0000	RB/STB
Oil Volume Factor	1.2340	RB/STB
CO_2 Compressibility Factor	0.3280	1/psi
CO_2 Volume Factor	0.4450	RB/MCF
Water Density	0.9927	g/cc
CO_2 Density	0.7870	g/cc
CO_2 Density	49.1	lb/cu ft
CO_2 Solubility in Water	172.9	SCF/BBL
Oil Solution Gas Content	400.0	SCF/BBL
Relative Perm Curves		
Oil Relative Perm Curvature	2.00	
Water Relative Perm Curvature	2.00	
Oil Relative Perm End-Point	0.700	
Water Relative Perm End-Point	0.350	
Irreducible Water Saturation	0.150	
Residual Oil Saturation	0.400	

TABLE 4 (Cont.)

RELATIVE PERMEABILITY TABLE

Water Saturation	Oil Kro	Water Krw	Fraction Water	Deriv DFW/DSW
0.1500	0.7000	0.0000	0.0000	0.000
0.1725	0.6317	0.0009	0.0022	0.202
0.1950	0.5670	0.0035	0.0096	0.469
0.2175	0.5057	0.0079	0.0239	0.812
0.2400	0.4480	0.0140	0.0467	1.238
0.2625	0.3937	0.0219	0.0802	1.740
0.2850	0.3430	0.0315	0.1260	2.330
0.3075	0.2957	0.0429	0.1853	2.950
0.3300	0.2520	0.0560	0.2586	3.550
0.3525	0.2118	0.0709	0.3444	4.054
0.3750	0.1750	0.0875	0.4397	4.380
0.3975	0.1418	0.1059	0.5396	4.461
0.4200	0.1120	0.1260	0.6384	4.275
0.4425	0.0858	0.1479	0.7302	3.849
0.4650	0.0630	0.1715	0.8103	3.253
0.4875	0.0438	0.1969	0.8760	2.576
0.5100	0.0280	0.2240	0.9262	1.898
0.5325	0.0158	0.2529	0.9618	1.280
0.5550	0.0070	0.2835	0.9845	0.753
0.5775	0.0018	0.3159	0.9965	0.328
0.6000	0.0000	0.3500	1.0000	0.156

Layer Multipliers based on Dykstra-Parsons = 0.600

Layer	Perm,md	Rate Mult	Dim Pore Vol Mult
1	15.60	0.63411	1.90234
2	6.41	0.26067	0.78202
3	2.59	0.10521	0.31564

FIGURE 1

PHASE BOUNDARIES PREDICTED IN TERNARY EQUILIBRIA

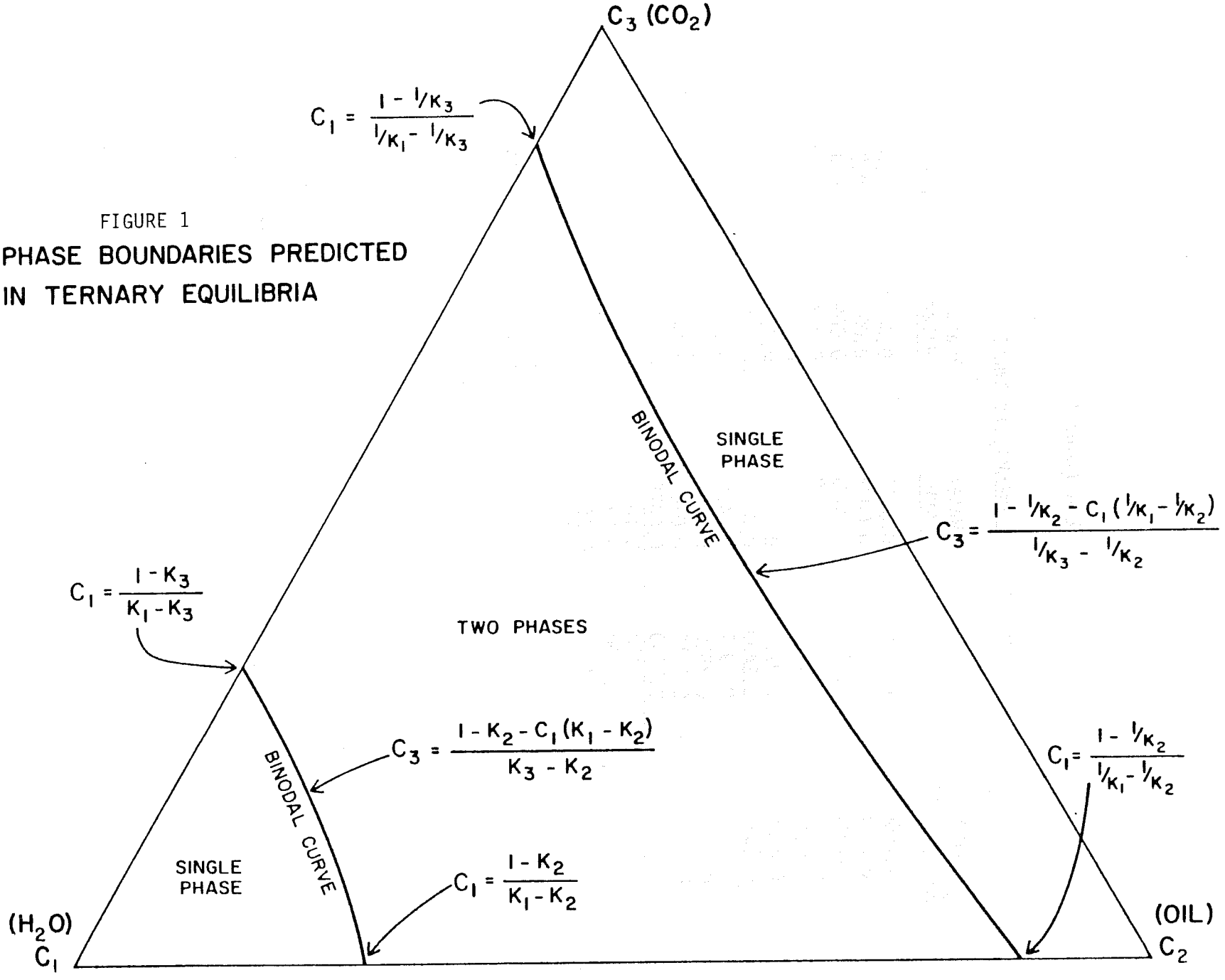

Figure 2a

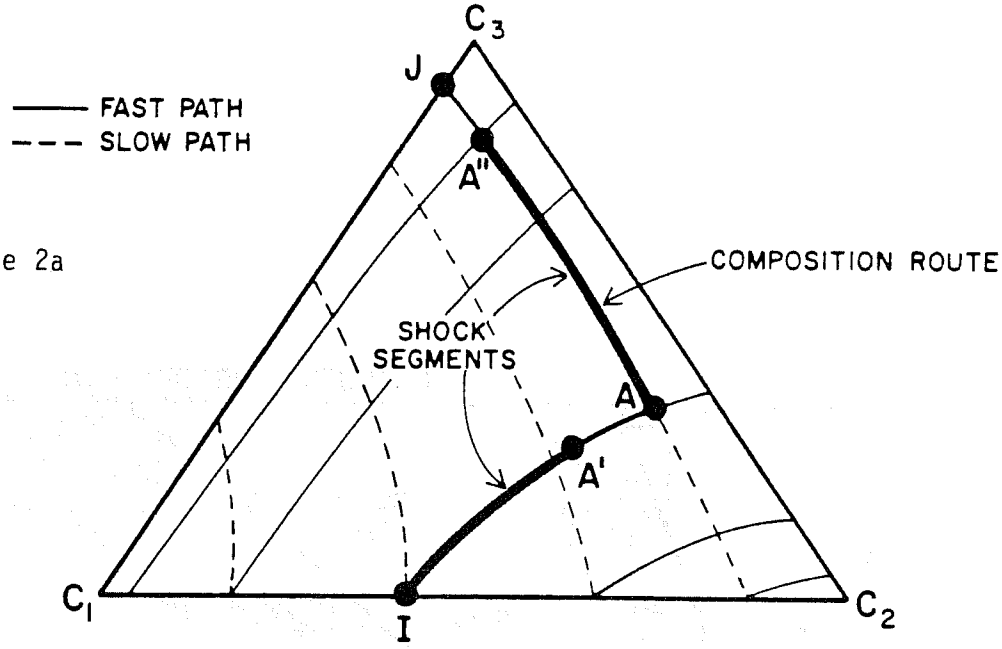

SCHEMATIC COMPOSITION PATH DIAGRAM

Figure 2b

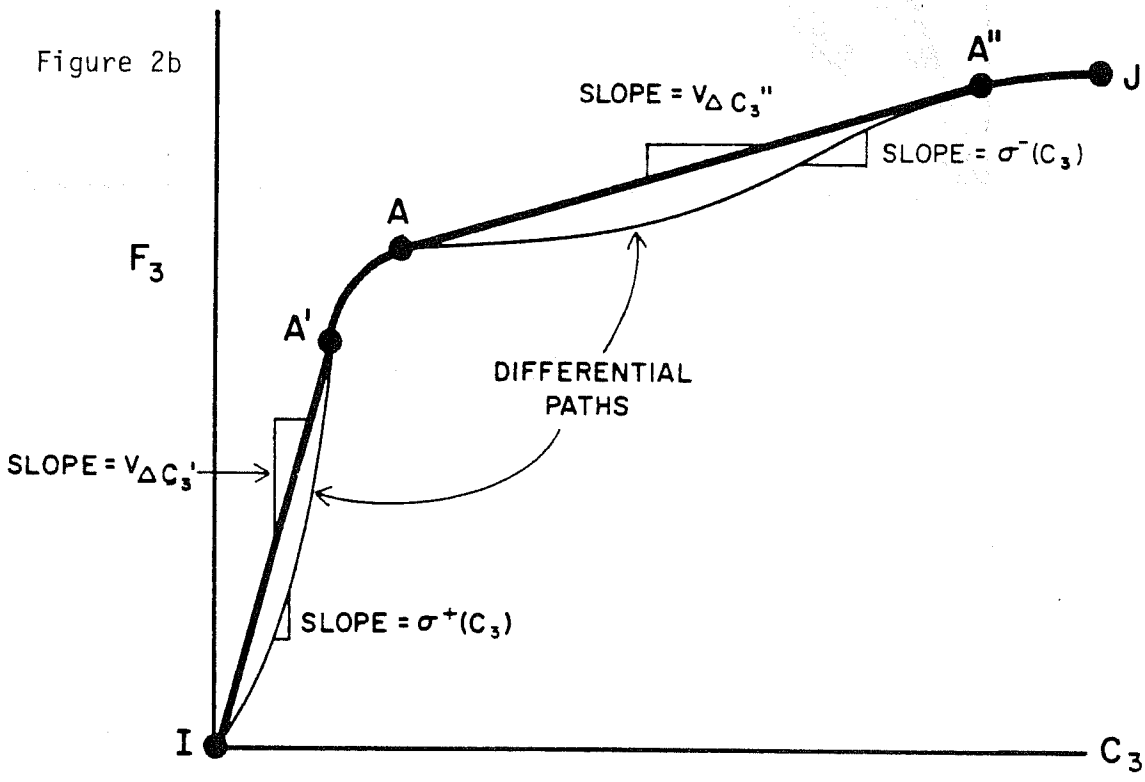

SCHEMATIC FLUX - CONCENTRATION PLOT

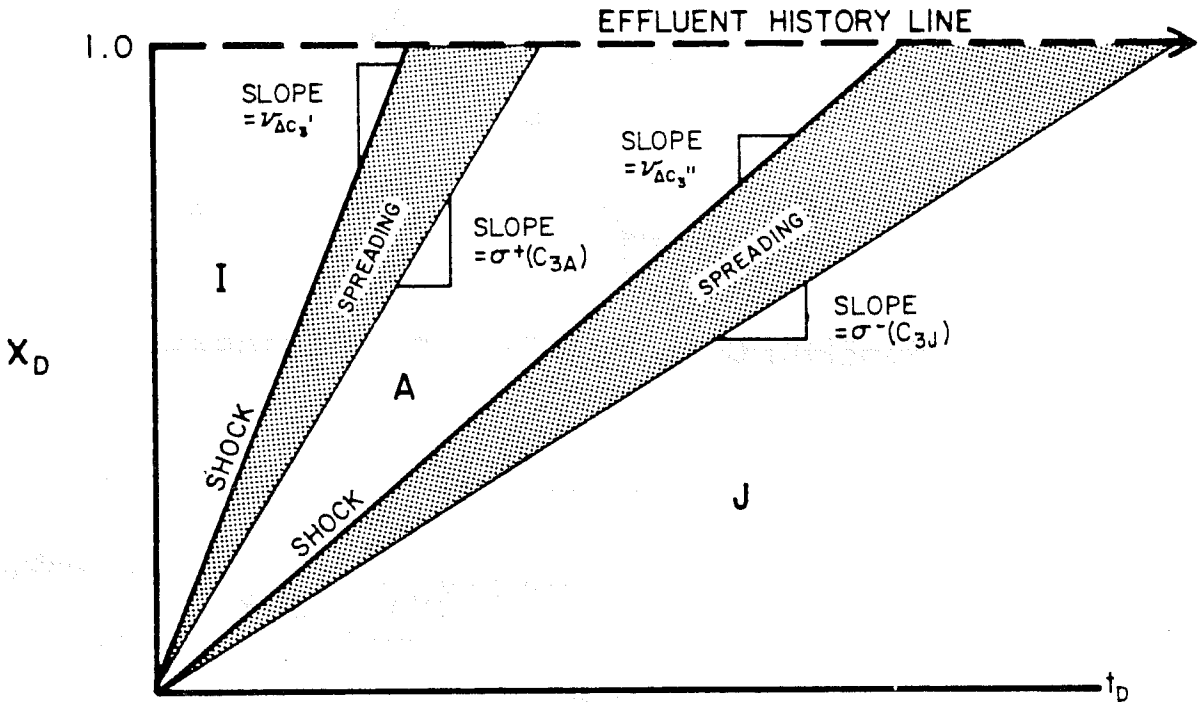

TIME-DISTANCE DIAGRAM

Figure 2c

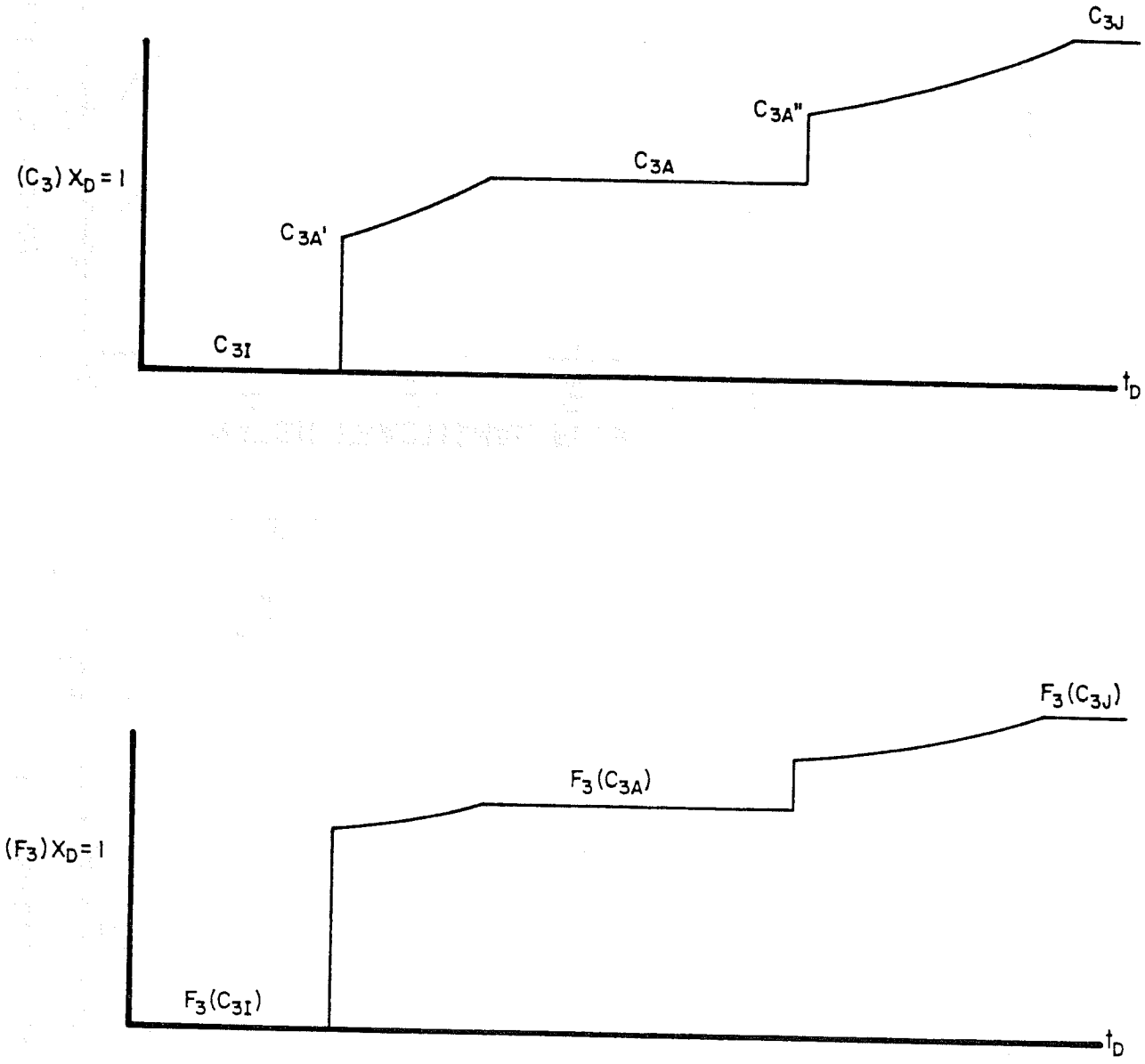

EFFLUENT HISTORIES

Figure 2d

Figure 3

RELATIVE PERMEABILITIES AND FRACTIONAL FLOW FOR SACROC EXAMPLE

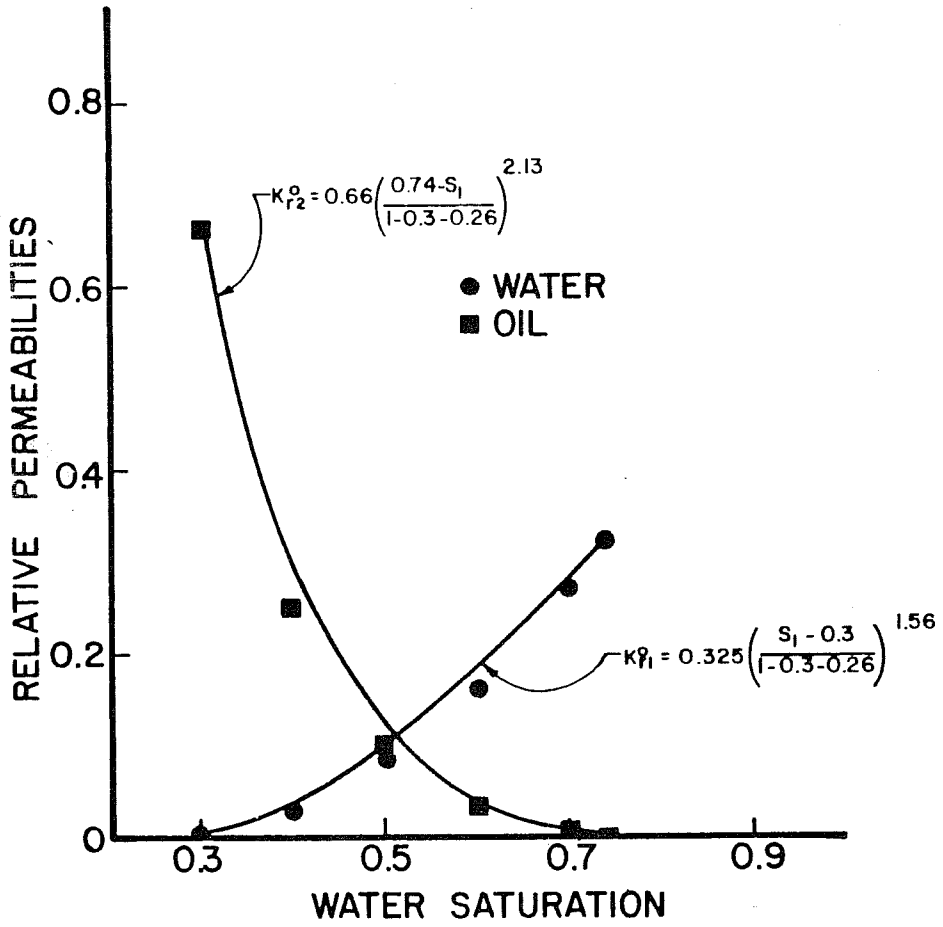

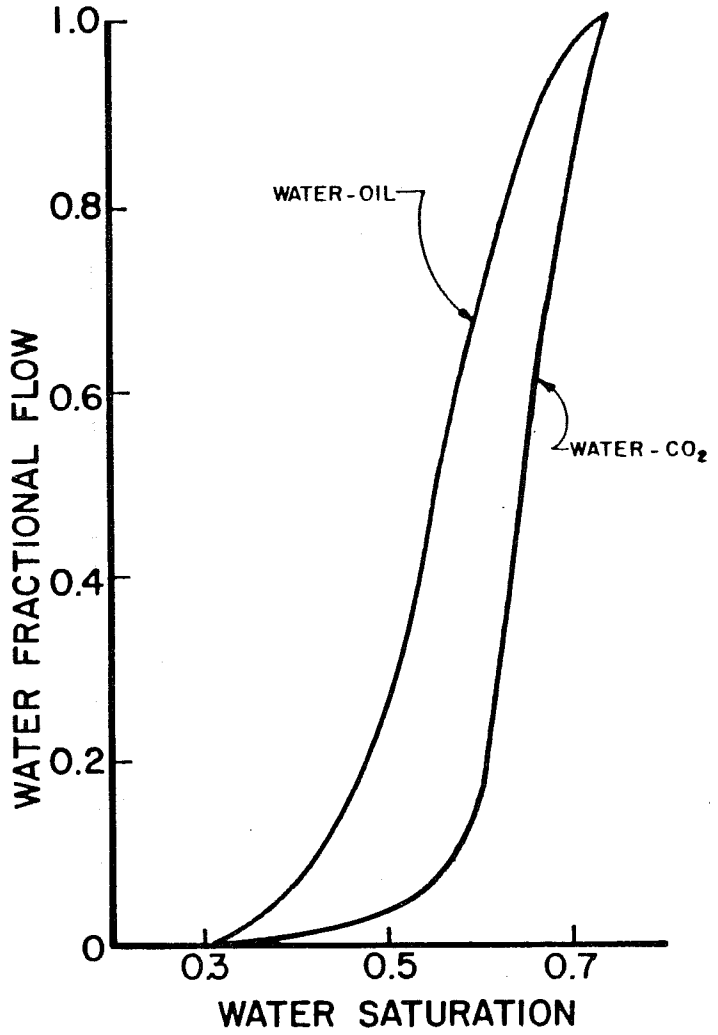

Figure 4

COMPOSITION PATH DIAGRAM FOR NO FINGERING CASES

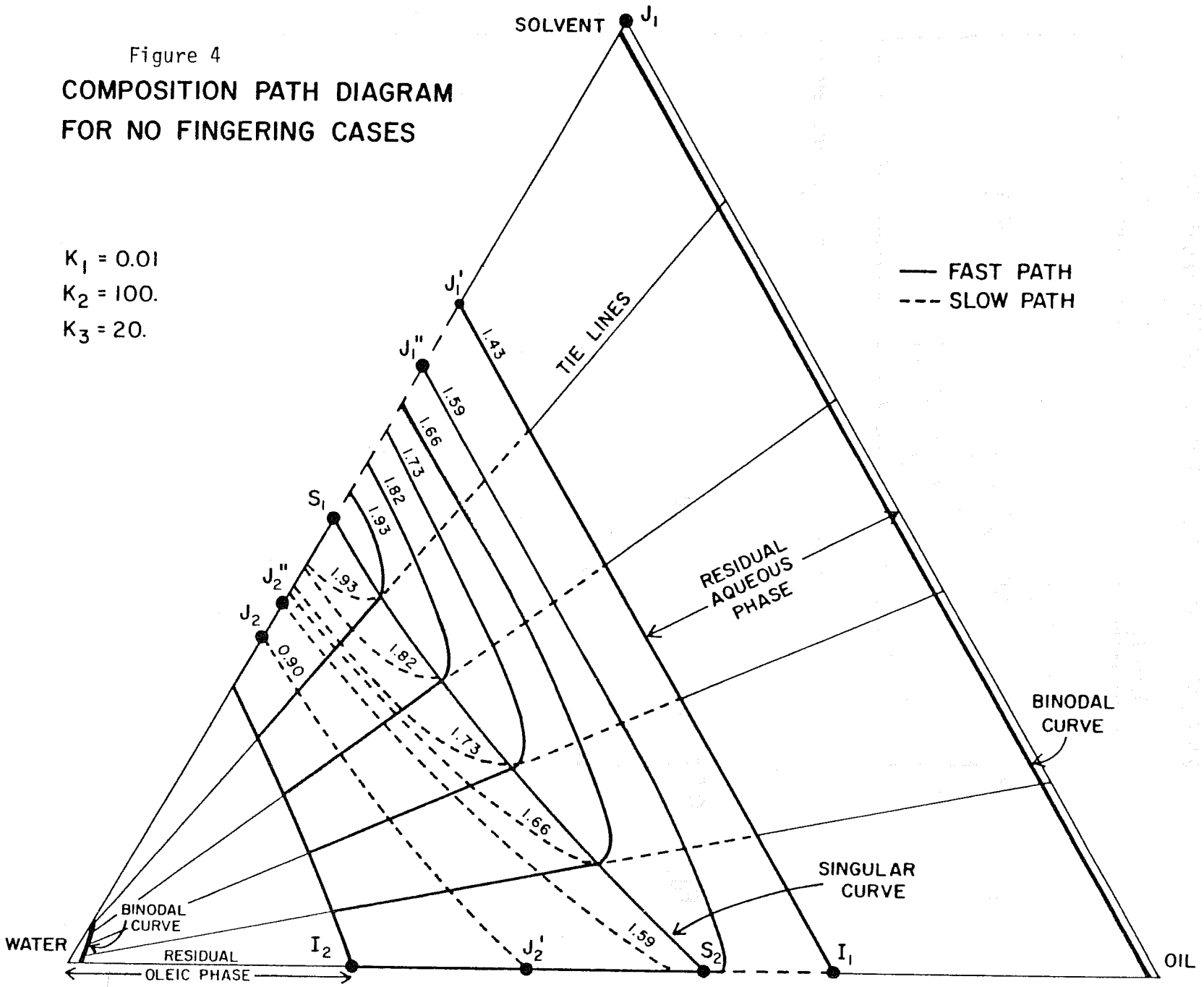

Figure 5

EFFLUENT HISTORIES FOR FOUR NO FINGERING CASES

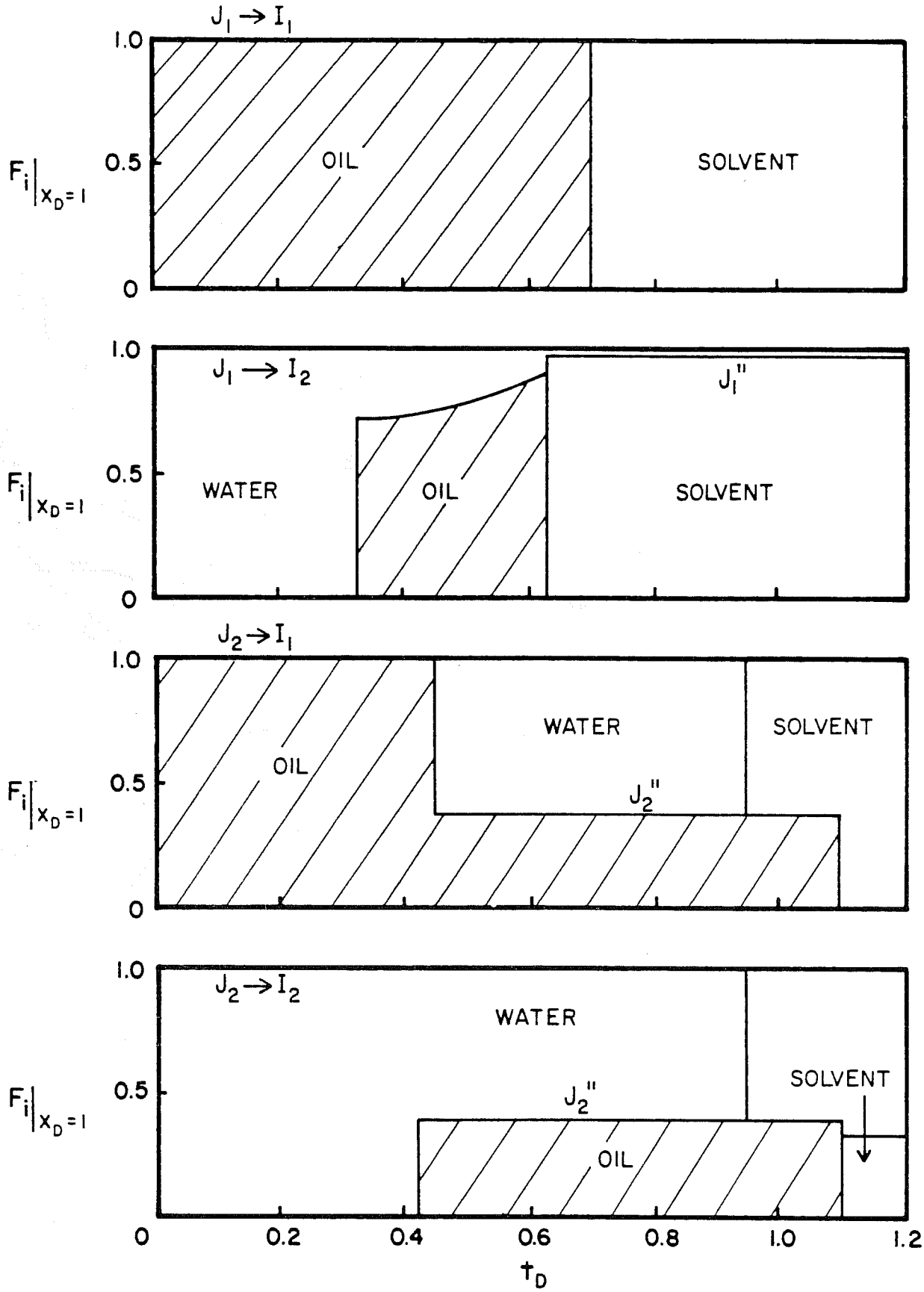

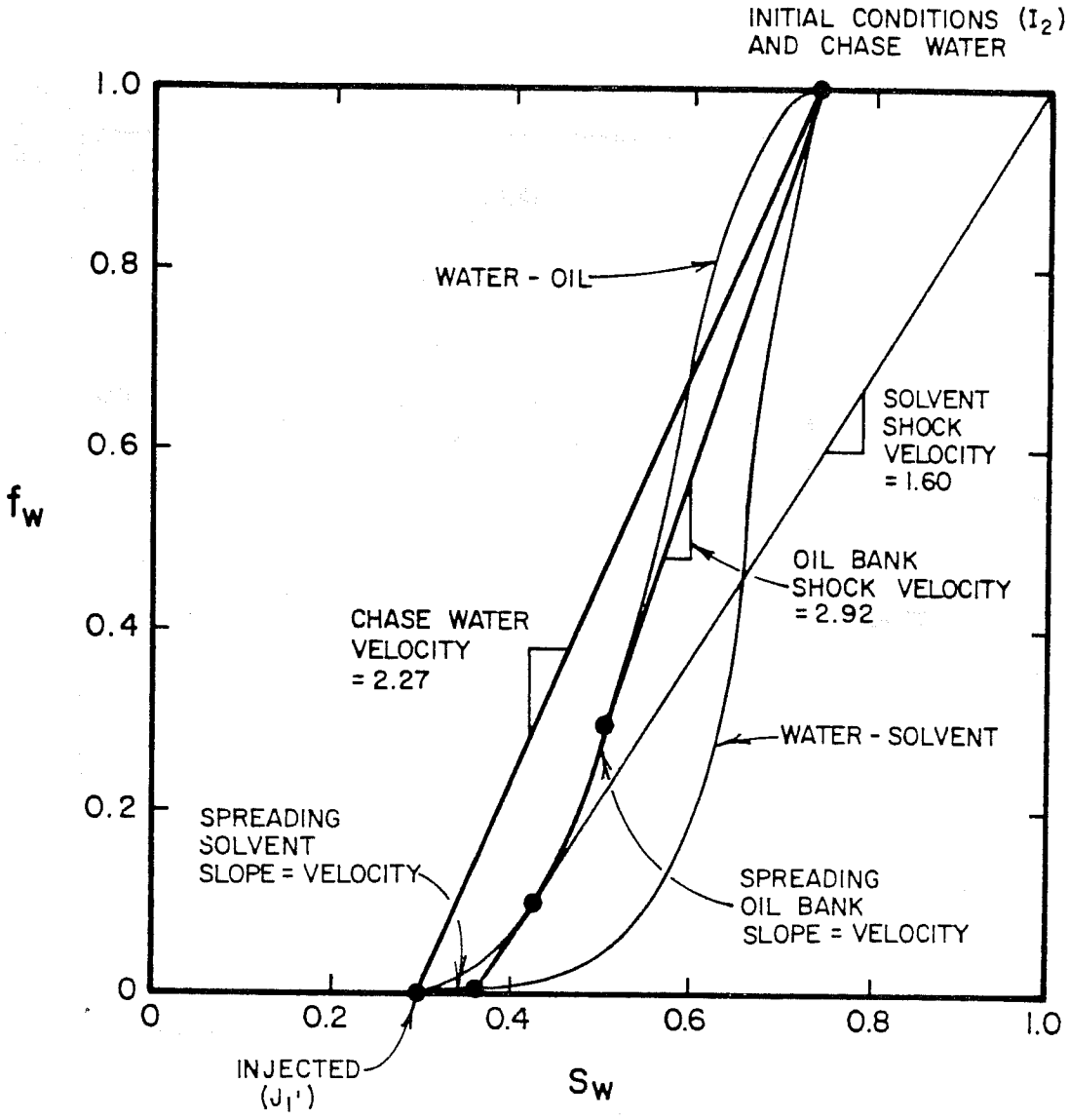

FRACTIONAL FLOW CONSTRUCTION FOR $J_1' \rightarrow I_2$

Figure 6

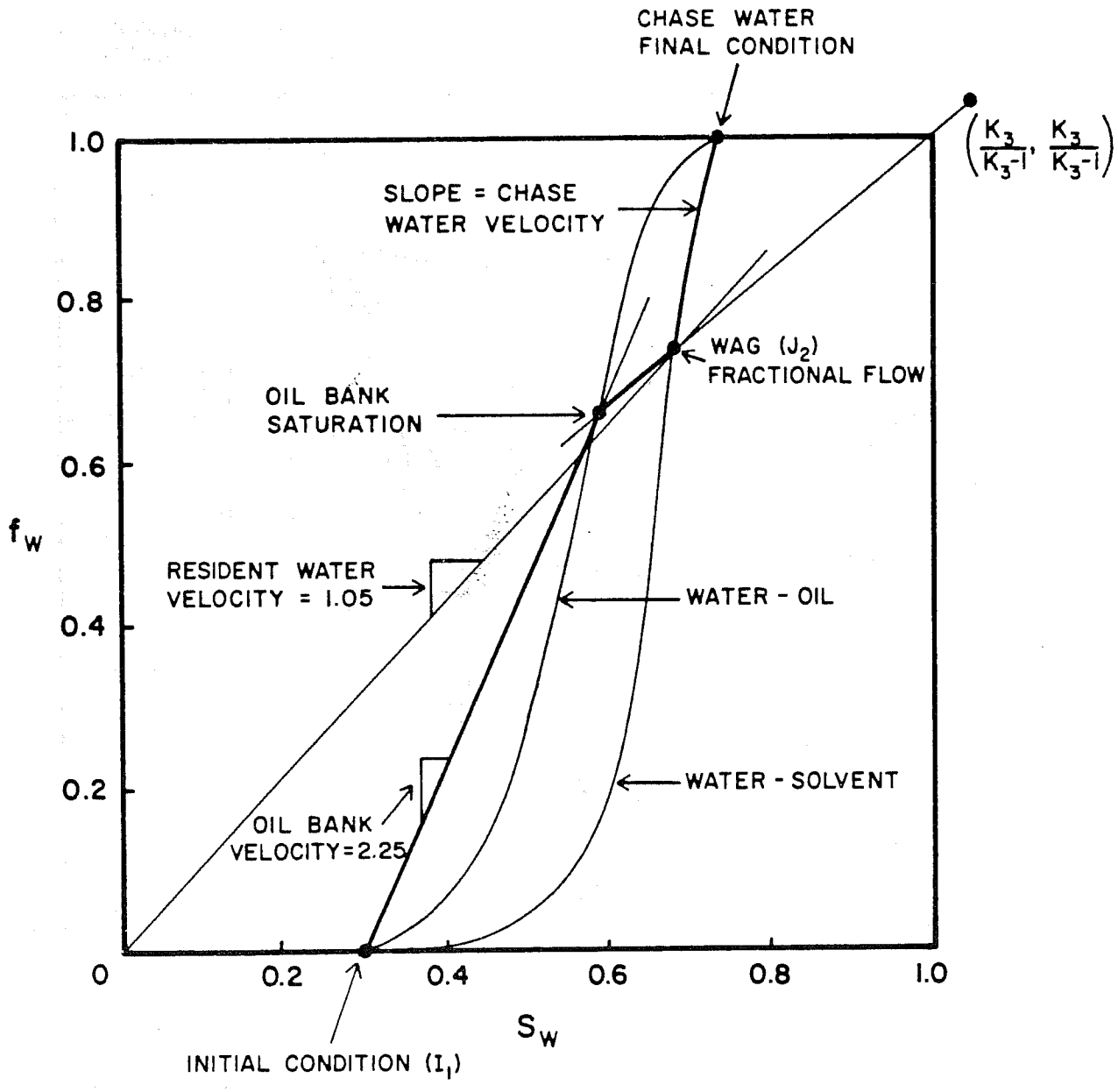

FRACTIONAL FLOW CONSTRUCTION FOR $J_2 \rightarrow I_1$

Figure 7

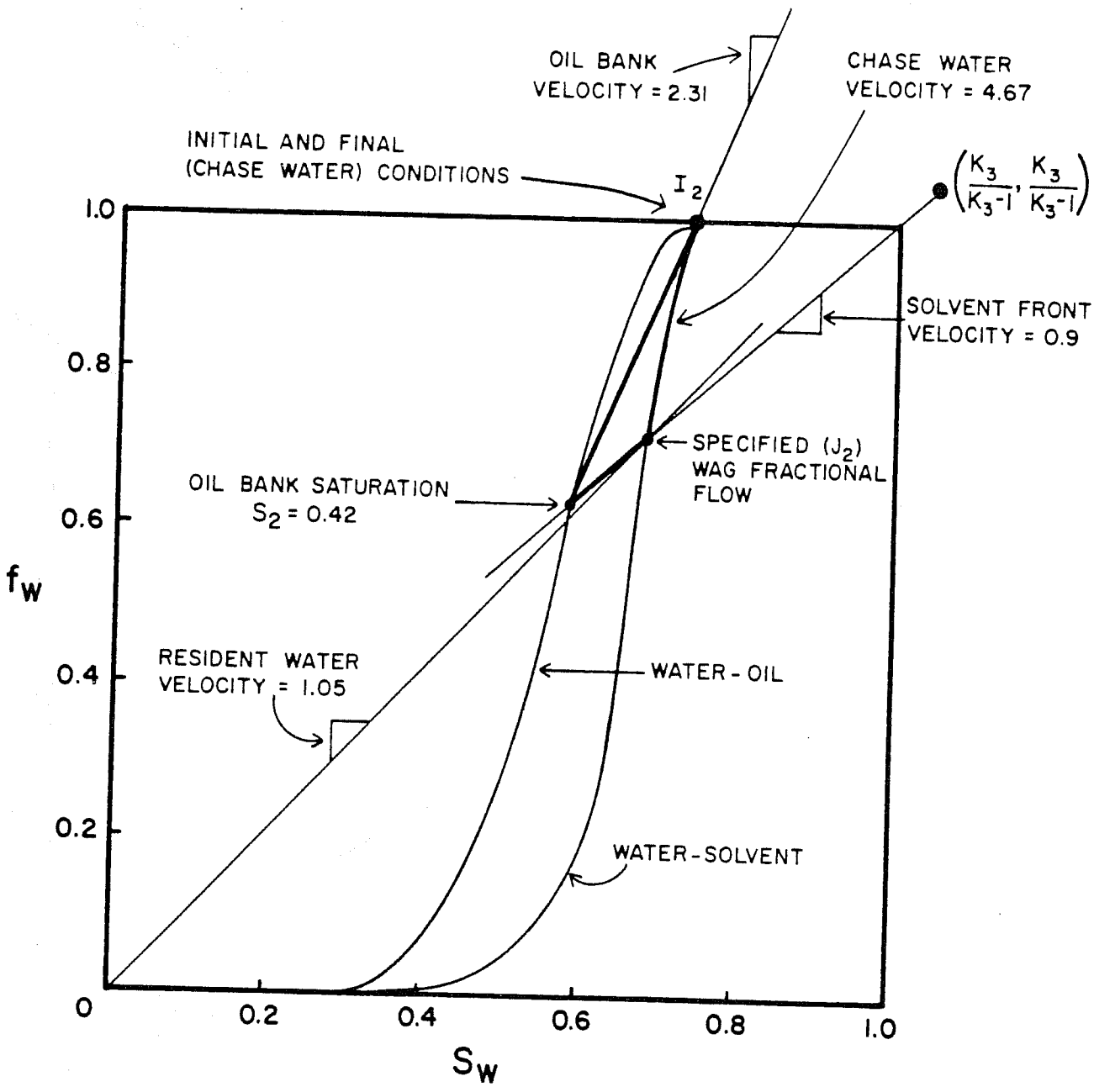

FRACTIONAL FLOW CONSTRUCTION FOR $J_2 \rightarrow I_2$

Figure 8

Figure 9

COMPOSITION PATH DIAGRAM FOR FINGERING CASES

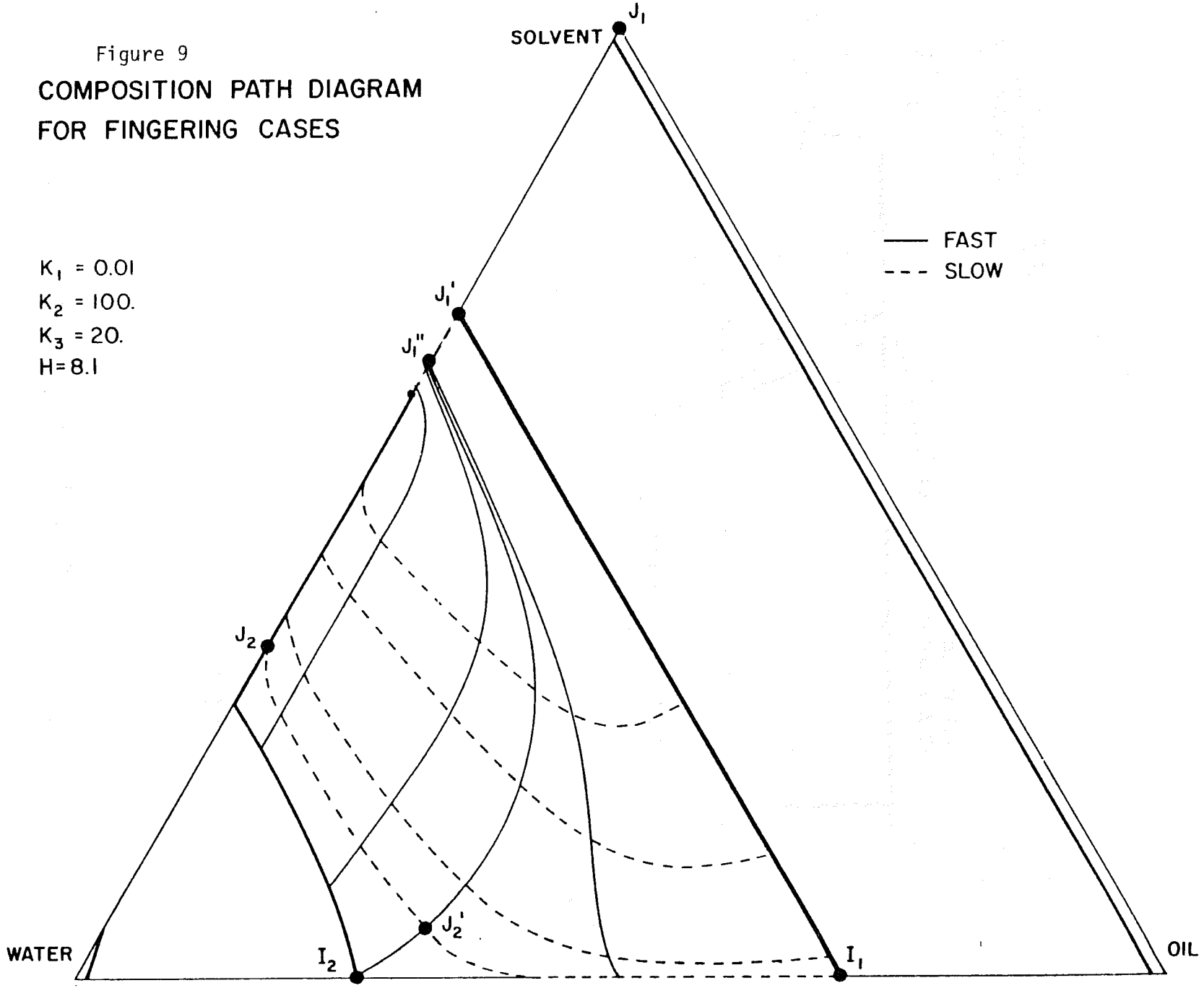

Figure 10

EFFLUENT HISTORIES FOR FOUR FINGERING CASES

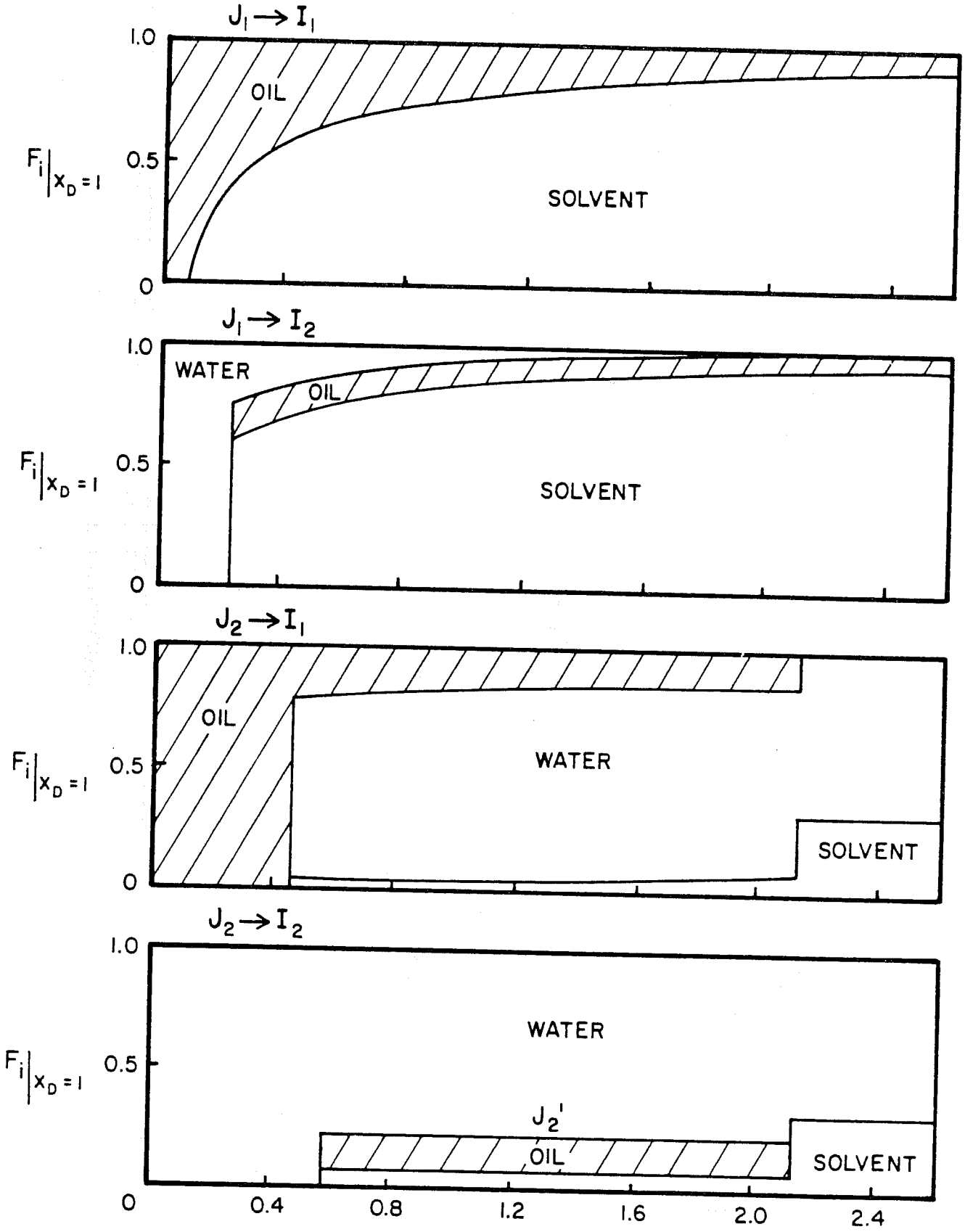

Figure 11

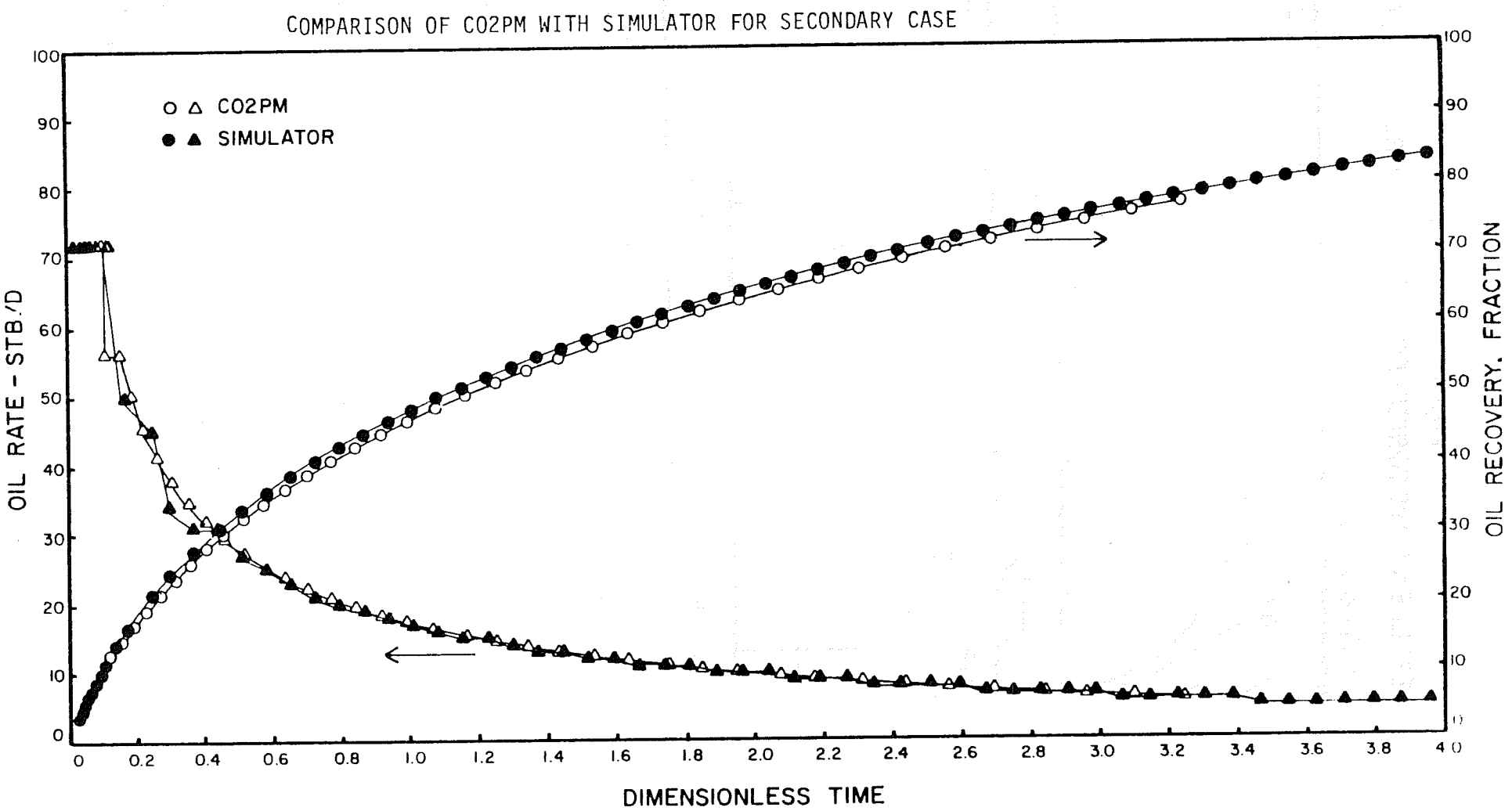
COMPARISON OF CO2PM WITH SIMULATOR FOR SECONDARY CASE
CO2PM
SIMULATOR
OIL RATE - STB/D
OIL RECOVERY, FRACTION
DIMENSIONLESS TIME
0
10
20
30
40
50
60
70
80
90
100
0.2
0.4
0.6
0.8
1.0
1.2
1.4
1.6
1.8
2.0
2.2
2.4
2.6
2.8
3.0
3.2
3.4
3.6
3.8
4.0

Figure 12

COMPARISON OF CO2PM WITH SIMULATOR FOR TERTIARY CASE

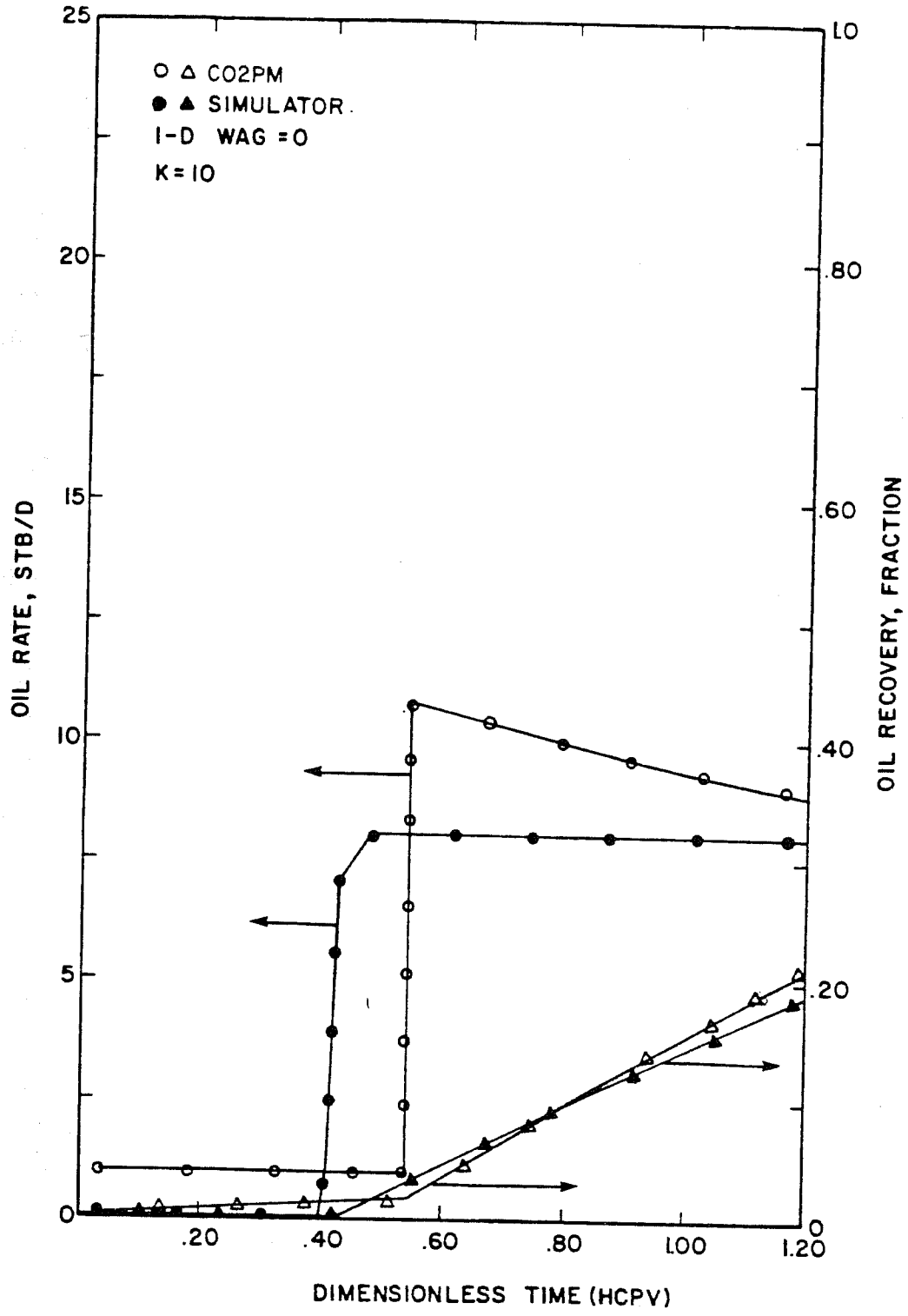

Figure 13

COMPARISON OF CO2PM WITH SIMULATOR FOR TERTIARY CASE

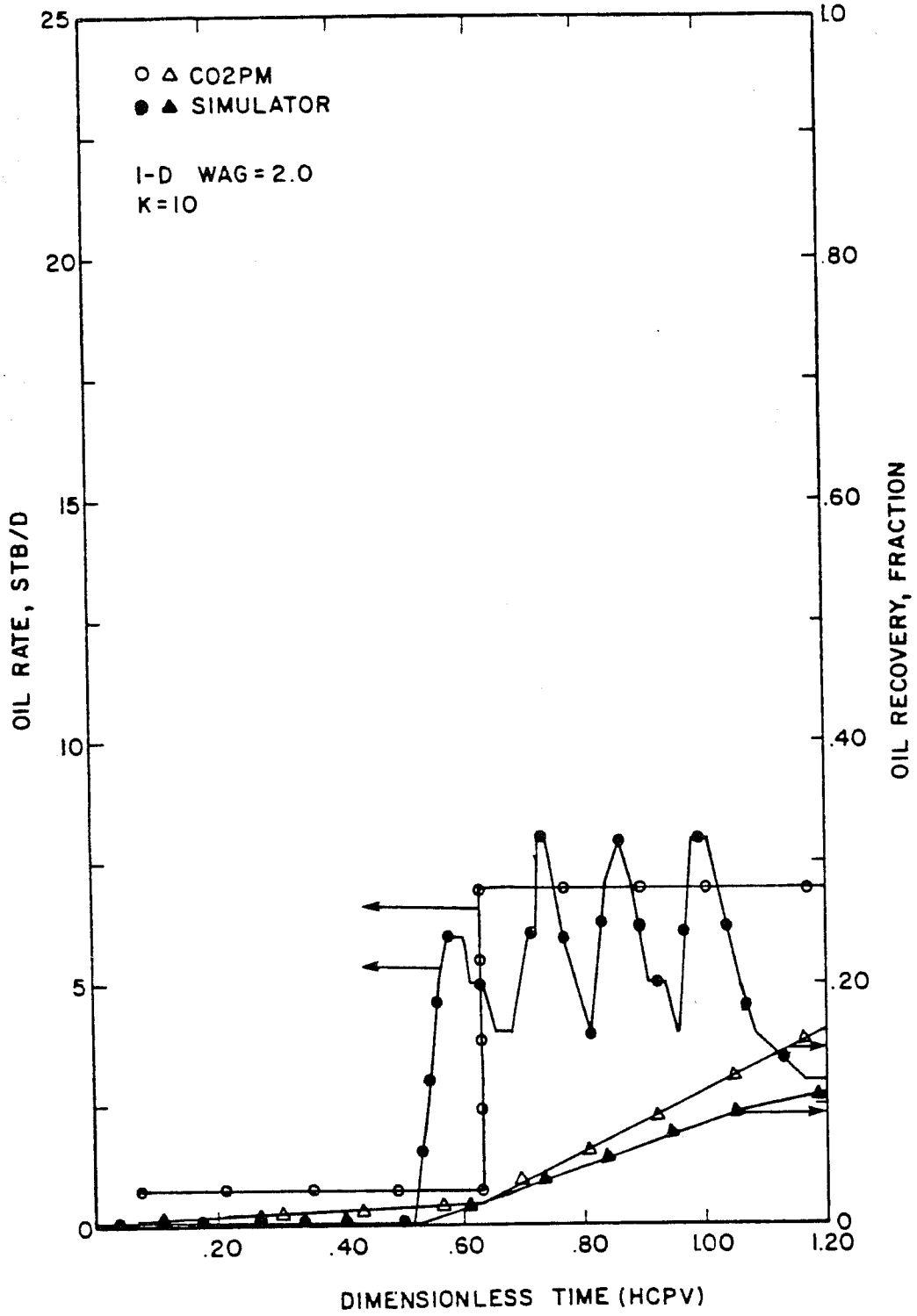

Figure 14

COMPARISON OF CO2PM WITH SIMULATOR FOR TERTIARY CASE

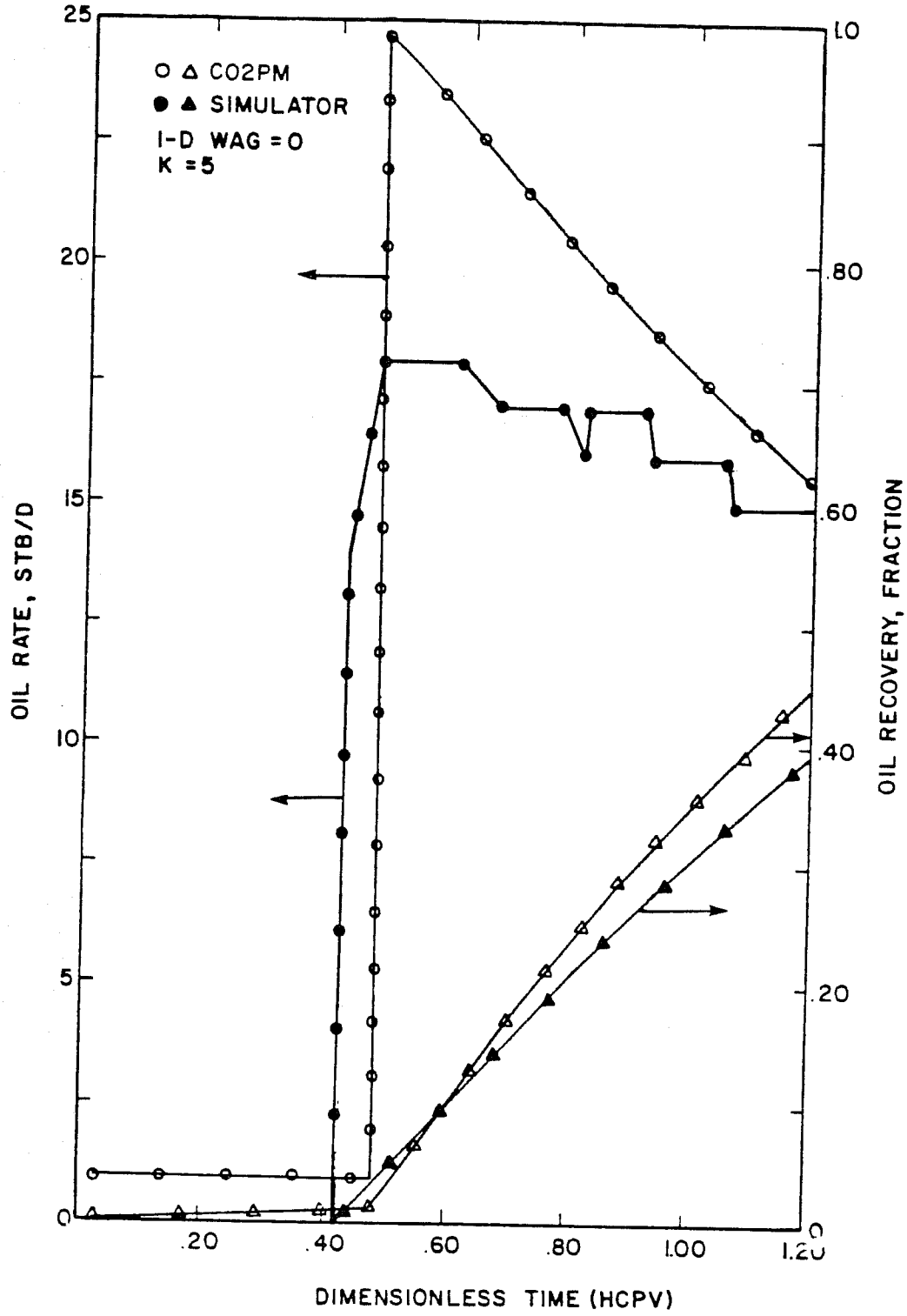

Figure 15

CUMULATIVE PRODUCTION OF WATER, OIL, AND GAS FOR BROOKHAVEN CRUDE IN A 6 FT. CONSOLIDATED CORE AT 1800 psig AND 109°F (FROM WHITEHEAD ET. AL.[19])

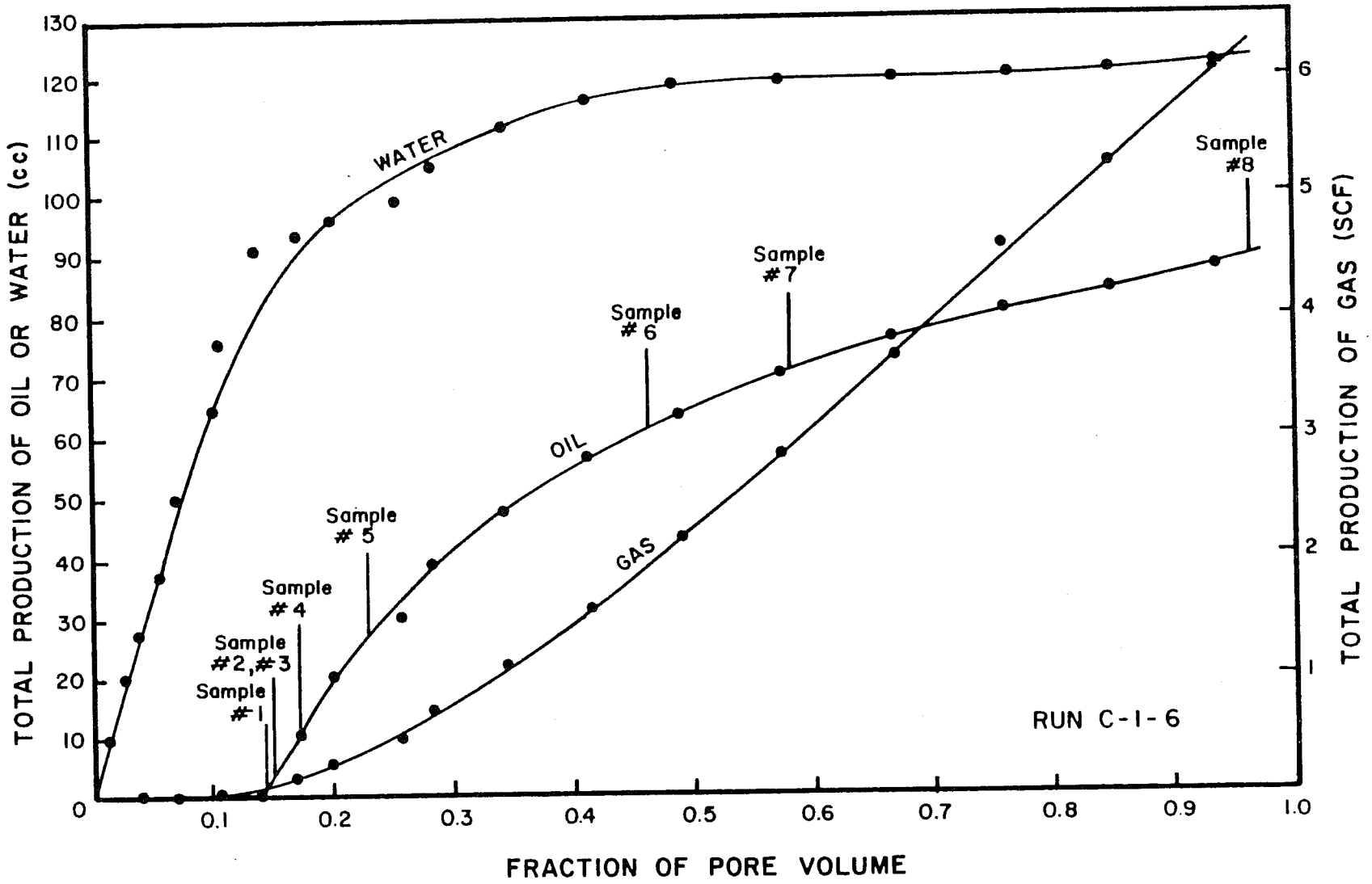

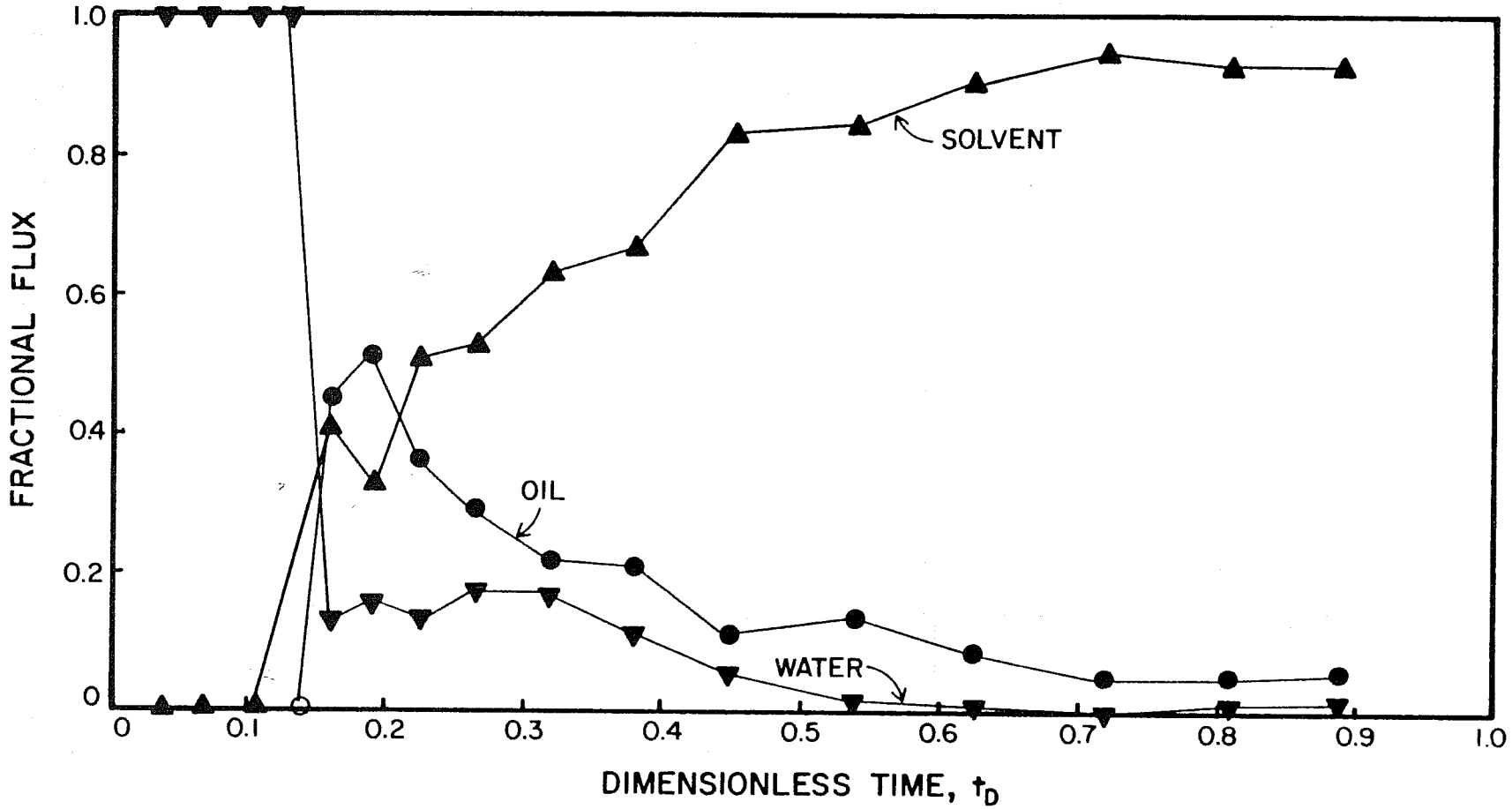

FRACTIONAL FLUXES OF COMPONENTS IN EXPERIMENT C-I-6

Figure 16

Figure 17

COMPARISON OF EXPERIMENTAL DATA & CO2PM RESULTS

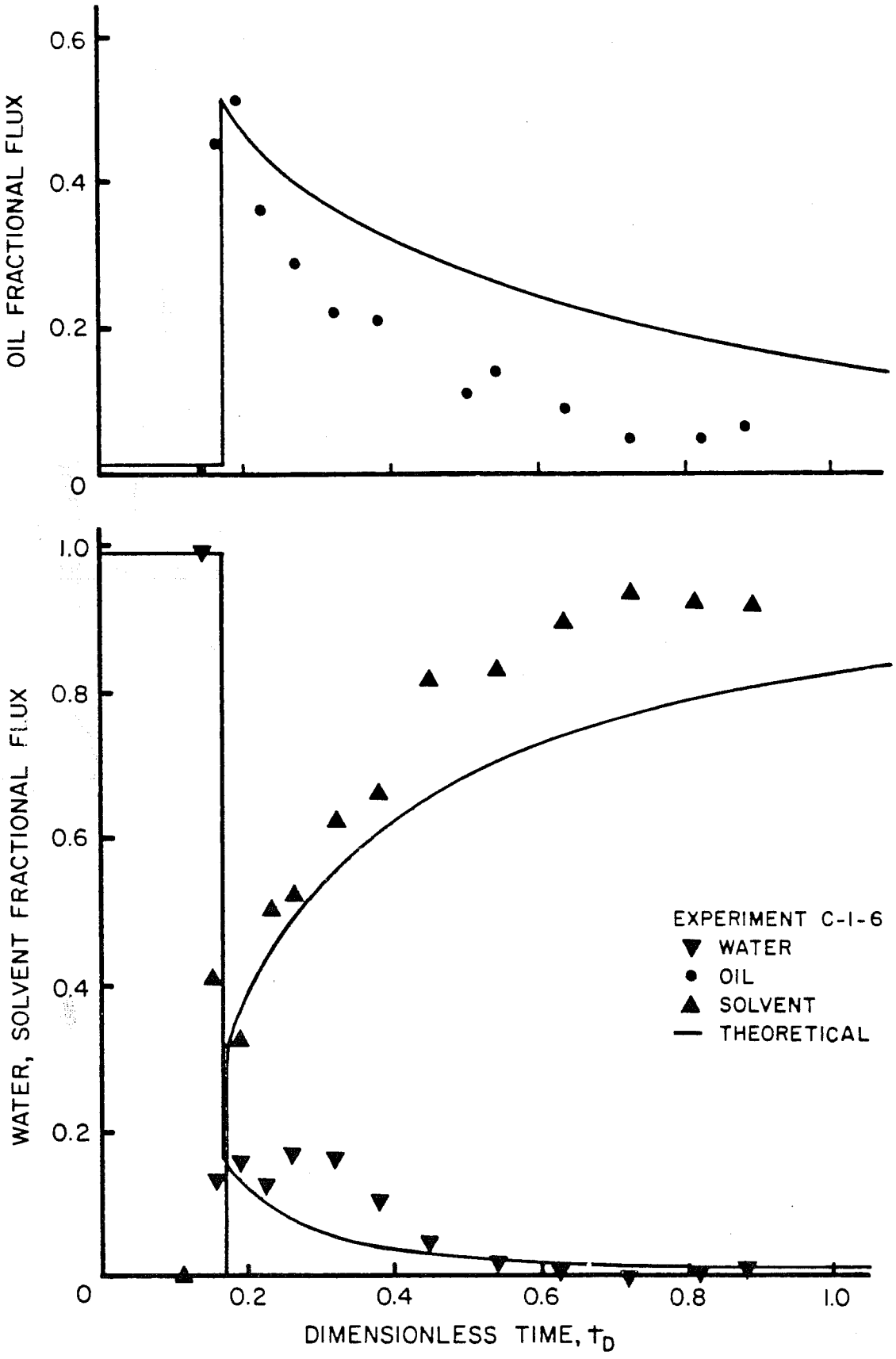

Figure 18

SCHEMATIC OF FRACTIONAL FLUX - CONCENTRATION CURVE (a), AND FLUX PROFILE (b)

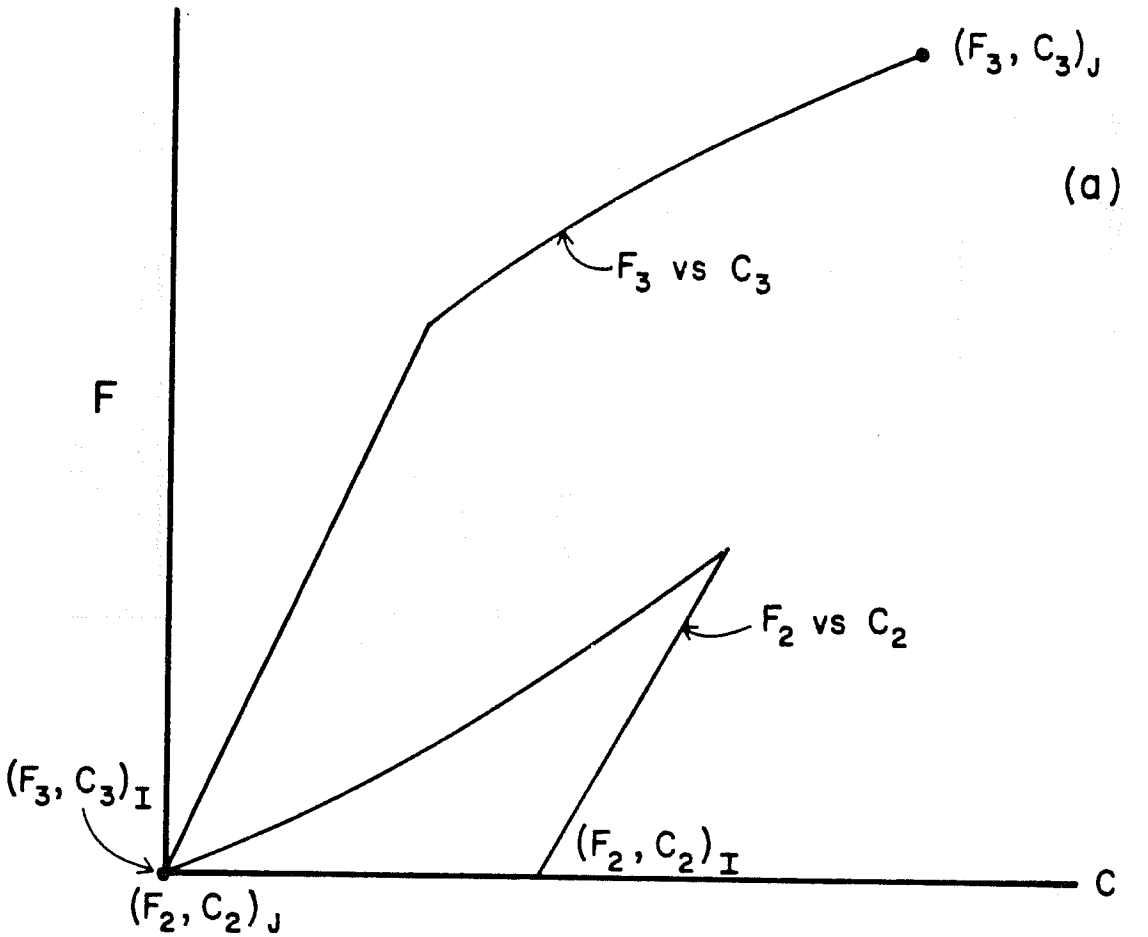

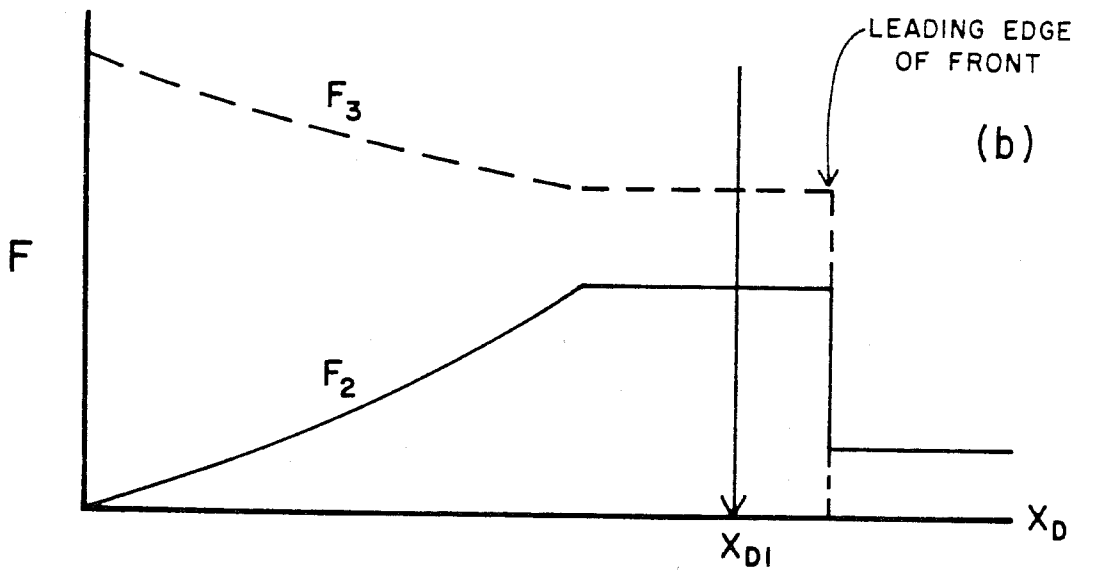

Figure 19

AVERAGE CONCENTRATION BEHIND THE FRONT FOR EXPERIMENT C-I-6

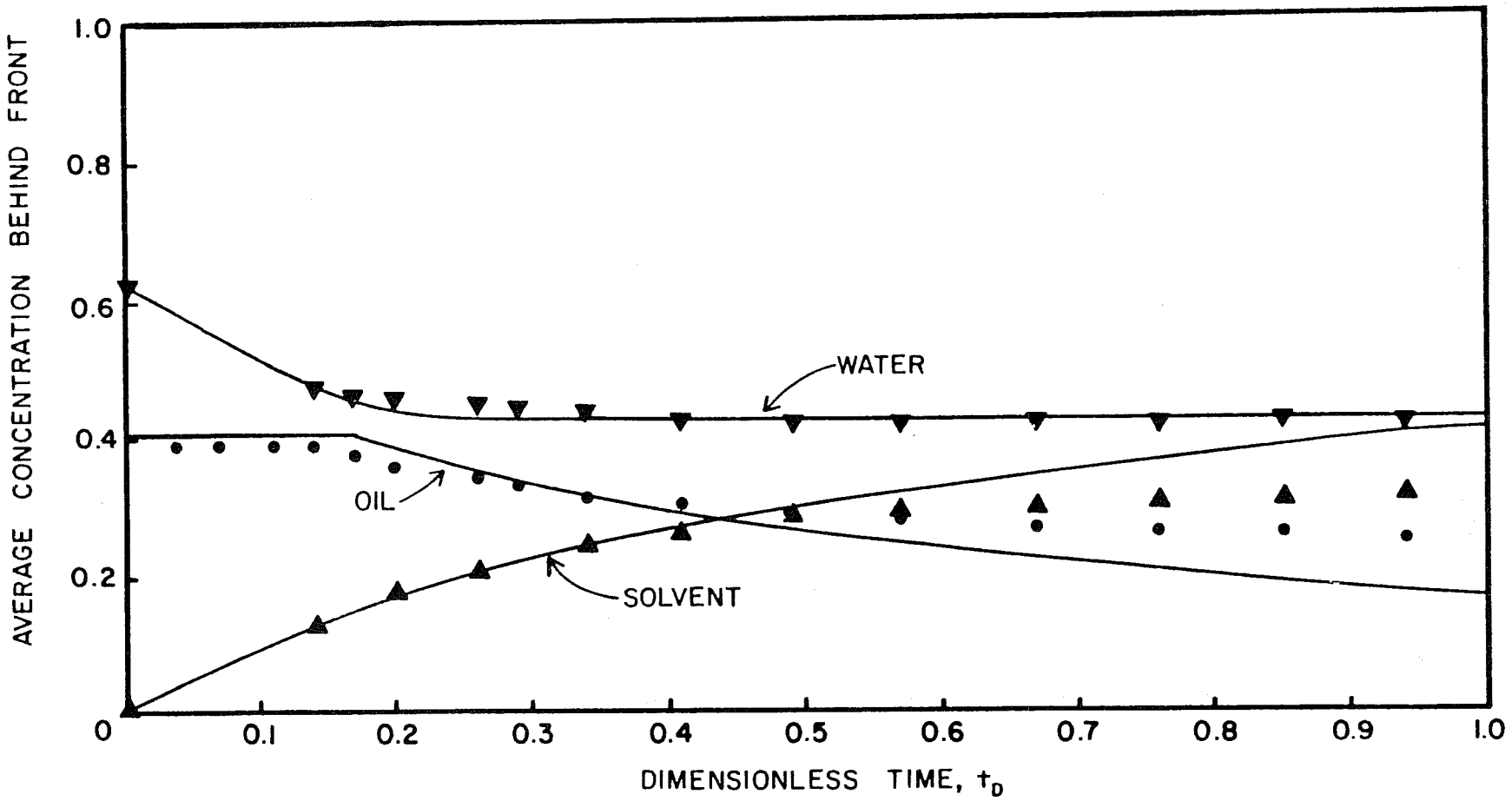

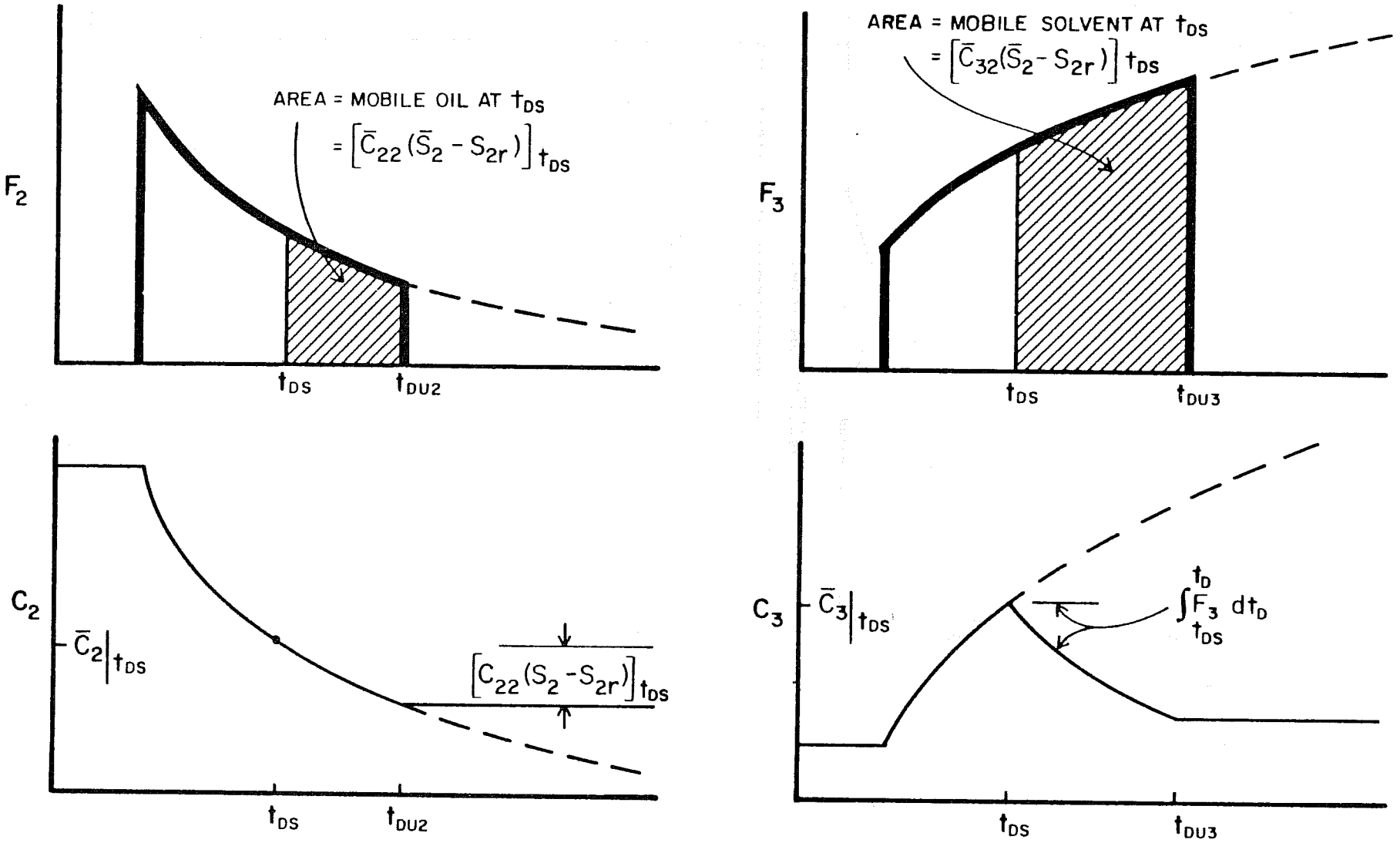

CORRECTION FOR FINITE SLUG SIZE

Figure 20

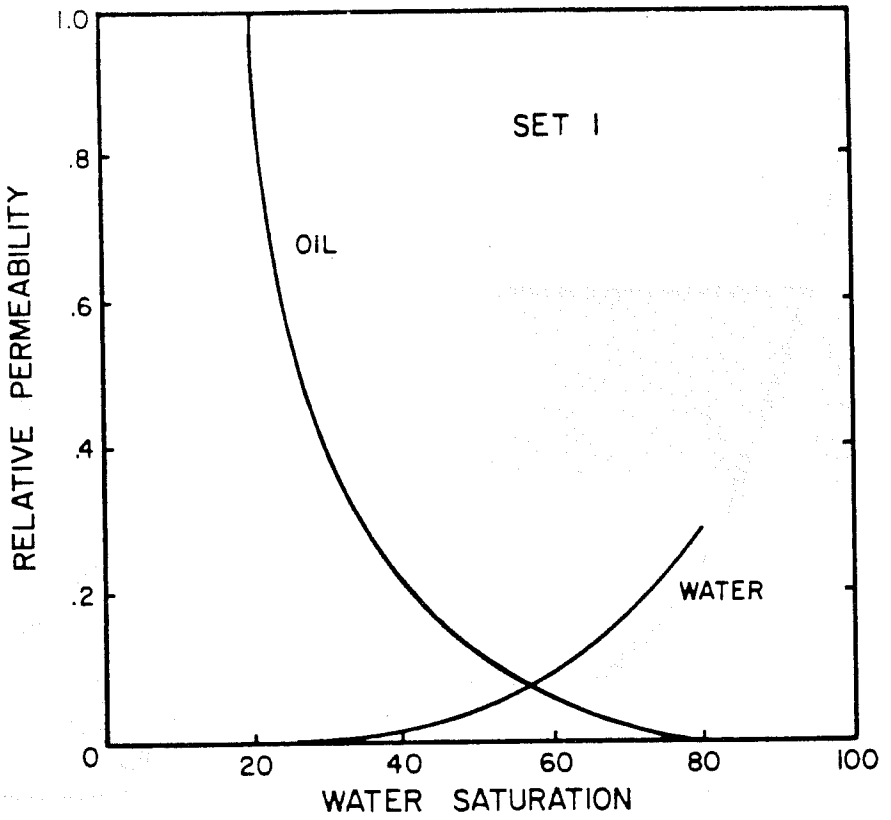

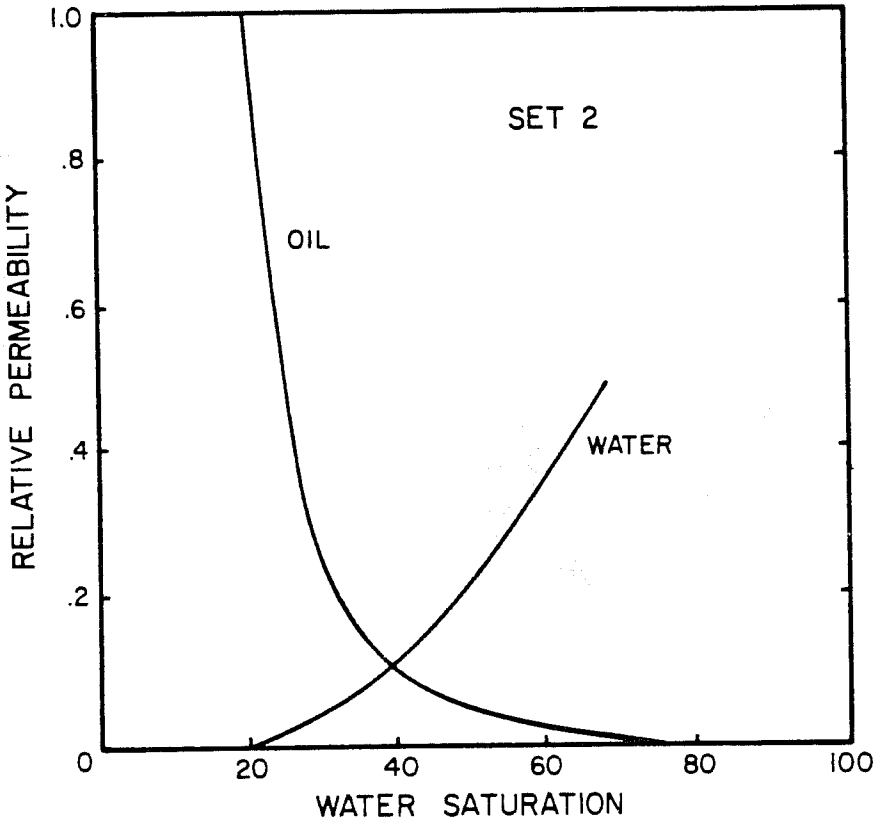

RELATIVE PERMEABILITY CURVES USED IN GRAVITY RUNS

Figure 21

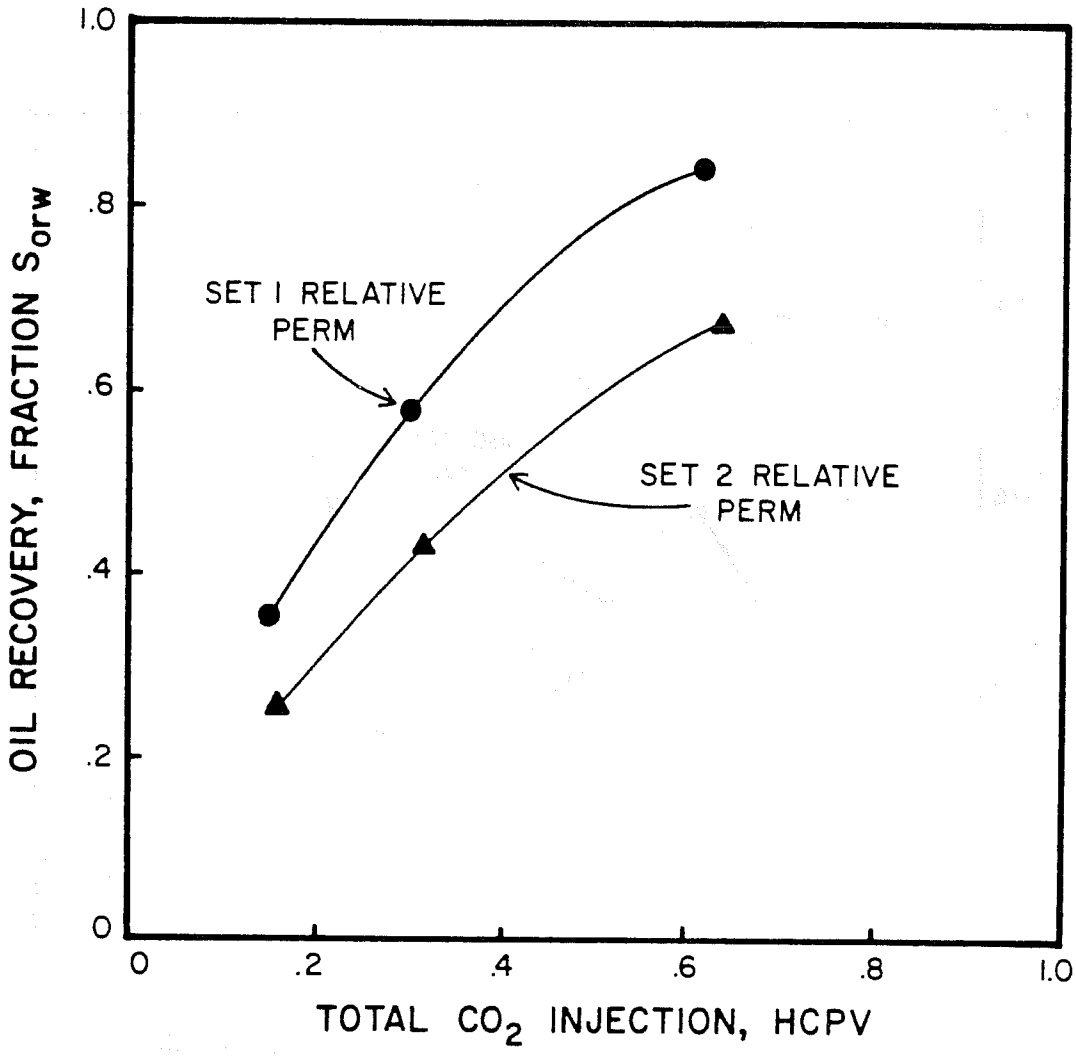

EFFECT OF RELATIVE PERMEABILITY CURVES ON SINGLE LAYER ($t_h/t_v = 0$) OIL RECOVERY

Figure 22

Figure 23

EFFECT OF PATTERN SIZE ON RECOVERY
FOR 5-SPOT PATTERN

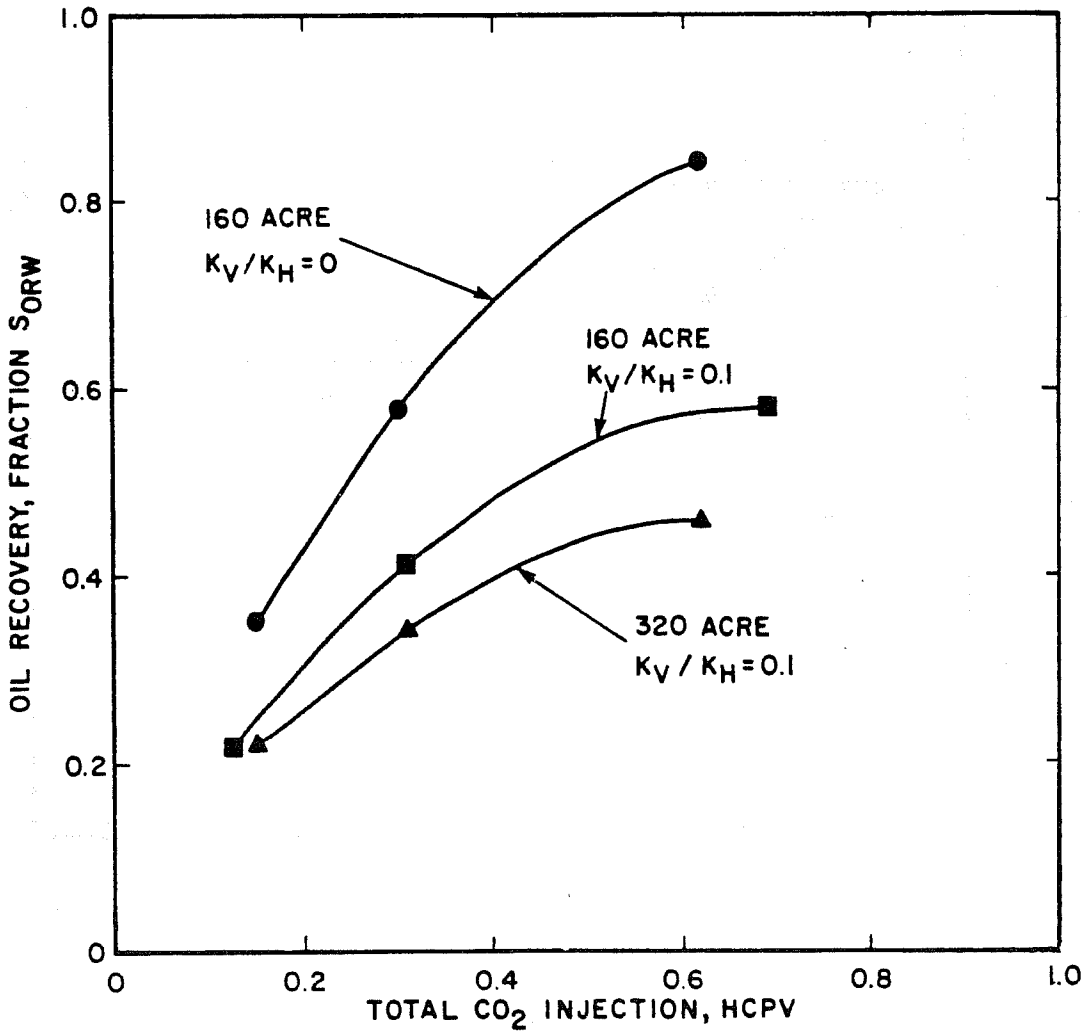

Figure 24

Normalized vs. t_h/t_v

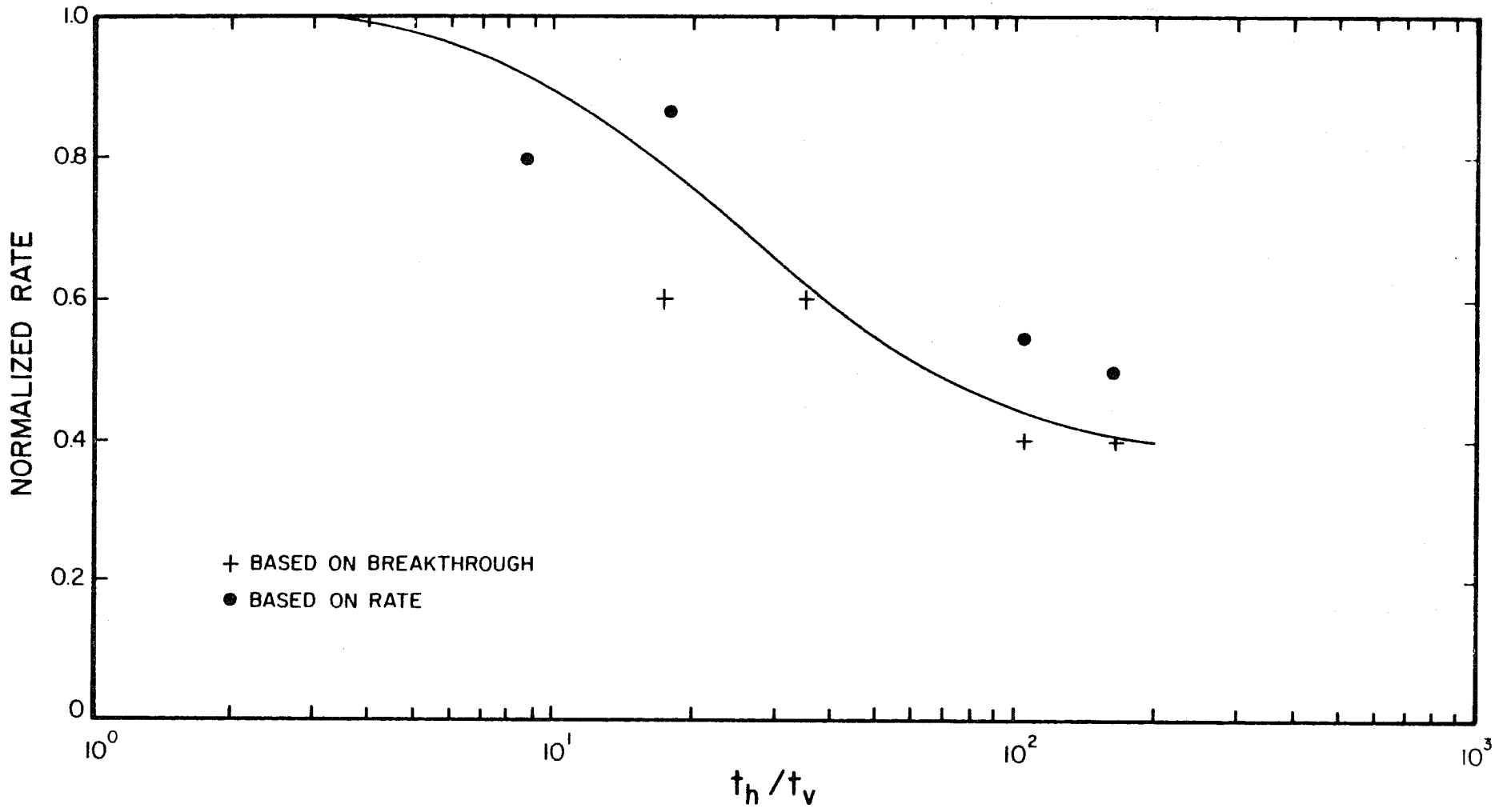

Figure 25

Normalized Rate vs. Koval Factor

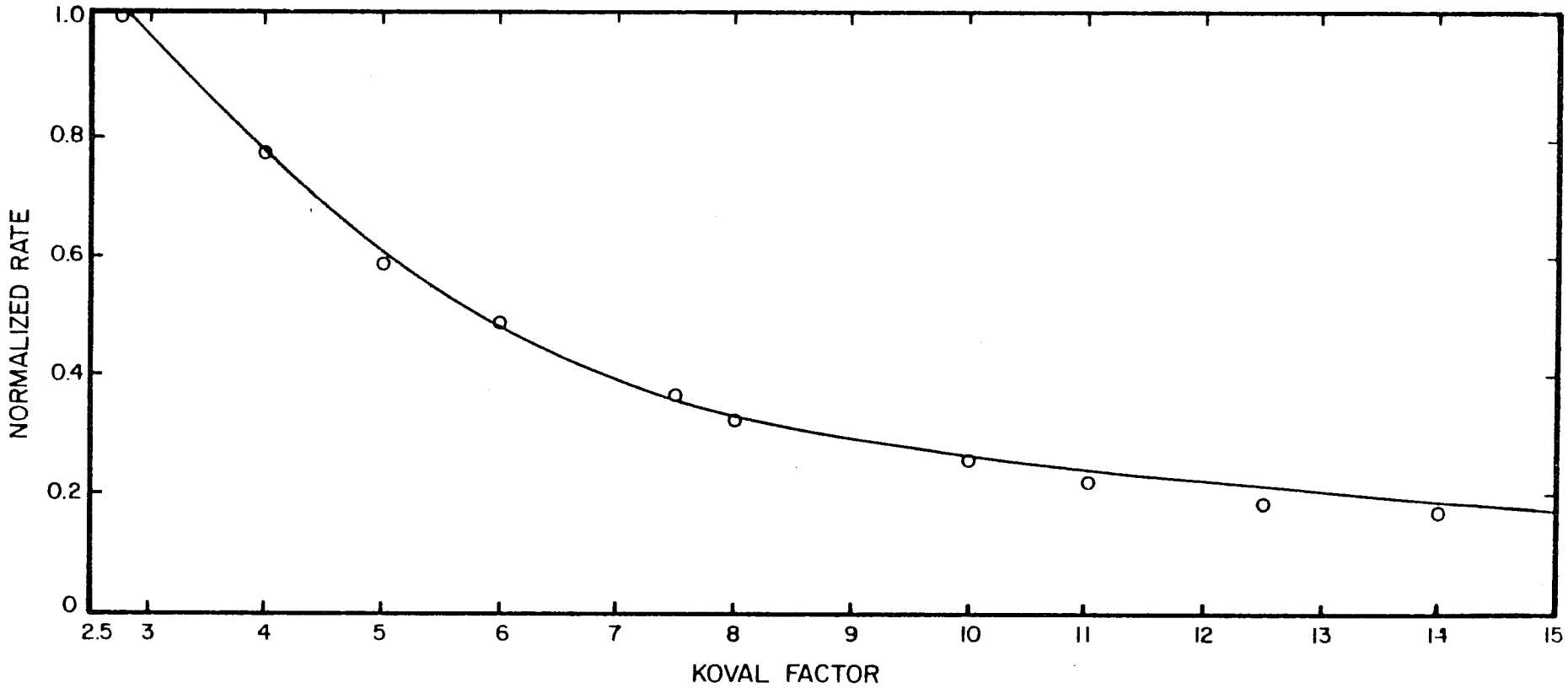

Figure 26

Gravity Correction Factor vs. t_k/t_v

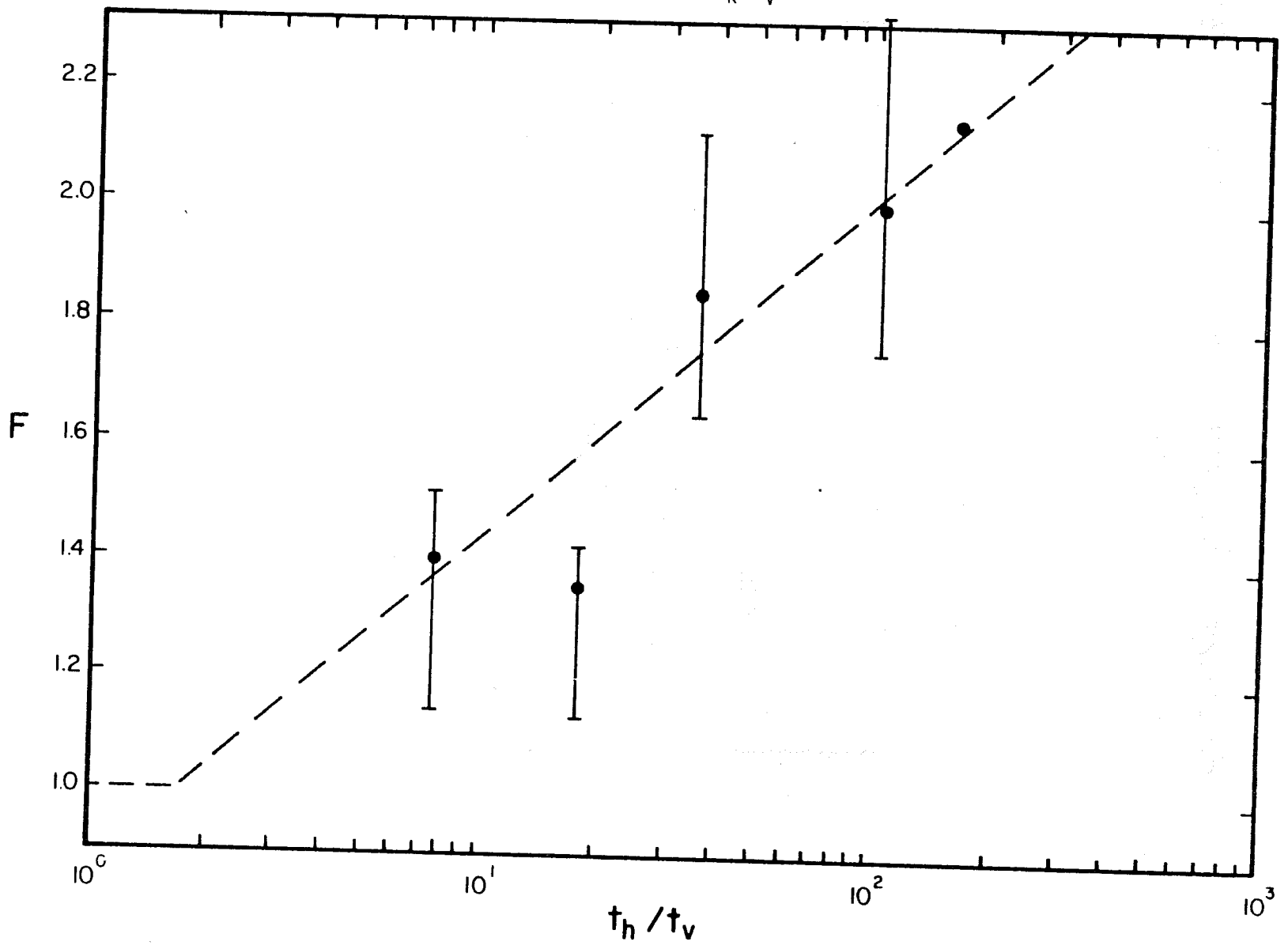

Figure 27

SCHEMATIC ILLUSTRATIONS OF CONTACTED AND INVADED AREA IN 1/4 5-SPOTS

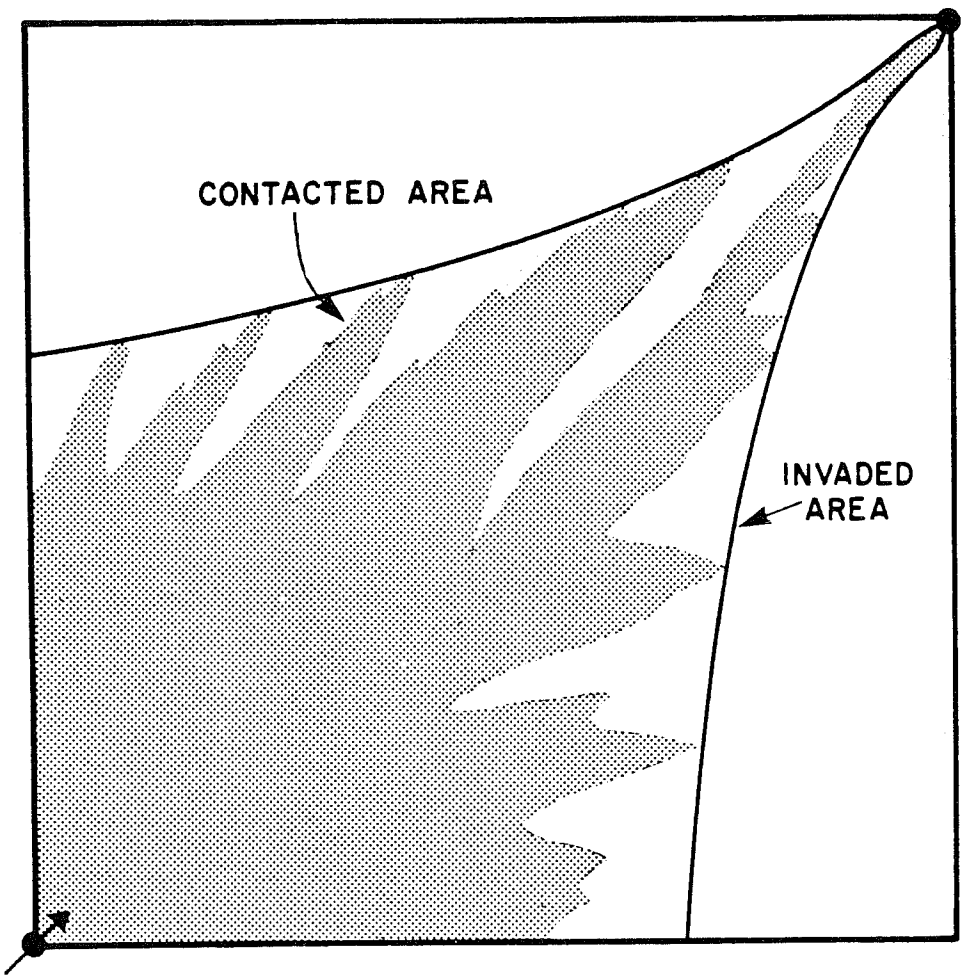

Figure 28

AREAL SWEEP CORRELATIONS FROM CLARIDGE

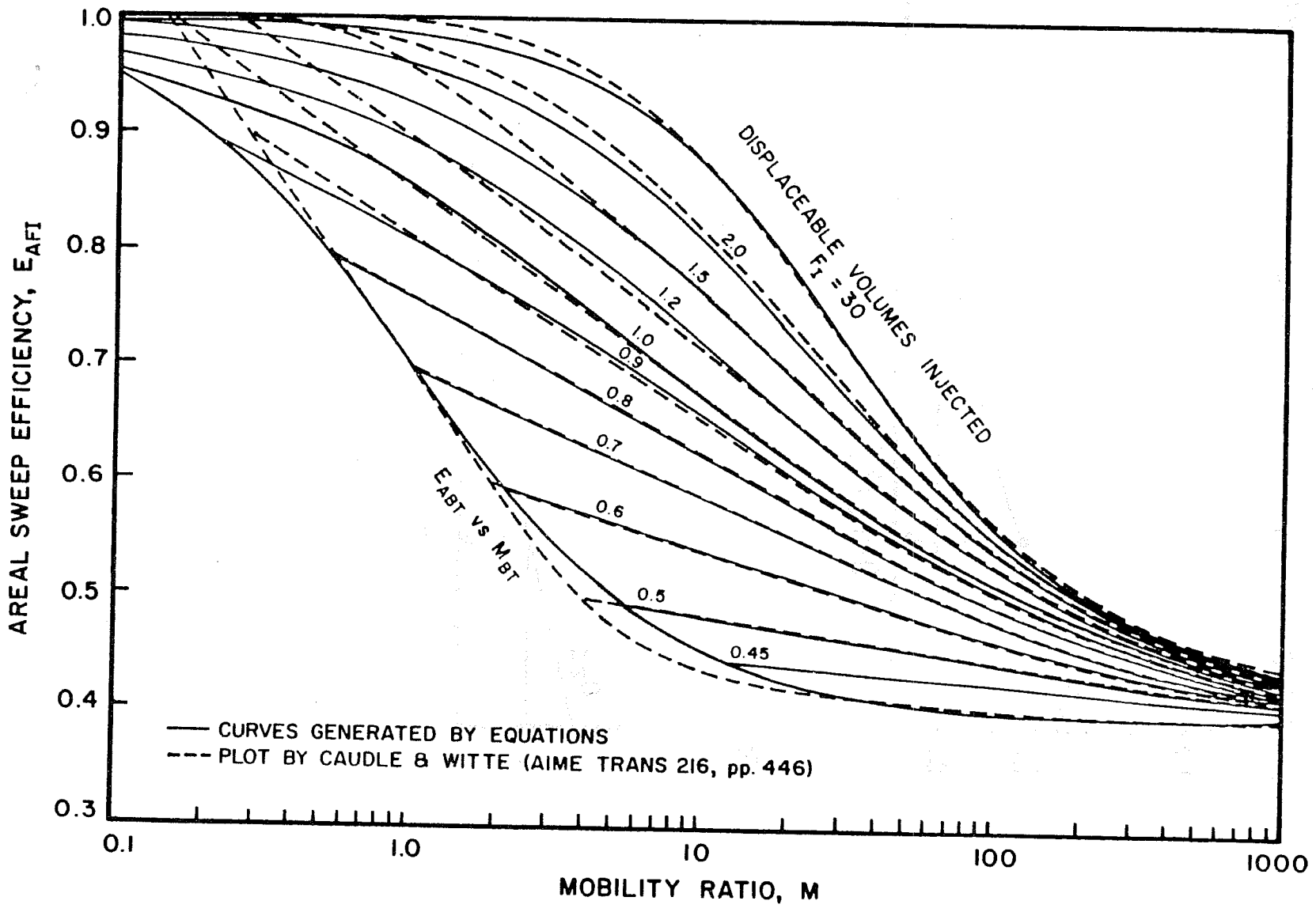

Figure 29

SCHEMATIC OF THE BEHAVIOR OF AVERAGE CONCENTRATIONS

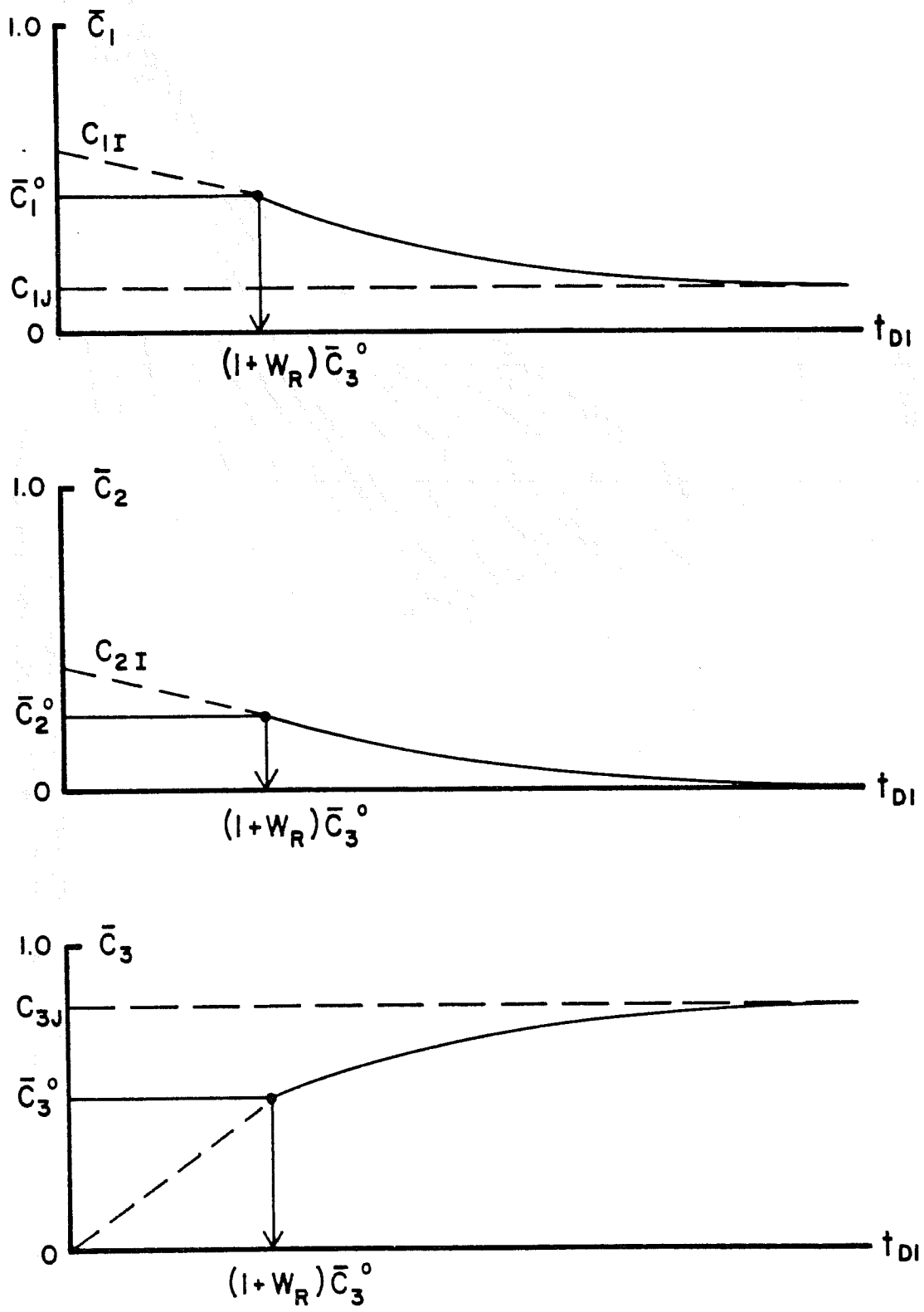

Figure 30

CUMULATIVE OIL PRODUCED FOR EXPERIMENT C-I-6

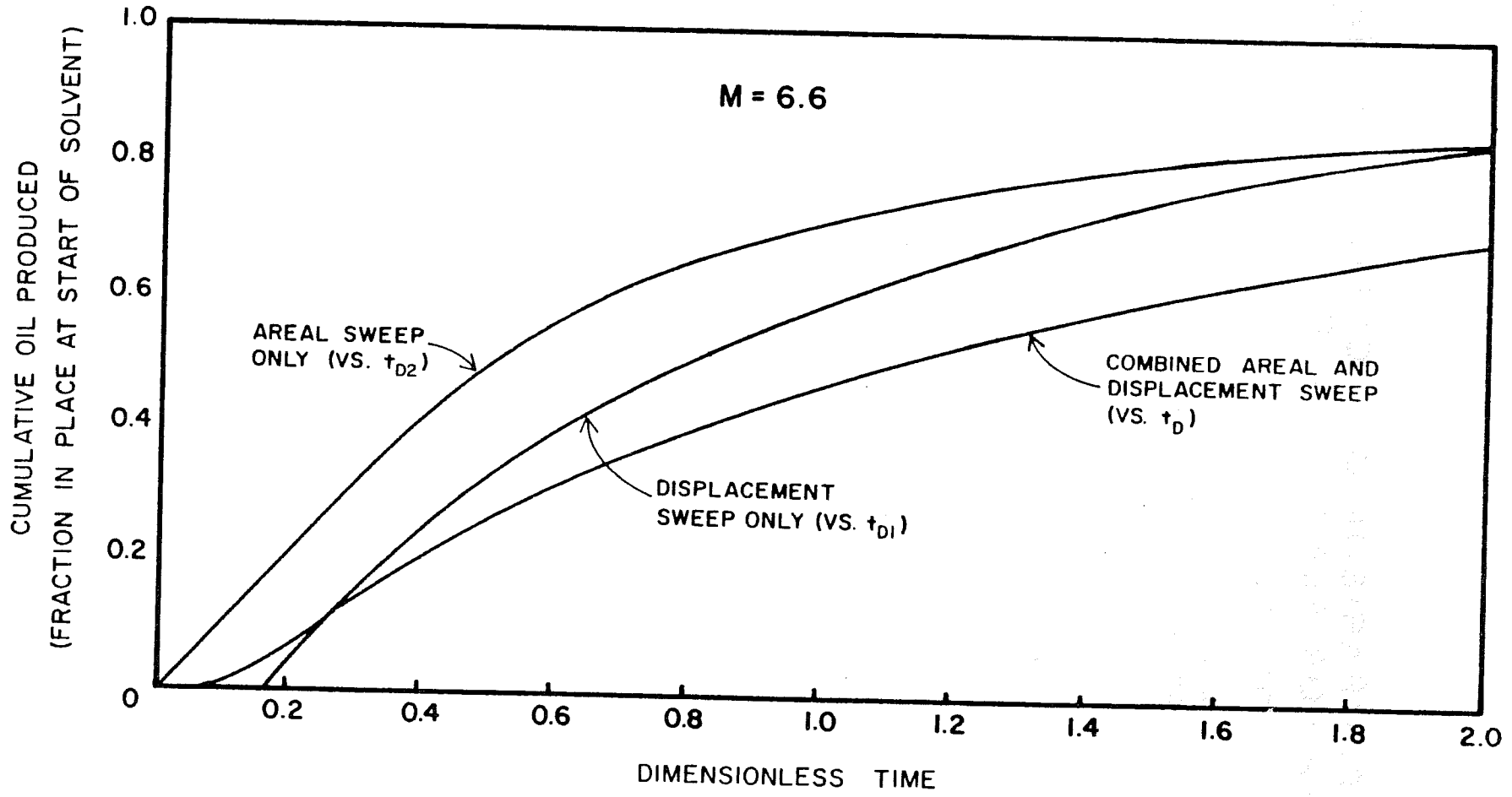

Figure 31

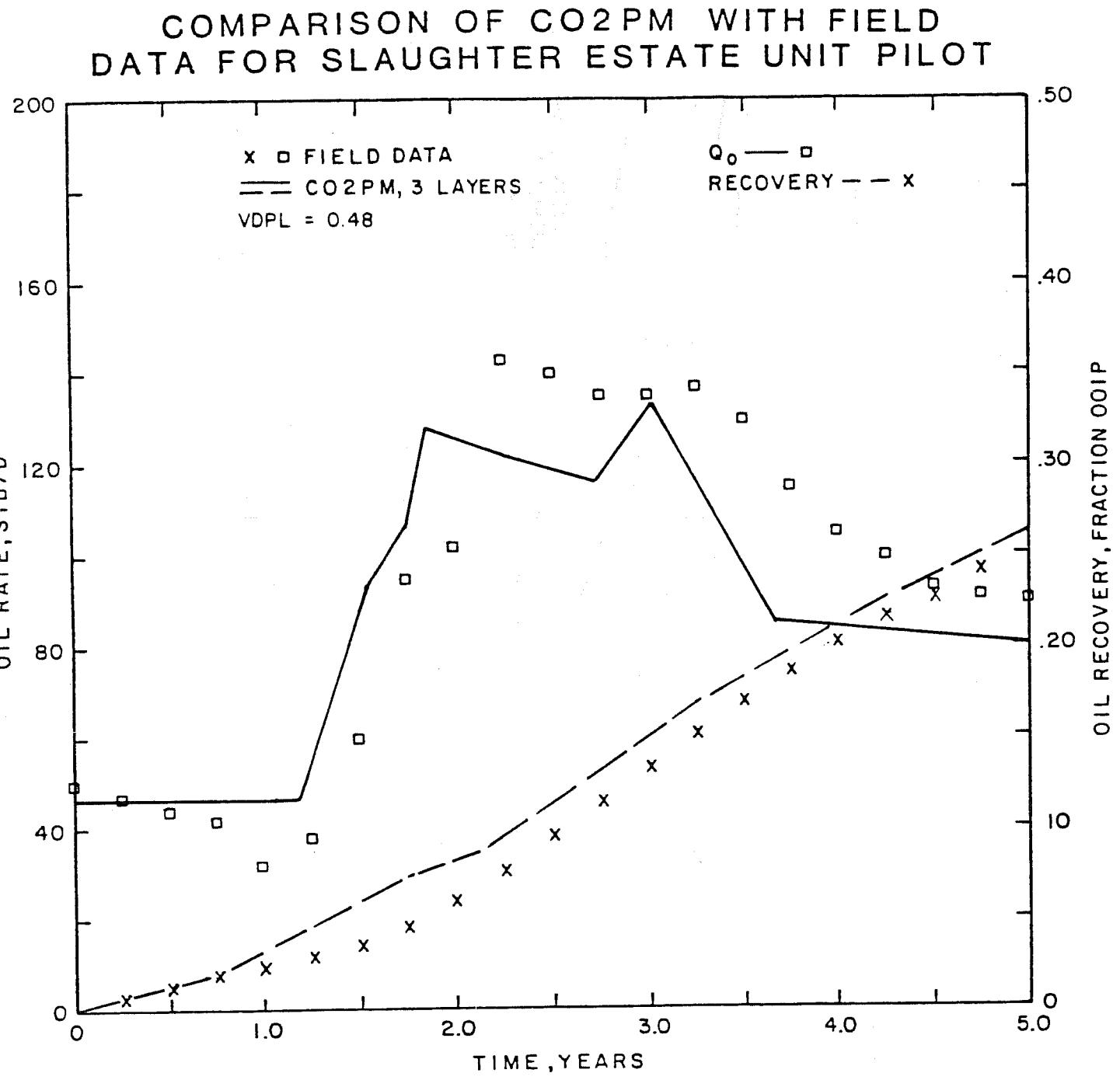
COMPARISON OF CO2PM WITH FIELD DATA FOR SLAUGHTER ESTATE UNIT PILOT
x □ FIELD DATA
CO2PM, 3 LAYERS
VDPL = 0.48
Q_o —— □
RECOVERY — — x
OIL RATE, STB/D
OIL RECOVERY, FRACTION OOIP
TIME, YEARS
0
40
80
120
160
200
0
10
.20
.30
.40
.50
1.0
2.0
3.0
4.0
5.0

Figure 32

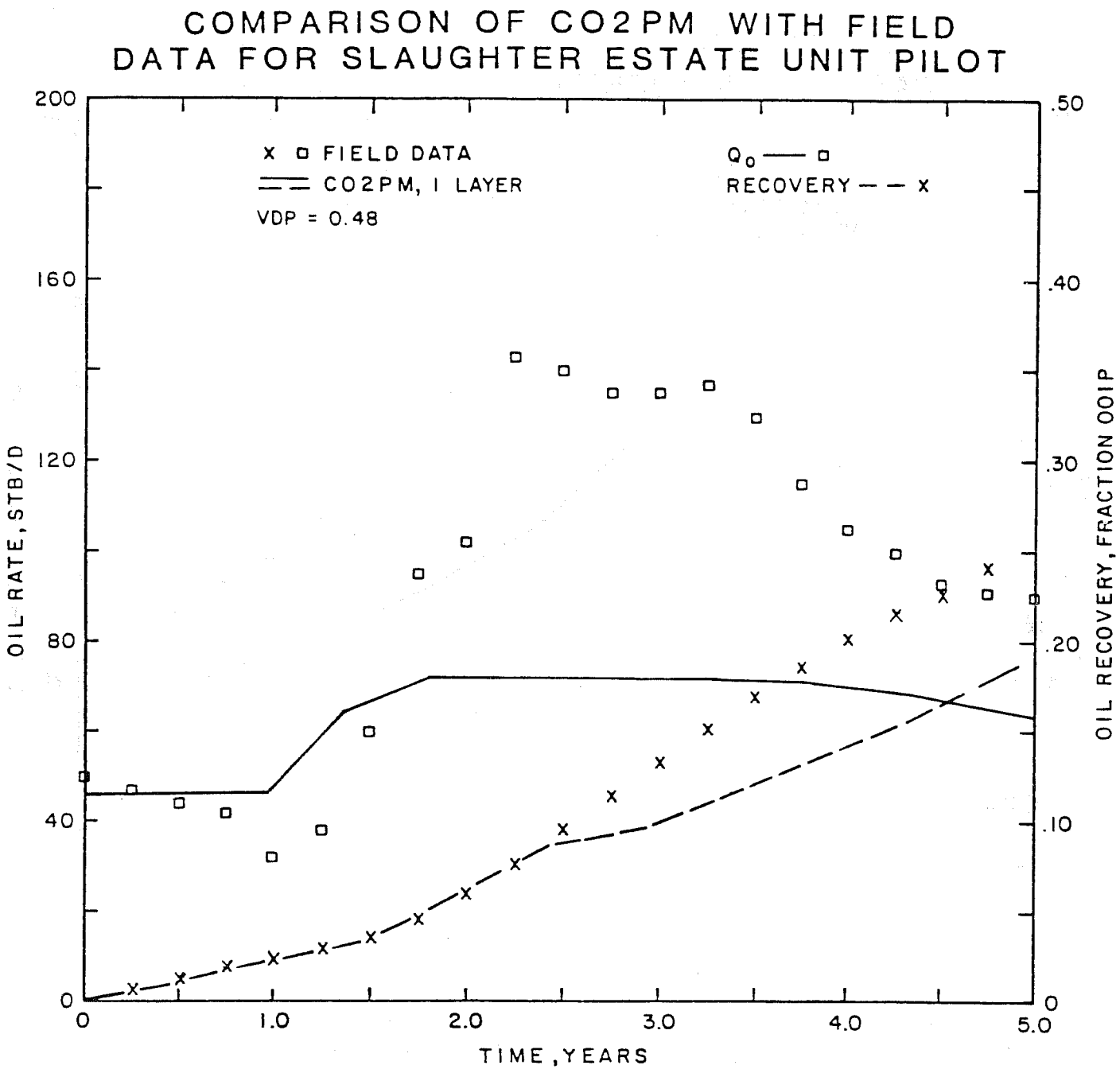
COMPARISON OF CO2PM WITH FIELD DATA FOR SLAUGHTER ESTATE UNIT PILOT
X □ FIELD DATA
CO2PM, 1 LAYER
VDP = 0.48
Q0 —— □
RECOVERY — — X
OIL RATE, STB/D
OIL RECOVERY, FRACTION OOIP
TIME, YEARS
0
40
80
120
160
200
0
.10
.20
.30
.40
.50
0
1.0
2.0
3.0
4.0
5.0

Figure 33

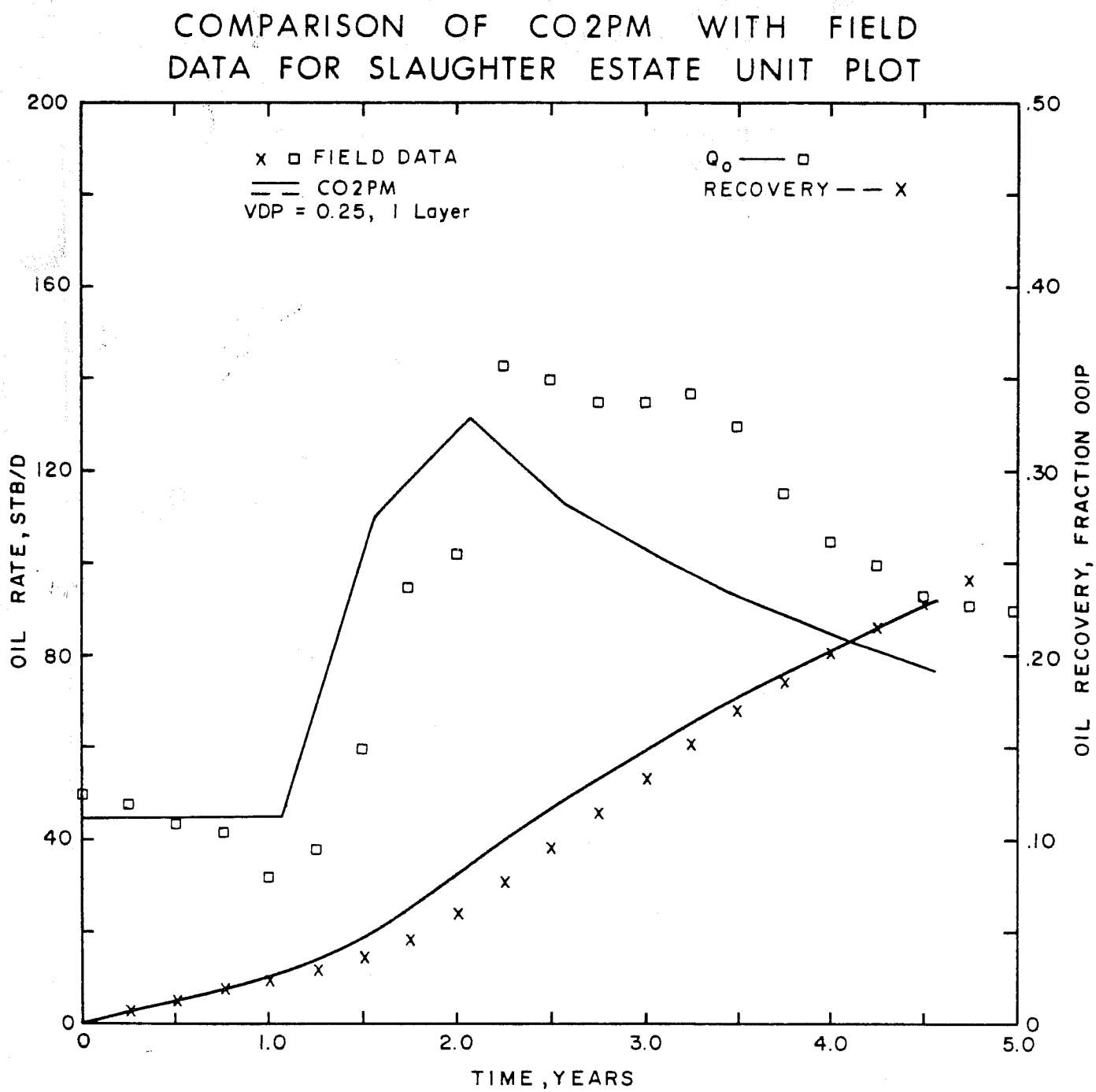
COMPARISON OF CO2PM WITH FIELD DATA FOR SLAUGHTER ESTATE UNIT PLOT
x □ FIELD DATA
CO2PM
VDP = 0.25, 1 Layer
Q_o —— □
RECOVERY — — X
OIL RATE, STB/D
OIL RECOVERY, FRACTION OOIP
TIME, YEARS
200
160
120
80
40
0
.50
.40
.30
.20
.10
0
1.0
2.0
3.0
4.0
5.0

FIGURE 34

SAN ANDRES ZONE V WATER-OIL RELATIVE PERMEABILITY CURVES

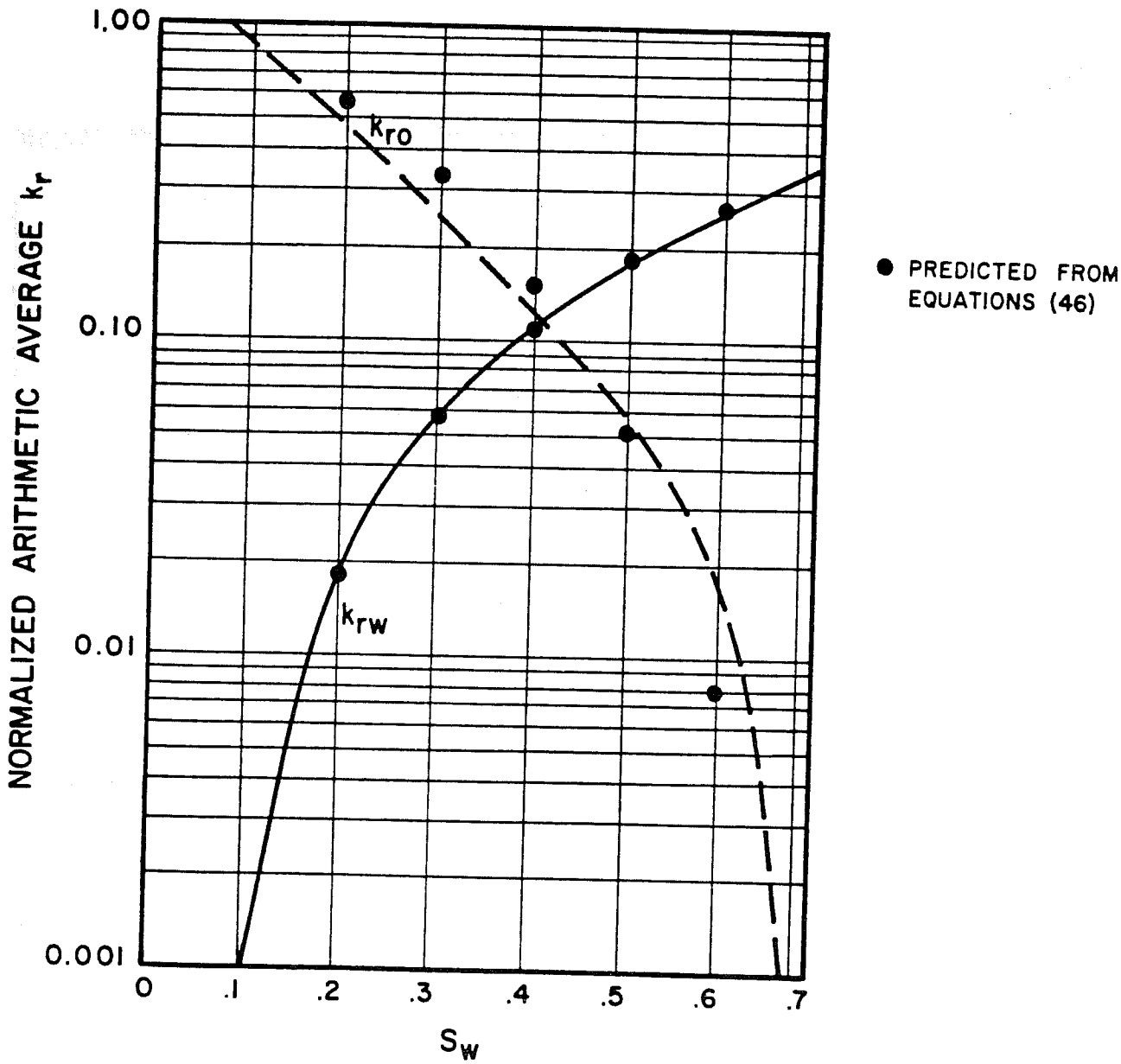

Figure 35

COMPARISON OF FLOW CAPACITY-STORAGE CAPACITY RELATIONS

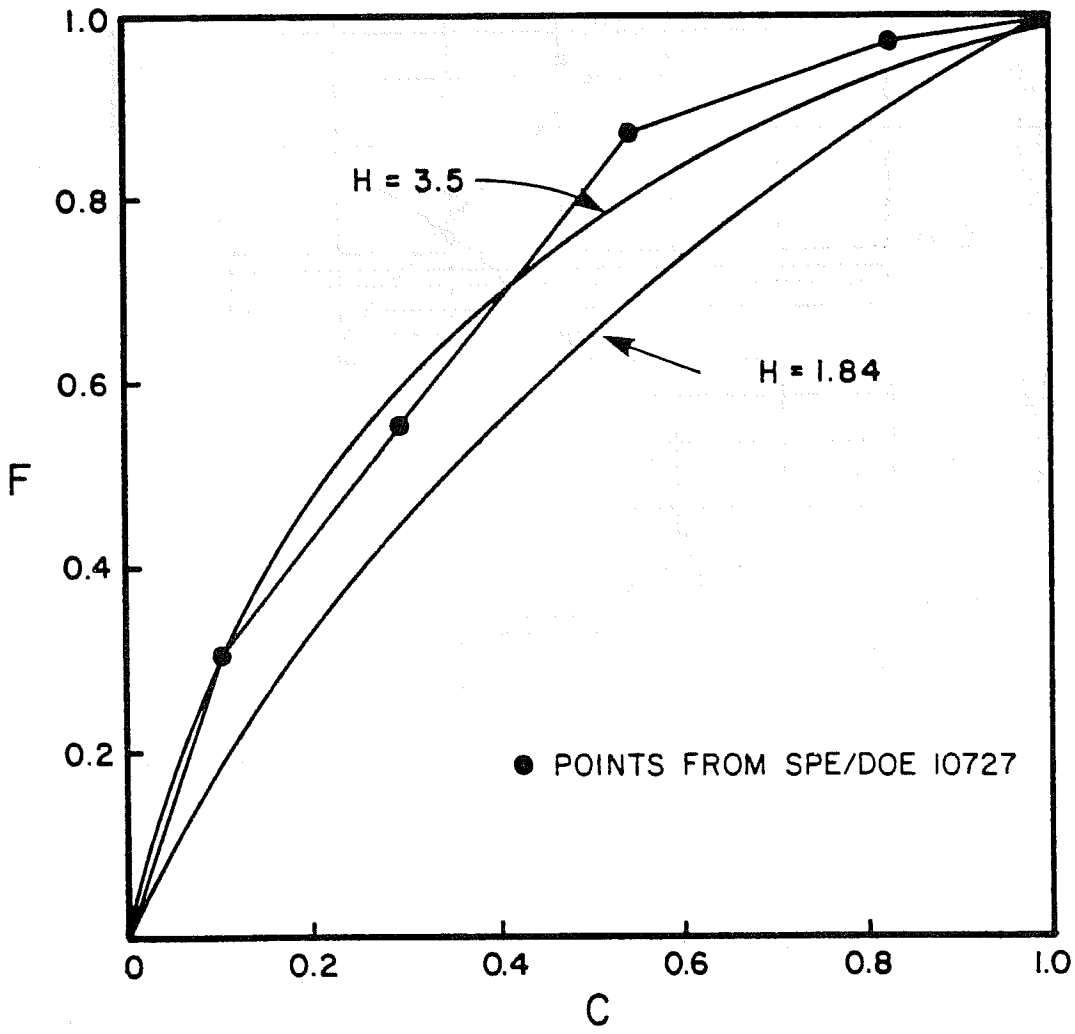

Figure 36

COMPARISON OF CO2PM AND WASSIM SIMULATOR FOR DENVER UNIT

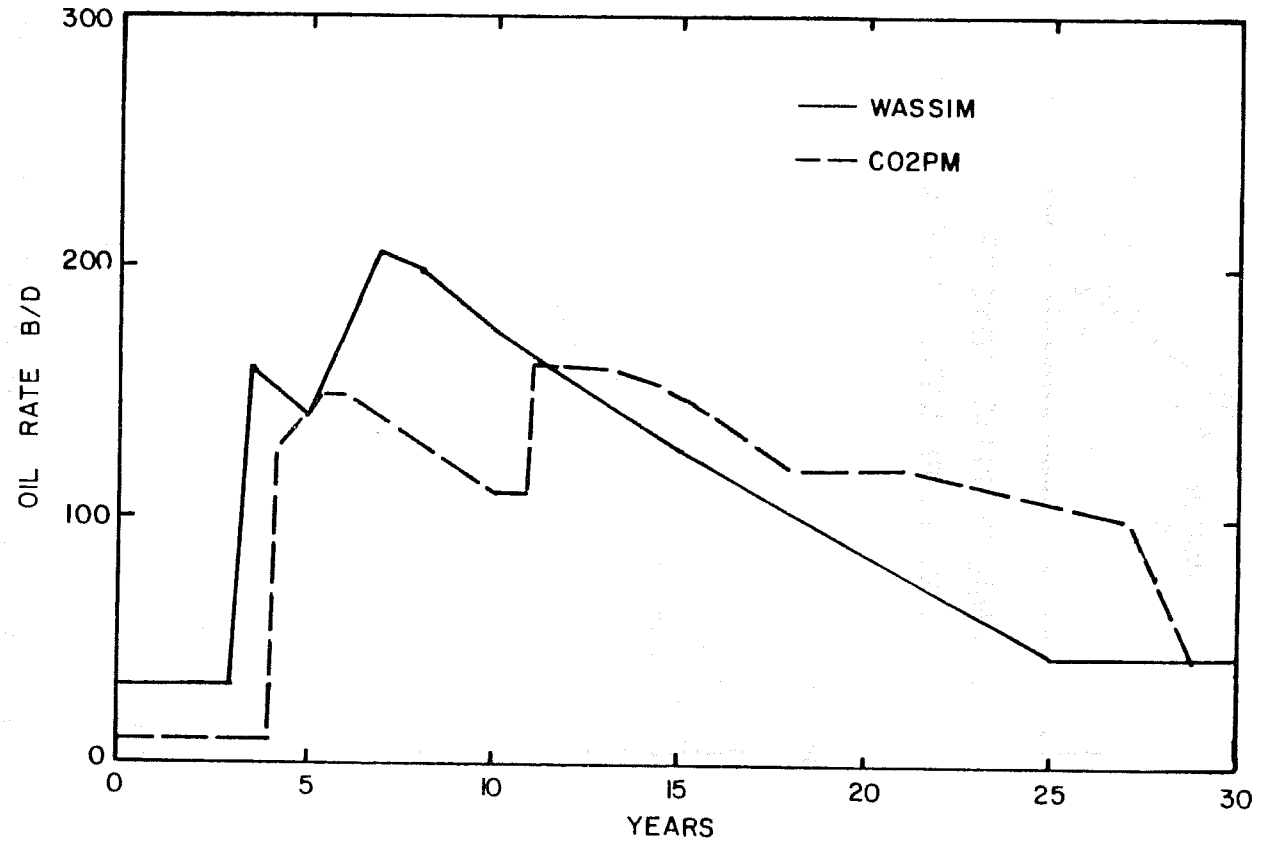

Figure A-1a

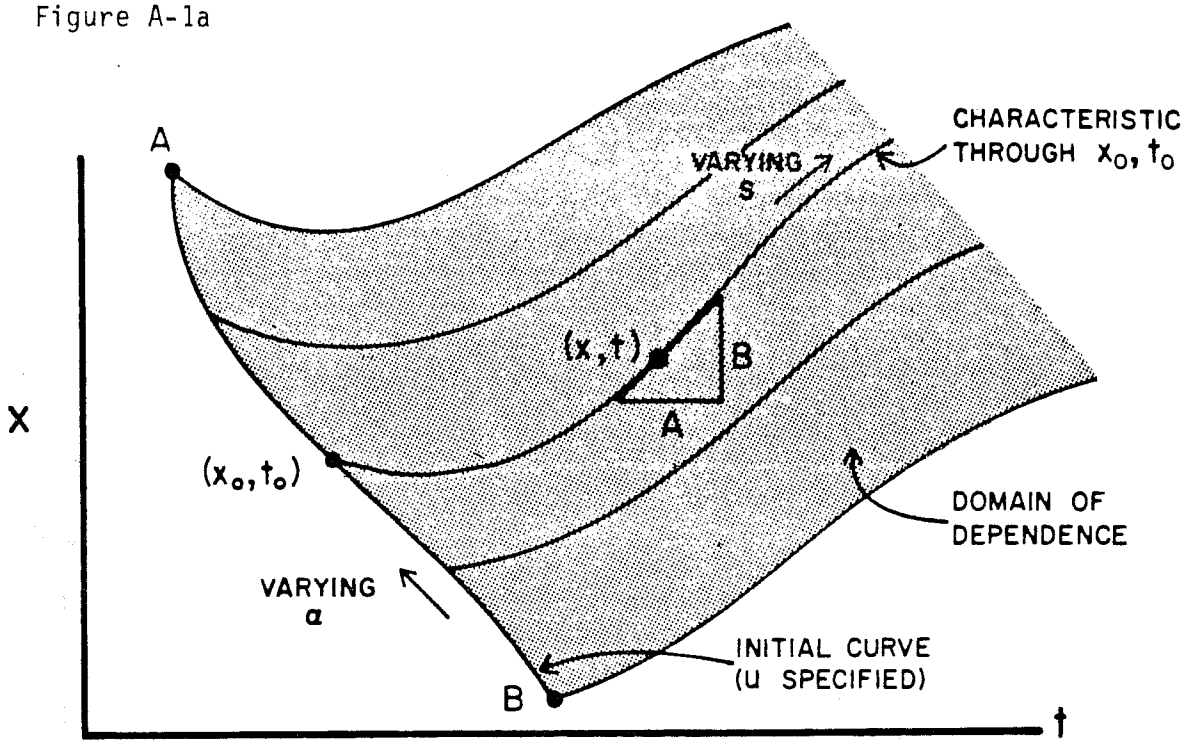

CHARACTERISTIC CONSTRUCTION FOR GENERAL ONE DEPENDENT VARIABLE PROBLEM

Figure A-1b

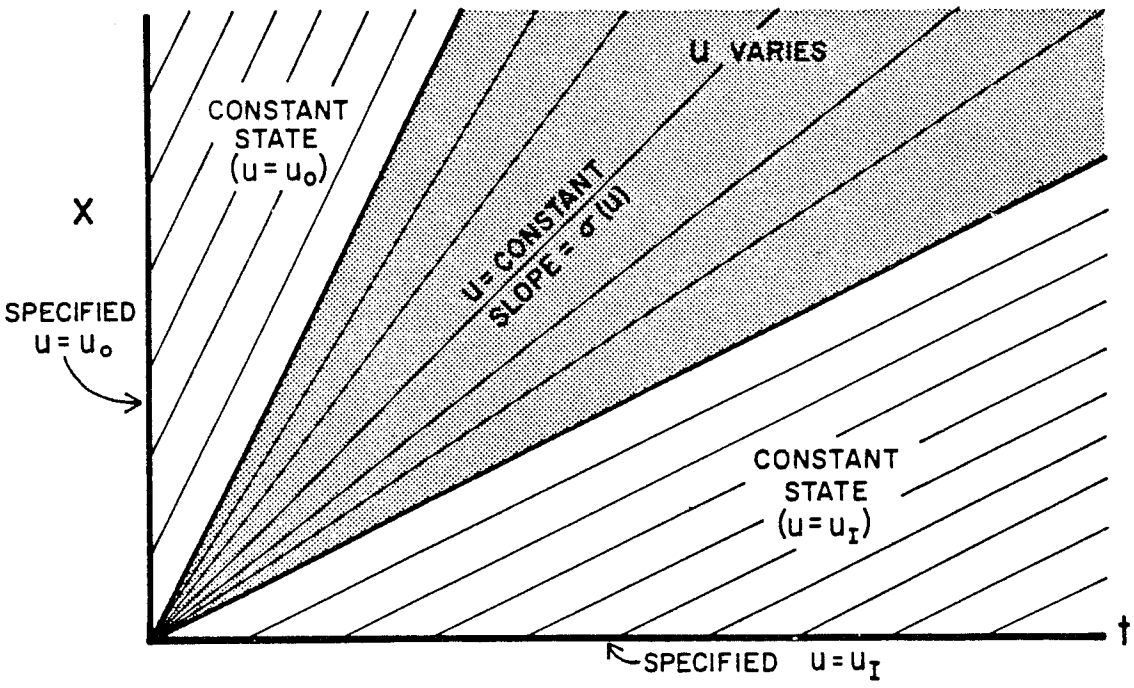

CHARACTERISTIC CONSTRUCTION FOR SPECIAL CASE

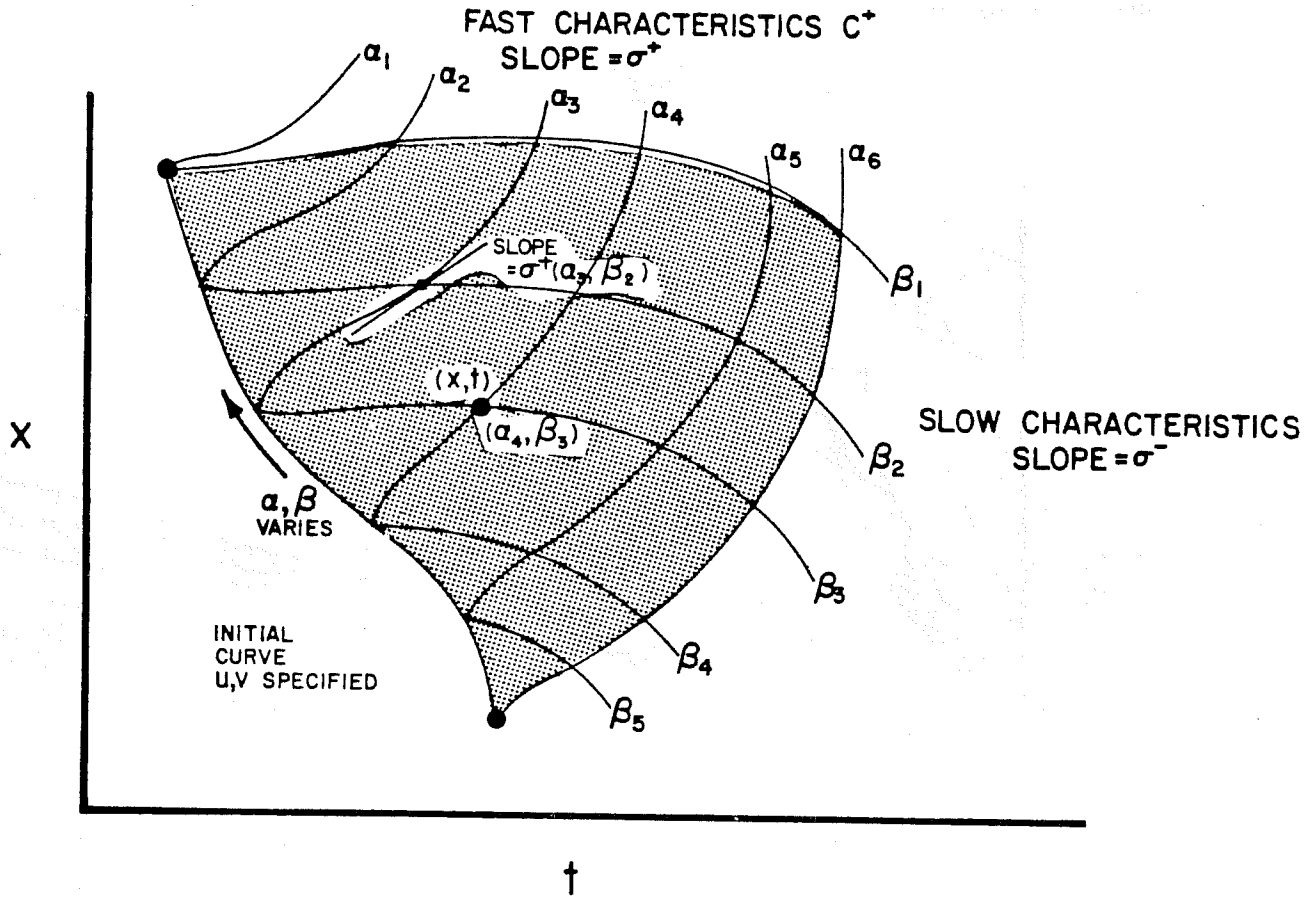

CHARACTERISTICS FOR TWO-VARIABLE PROBLEM

Figure A-2C

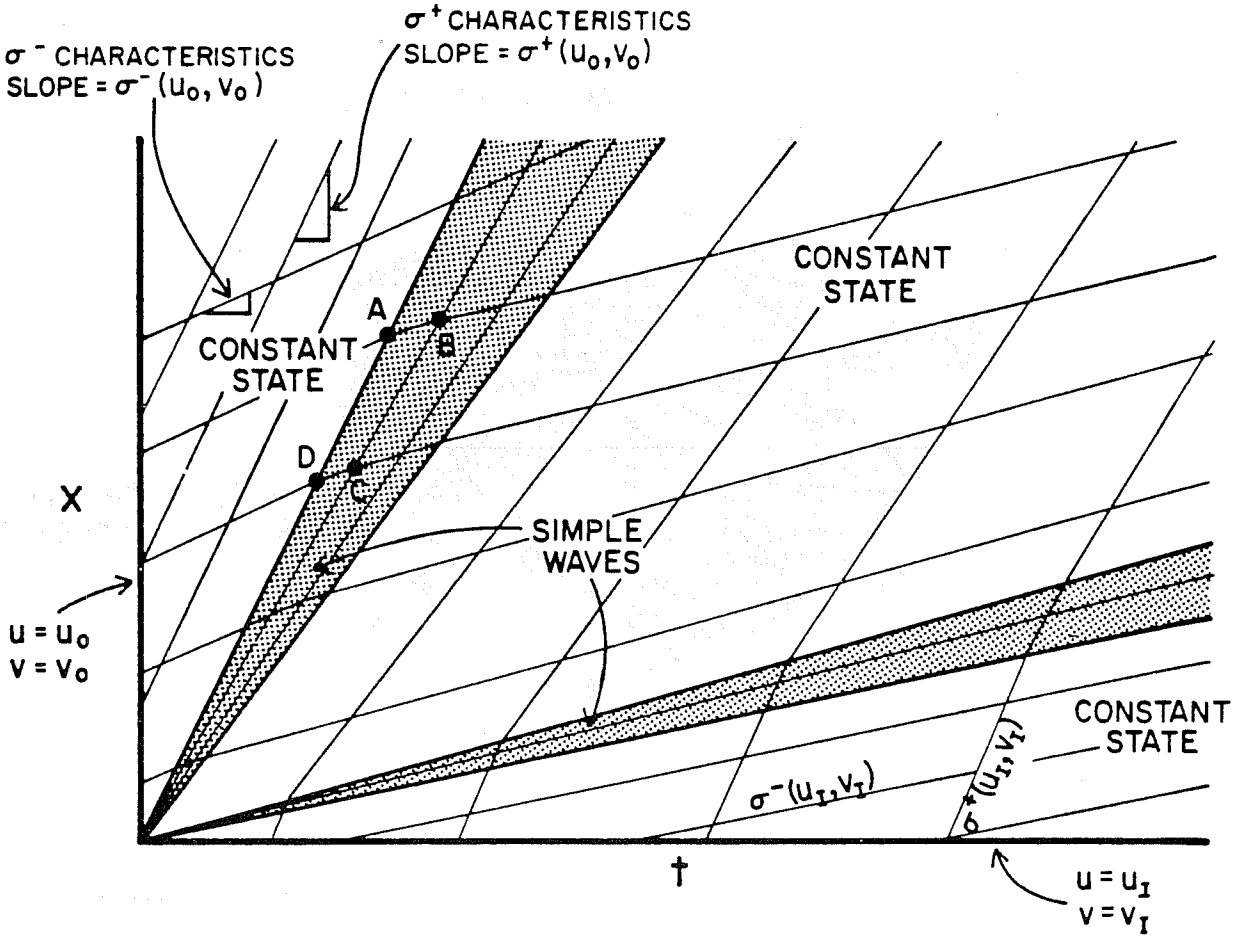

CHARACTERISTICS FOR CENTERED SIMPLE WAVE

Figure A-2b

FIGURE D-1

CO2PM FLOW DIAGRAM

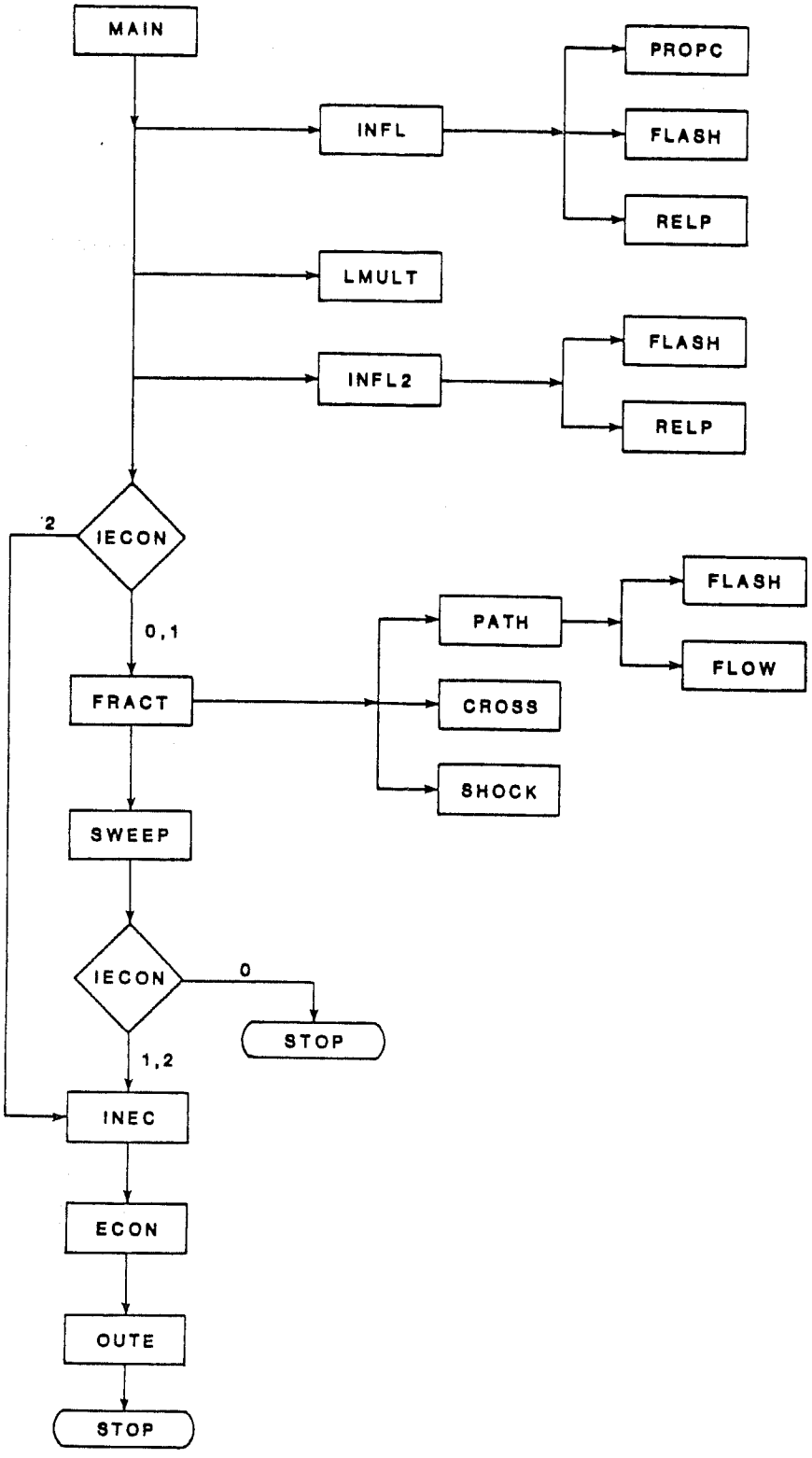

APPENDIX A

METHOD OF CHARACTERISTICS FUNDAMENTALS

This appendix gives a brief summary of the derivation of the coherence condition from the method of characteristics (MOC). Readers interested in more detail should consult standard references.[31-35]

A. Method of Characteristics

The fundamental principle in the MOC is to solve partial differential equations (PDE's) by first converting them to a set of ordinary differential equations (ODE's) which may then be integrated simultaneously. This set of ODE's can rarely be integrated in closed form, but there is a large class of porous media flow problems for which the integrations can be presented in a general form. To illustrate these ideas we consider first a single PDE, then pairs of PDE's in the dependent variables u and v. The theory may be generalized to more than two PDE's, but the procedures become quite cumbersome in practice.[35]

Consider the following partial differential equation for u(x,t)

$$L = Au_t + Bu_x + E = 0 \tag{A-1}$$

where A, B, and E are known functions of u, x, and t (the operator L is linear in the derivatives of u). The notation u_x and u_t means partial differentiation with respect to x and t.

We want solutions to (A-1) in the form u(x,t) subject to the appropriate initial and boundary conditions. In the MOC we seek these solutions in the form u(s) where s is a parameter along a curve C in x-t space such that x = x(s) and t = t(s). We may, therefore, write the total derivative of u with respect to s as

$$u_s = t_s\, u_t + x_s\, u_x \quad . \tag{A-2}$$

Note that Equation (A-2) is a mixture of total derivatives u_s, t_s, and x_s, and partial derivatives u_t and u_x. We use the same notation for both types of derivatives, however, since the type of derivative should be clear from the usage. Comparing Equations (A-1) and (A-2) leads to

$$t_s = A \tag{A-3a}$$
$$x_s = B \tag{A-3b}$$
$$u_s = -E \quad , \tag{A-3c}$$

an identification which implies that L is nothing more than a directed derivative along C. Equations (A-3) are a set of three ODE's which may be integrated from an initial curve, as shown in Figure A-1a, to give a curve C in x-t space along which u varies as given by the integration of Equation (A-3c). The various integrations are possible only if C is nowhere tangent to the initial curve. Figure A-1a shows schematically the integration of these equations for a curve C which begins at the point (x_0, t_0) on the initial curve. It is apparent that we could take other points on the initial curve, and thereby cover the shaded domain of dependence in Figure A-1a defined by the characteristics through the points A and B on ends of the initial curve. If α is a parameter along the initial curve then the solutions to Equations (A-3) may be regarded at $t = t(s, \alpha)$, $x = x(s, \alpha)$, and $u = u(s, \alpha)$. The parameters s and α may be thought of as the coordinate distance of a natural or canonical, generally-curved, coordinate system for Equation (A-1). Since α, in effect, determines which curve C passes through the point (x,t), at which the value of u is desired, the characteristics for Equation (A-1) are a one-parameter (α) family of curves, and α is a label for this one-parameter family. An important observation is that at every point (s,t) in the shaded region in Figure A-1a, the slope of the characteristic curve is given by

$$\frac{x_s}{t_s} = \left(\frac{dx}{dt}\right)_C = \frac{B}{A} \equiv (u,x,t) \tag{A-4}$$

where σ is called the characteristic direction at a given (x,t). Equation (A-4) implies that it will generally be unnecessary to determine $t = t(s, \alpha)$ and $x = x(s, \alpha)$ since $u = u(s, \alpha)$ follows directly from (A-4) and (A-3c).

Consider now a special case of Equation (A-1) where E = 0, and A and B are functions of u only. Further, we take as initial data a curve that coincides with the x-axis, where us = u_I, and then coincides with the t-axis, where u = u_J. The boundary (x = 0) and initial (t = 0) data are, therefore, uniform except for a step change at the origin, at which point all values of u between u and u_I exist. It follows immediately from Equations (A-3c) and (A-4) that u is constant along the characteristics C which are themselves straight lines. Figure A-1b shows the characteristics for this case. In regions adjacent to the x- and t-axis the characteristics are parallel with slopes σ (u_I) and σ (u_J) respectively. These regions are constant state regions. The shaded region in Figure A-1b is a fan-like region where σ changes continuously between the limits imposed by the constant state regions. Each ray emanating from the origin carries a particular constant σ from the multiplicity of u's between u_I and u_J, and each has a slope σ evaluated at that u. The shaded region in Figure A-1b is, therefore, a wave,[31] since in any non-characteristic direction u is changing. It is clear from Figure A-1b that the characteristics cannot cross, but there is nothing that requires σ to decrease monotonically as in the case shown. When σ does not decrease monotonically, a mathematically valid solution exists that leads to the formation of discontinuous or shock waves if u is a physical variable. We defer discussion of shocks to later. Finally, the characteristic direction σ may clearly be interpreted as a velocity (if x and t are distance and time), and written as

$$\sigma = \left(\frac{dx}{dt}\right)_C = \left(\frac{dx}{dt}\right)_u \qquad \text{(A-5)}$$

With the appropriate forms for A, B, t, and x, Equation (A-5) would become the well known Buckley-Leverett equation for water displacing oil in a porous medium.

Let us consider now a pair of PDE's in the dependent variables u(x,t) and v(x,t)

$$L_1 = A_1\, u_t + B_1\, u_x + C_1\, v_1 + D_1\, v_x + E_1 = 0 \qquad \text{(A-6a)}$$

$$L_2 = A_2\, u_t + B_2\, u_x + B_2\, u_x + C_2\, v_t + D_2\, v_x + E_2 = 0 \qquad \text{(A-6b)}$$

Initially we consider the most general case of the coefficients A-E being functions of x, t, u, and v. The first four terms in the linear operators L_1 and L_2 may be regarded as directed derivatives of u and v. There are four such directions ($A_1 u_t + B_1 u_x$, $C_1 v_t + D_1 v_x$, etc.), but, in order to transform the pair to a set of ODE's, we will seek a curve in (x,t) space where u = u(s), v = v(s), x = x(s), and t = t(s). We therefore will seek a combination $L = \lambda_1 L_1 + \lambda_2 L_2$ such that L is a linear combination of total derivatives u_s and v_s. As before, s is a parameter along such a curve. For solutions to the equations, the operator L must be equal to zero, hence:

$$L = (A_1 \lambda_1 + A_2 \lambda_2)u_t + (B_1 \lambda_1 + B_2 \lambda_2)u_x + (C_1 \lambda_1 + C_2 \lambda_2)v_t + (D_1 \lambda_1 + D_2 \lambda_2)v_x + (E_1 \lambda_1 + E_2 \lambda_2) = 0 \quad . \tag{A-7}$$

For the directed derivatives of u and v to be co-linear it is necessary that

$$\frac{x_s}{t_s} = \sigma = \frac{B_1 \lambda_1 + B_2 \lambda_2}{A_1 \lambda_1 + A_2 \lambda_2} = \frac{D_1 \lambda_1 + D_2 \lambda_2}{C_1 \lambda_1 + C_2 \lambda_2} \quad , \tag{A-8}$$

The two equations in (A-8) may be written as

$$(A_1 x_s - B_1 t_s) \lambda_1 + (A_2 x_s - B_2 t_s) = 0 \quad . \tag{A-9a}$$

$$(C_1 x_s - D_1 t_s) \lambda_1 + (C_2 x_s - D_2 t_s) = 0 \quad . \tag{A-9b}$$

In order for non-trival λ_1 and λ_2 it is necessary for the determinant of the coefficient matrix to be zero, hence:

$$(A_1 C_1 - A_2 C_2) \sigma^2 + (A_2 D_1 - D_2 A_1 + C_1 B_2 - C_2 B_1) \sigma + (B_1 D_2 + D_1 B_2) = 0 \tag{A-10}$$

where we have substituted the characteristic direction σ from Equation (A-8). Immediately, it is apparent that there are in general two characteristic directions, not one as there was in the analogous

expression, Equation (A-4), for the one variable problem. Whether or not these directions are real for all (x,t) depends on the form of the coefficients. For porous media flow problems σ is real in at least some, usually all, of the domain (x,t). This, in fact, is the definition of hyperbolic PDE's. Furthermore, the roots to Equation (A-10) are generally distinct. Let σ^+ designate the larger root of (A-10) and σ^- the smaller. Clearly, the corresponding characteristic curves C^+ and C^- cover the domain of dependence in (x,t) since the slope of C^+ is everywhere larger than the slope of C^-. These curves are shown in Figure A-2a. The shaded domain of dependence is bounded for the two-variable problem by the "fast" σ^+ characteristic through B, and the "slow" characteristic σ^- through A.

Each point in the domain of dependence is on the intersection of an σ^+ and σ^- characteristic. The coordinates of a point may then be located as a distance s along a particular characteristic having label x (say), that is, $x = x(s, \alpha)$ and $t = t(s, \alpha)$. Alernatively, the coordinates may be located by giving the labels of both characteristics passing through it, or $x = x(\alpha, \beta)$ and $t = t(\alpha, \beta)$, where β is now the label on the other characteristic. The notion of labels is somewhat confusing since α and β can take on the same numerical values on the initial curve; in the interior of the domain of influence they are distinct.

The characteristic curves cannot be obtained, in general, unless it is known how u and v change along the characteristic directions. This may be obtained by replacing the coefficients of u_x and v_x by the denominators of the Equations (A-8),

$$(A_1 \lambda_1 + A_2 \lambda_2)u_s + (C_1 \lambda_1 + C_2 \lambda_2)v_s + (E_1 \lambda_1 + E_2 \lambda_2)t_s = 0. \quad \text{(A-11a)}$$

A similar procedure on u_t and v_t gives

$$(B_1 \lambda_1 + B_2 \lambda_2)u_s + (D_1 \lambda_1 + D_2 \lambda_2)v_s + (E_1 \lambda_1 + E_2 \lambda_2)x_s = 0. \quad \text{(A-11b)}$$

These equations, rearranged, are

$$(A_1 u_s + D_1 v_s + E_1 x_s) \lambda_1 + (A_2 u_s + C_2 v_s + E_2 t_s) \lambda_2 = 0 \quad , \text{(A-12a)}$$

$$(B_1 u_s + D_1 v_s + E_1 x_s) \lambda_1 + (B_2 u_s + D_2 v_s + E_2 x_s) \lambda_2 = 0 \quad . \text{(A-12b)}$$

Again, for non-trival λ_1 and λ_2 the determinant of the coefficient matrix must be zero; again the characteristic equation has two real, distinct roots for u_s and v_s. The roots of these equations form, along with the two roots to Equation (A-10), four ODE's which may be integrated simulataneously for u, v, x, and t from an initial curve.

Rather than expound further on the above, let us consider the special case where $E_1 = E_2 = 0$ and the remaining coefficients are functions of u and v only. Such equations are said to be reducible. The characteristic directions from Equation (A-10) are a known function of u and v only. Furthermore, along each characteristic curve there is a relation between u and v given by

$$\left[B_2 A_1 - B_1 A_2 \frac{du}{dv}\right] = B_1 C_2 - C_1 B_2 + \sigma^{\pm} \left[C_1 A_2 - A_1 C_2\right] \qquad \text{(A-13)}$$

from Equations (A-9a) and (A-12a). There are three equivalent forms to this equation, but the important point is that u and v are related to each other along the $C^{\pm}$ curves in x-t space, since all the coefficients in (A-13) are known functions of u and v. The u-v plot which contains the above solution is said to be the image, or hodograph, space. The function $u = u(v)$ for C^+ is the image curve Γ^+ of C^+ as is $u = u(v)$ for Γ^- the image curve for C^-. In the coherence theory section we shall call the u-v space the composition path diagram, and the Γ^+ and the Γ^- curves the composition paths.

In addition to the restriction to reducible PDE's, let us now consider the special case of $u = u_I$ and $v = v_I$ being specified on the x-axis, and $u = u_J$ and $v = v_J$ being specified on the t-axis. As before, this means that all (u,v) values between (u_I, v_I), and (u_J, v_J) exist at the origin. As before also, there are regions of constant state adjacent to both axis where the characteristic directions, and, hence, the labels α and β are constant. Unlike before, however, there are now two fan-shaped regions (Figure A-2b) where first the fast or α characteristics change slope, and then the β characteristics change. The regions cannot overlap or there would be finite regions where $\sigma^+ < \sigma^-$. This fact causes the creation of a new constant state region (u,v) between the fans that is, in general, different from either (u_I, v_I) or (u_J, v_J). Within the fan-shaped regions, the α - β- characteristics cannot both be straight or else these would be constant state regions. One of the characteristic

directions is constrained to be straight, however, in each region ($\sigma+$ in the first shaded region of Figure A-2b, and $\sigma-$ in the second). This is so because two points A and D on the boundary have the same (u,v) values since they can be regarded as being in the constant state region. This must be true of all other rays in the fan-shaped region, for example, the ray passing through C and B. Otherwise the ray could be curved (from Equation (A-10)) and would ultimately intersect either of the constant state regions. It follows, then, that all points on the straight line characteristic carry the same (u,v) value. Since $(u,v)_A = (u,v)_B$ and $(u,v)_C = (u,v)_D$, it follows that $\sigma_B = \sigma_C$ and the slope of the $\sigma-$ characteristics is the same as all of the $\sigma+$ characteristics. This means that the u = u(v) relationship defined by Equation (A-13) is the same on any slow characteristic in the region. Thus (du/dv) - and (du/dv) + uniquely determine the variations in u and v in the respective fan-shaped regions. Note that the function u = u(v) is always calculated based on the curved characteristic.

The above concepts apply generally to reducible sets of PDE's in any number of dependent variables. The observations, stated concisely, are,

1. Adjacent to any constant state region there is a region having at least one straight line characteristic. The second region is called a simple wave region.

2. Within a simple wave region the dependent variables are related to each other through a set of ODE's.

3. For boundary and initial conditions that are uniform except for a step change at the origin, the entire (x,t) domain consists of alternating constant state and simple wave regions. The simple waves in this case are centered simple waves.

B. Coherence

The previous information may be restated more concisely, and with more physical insight, by referring to simple waves in the terminology of coherent waves.[31] Since (u,v) is constant on a straight line characteristic in a simple or coherent wave region, and since σ is a function of u and v only, it follows that

$$\left(\frac{dx}{dt}\right)_u = \left(\frac{dx}{dt}\right)_v \tag{A-14a}$$

for all simple wave regions. For N dependent variables u_i this becomes

$$\left(\frac{dx}{dt}\right)_{u_1} = \left(\frac{dx}{dt}\right)_{u_2} \cdots = \left(\frac{dx}{dt}\right)_{u_N} \tag{A-14b}$$

Equation (A-14b) states that the velocity of constant values of the dependent variables is the same--the coherence condition. The coherence theory offers no fundamental advancement of the MOC, but as was illustrated in Section II, the coherence method of calculating simple waves is far more direct that using the method of characteristics.

Probably the most important property of reducible equations is that the dependent and independent variables may be interchanged if the Jacobian of the transformation is not zero. This means that the mapping of C into the Γ space is one-to-one. In constant state and simple wave regions, however, the Jacobian is identically zero (every term is zero in the constant state region). Hence, as illustrated above, the mapping of C onto Γ is not one-to-one, and we find cases of curves in C being mapped onto points in Γ.

APPENDIX B

EFFECT OF GRAVITY SEGREGATION ON MISCIBLE FLOOD OIL RECOVERY

The time required for a particle to move from injection to production well (t_h) relative to the time required for a particle to move from the bottom to the top of the reservoir (t_v) should be a measure of the extent of gravity segregation occurring during a displacment process.

The average frontal velocity for a five-spot pattern was determined by Parsons[36] to be

$$\bar{v}_h = 0.016 \frac{Q}{h\sqrt{A}} \tag{B-1}$$

where Q is the injection rate in RB/D, h is the thickness of the reservoir, and A is the pattern area in acres. The distance between injection and production wells in a five-spot is

$$L = \sqrt{43560A} \;/\; 2\sin 45^\circ = 147.58\sqrt{A} \tag{B-2}$$

where L is in feet. Therefore, t_h is given by

$$t_h = \frac{L}{\bar{v}_h} = 9224 \frac{hA}{Q} \quad . \tag{B-3}$$

From Darcy's law, the fluid velocity in the vertical direction due to gravity forces is given by

$$v_v = 2.7401 \times 10^{-3} \frac{k_v}{\mu} \Delta \rho \tag{B-4}$$

where k_v is the vertical permeability in md, μ is hte viscosity in centipoise, and $\Delta\rho$ is the fluid density difference in gm/cc.

The time to move a distance h is then given by

$$t_v = \frac{h}{v_v} = \frac{h\,\mu}{2.7401 \times 10^{-3} k_v \Delta\rho} \qquad \text{(B-5)}$$

and the ratio of times is

$$\frac{t_h}{t_v} = 2.5271 \left(\frac{k_v}{k_h}\right)\left(\frac{A}{h}\right)(k_h h) \; \frac{\Delta\rho}{Q\,\mu} \qquad \text{(B-6)}$$

where k_h is the horizontal permeability.

APPENDIX C

CALCULATION OF RATE AND SLUG SIZE MULTIPLIERS FOR LAYERS

We assume N layers of equal thickness (h) and porosity. The cumulative probability of permeability for layer i is

$$P_i = h(i - \tfrac{1}{2})/H, \qquad \text{(C-1)}$$

or since the total thickness H = Nh,

$$P_i = (i - \tfrac{1}{2})/N \qquad \text{(C-2)}$$

The difference in probability of the mean permeability $\bar{k}$ (assumed equal to k_{50}) from the probability of any permeability k_i is obtained by integrating the normal probability density function

$$P_{50} - P_i = 0.5 - p_i = 1/\sqrt{2\pi} \int_0^y \exp(-y^2/2)dy \qquad \text{(C-3)}$$

where

$$y = -(\log k_i - \log K_{50})/\log(1 - VDPL) \qquad \text{(C-4)}$$

and where we have distinguished VDPL, the Dykstra-Parsons coefficient among gross layers, from VDP, the measure of heterogeneity within an individual layer. The latter coefficient is used to compute the Koval factor according to Equations 23a and 23b. Equation (C-4) is integrated numerically until the rhs equals 0.5 - p_i, then solved for k_i. The k_i's are normalized such that $\sum k_i h = kH$.

Once the k_i are obtained, the rate and slug size are apportioned among the layers by

$$q_i = q\, k_i / \sum_{i=1}^{N} k_i,$$

$$t_{DS_i} = N\,(q_i/q)\,t_{DS}$$

where q is the total rate and t_{DS} is the total HCPV of CO_2 and water injected.

APPENDIX D

DESCRIPTION OF CO2PM ROUTINES

The operations performed by the various CO2PM routines are given below. A flow design of the model is shown in Figure C-1.

MAIN: The MAIN program corrects for areal sweep and calculates production profiles. It calculates cumulative fluid recoveries and prints final summaries. The main program also calls the economic calculation routines.

INFL: This subroutine reads all of the input reservoir data and initializes the model. It checks all input data and assigns default values. It prints all the initialization data.

INFL2: Peforms essentially the same functions as INFL for multiple layer cases.

LMULT: Computes rate and CO_2 slug size multipliers for layers.

FRACT: Computes rate and CO_2 slug size multipliers for layers. This subroutine computes fractional flow of water/oil/CO_2 in two phases (aqueous and oleic). It uses the method of characteristics to compute the fractional flow. It also prints the recovery calculations for 1-D systems.

PATH: This subroutine computes concentrations of water/oil/CO_2 in two phases (aqueous and oleic) along a fast or slow path by the method of characteristics solution.

FLASH: This subroutine calculates aqueous and oleic phase saturations from a two-phase flash. It also calculates concentration of all components in each phase.

FLOW: This subroutine calculates fractional flow of each component in the system. It takes into account dispersion and fingering in the reservoir due to unstable miscible displacement by the method of Koval.

CROSS: This subroutine finds the intersection between slow and fast paths.

SHOCK: This subroutine finds a single shock along the fast path by finding the concentrations where the shock and concentration velocities are equal.

PROPC: This subroutine computes physical properties for CO_2 as a function of reservoir pressure and temperature. It calculates CO_2 density, viscosity, solubility in water, and compressibility factors.

RELP: This subroutine calculates oil/water relative permeability curves and the respective fractional flows.

SWEEP: This subroutine calculates areal sweep efficiency by Claridge's method.

INEC: This subroutine reads all of the economic data, pattern schedules, and case controls. It also assigns default values for economic data.

ECON: This routine computes profitability indices.

OUTE: This subroutine writes economic reports, including discounted cash flow versus time.

☆U.S. GOVERNMENT PRINTING OFFICE: 1984-769-029/412